Structural uncertainty identification using mode shape information

Siska Riefelyna

Submitted for the degree of Doctor of Philosophy

Engineering and Design

School of Engineering and Informatics

University of Sussex

September, 2012

Declaration

I hereby declare that this thesis has not been submitted, either in the same or different form, to this or any other university for a degree.

_____

Siska Riefelyna

Acknowledgements

First and foremost, I would like to thank my supervisor, Dr. Julian F Dunne, whose constant encouragement, continuous support, and belief in me, made this work possible. I will always be grateful for his guidance during the period, as well as his kindness and reliability.

I would also sincerely like to thank TPSDSP ITENAS for their 3 years scholarship and to DIKTI for 9 months additional funding for this research.

Special thanks to Taufan C Abadi, for his help and support for me from the beginning.

And a deep thank you, not only to my parents: Euis and Syarief but also to my sisters: Henny and Yuyun for their support forever, always being my number one supporters on whichever path I have taken in my life.

I would like to thank Sumarliah and Dayat Hidayat, they were always encouraging me with their best wishes.

There are a number of people I would like to thank here, not necessarily only for their support in my research, but also for their companionship while I was doing my research. Each of them has special meaning to me. If I am missing a name, it is simply a lack of memory and not ingratitude. Each one of them has a unique way to give the contribution on my research. Thank you to:

Abdullah, Agis, Alan, Amelia, Amich, Anna, Arifin, Ashish, Ayu, Barry, Chris, Derek, Diana, Eefan, Faisal, Ferry, Gabriella, Graham, Imran, Irma, Jessica, Kristyadi, Liang, Leo, Lionel, Luis, Martina, Mark, Max, Maya, Michael, Megya, Nelti, Nicholas, Novi, Nursetiawan, Obi, Pattarapong, Petra, Shrijit, Sue, Taufik, Thana, William, Wulan Yuhan, and, Zun.

To my lovely daughter, the light of my life,

Xyla Fellita Ayu Taufaniska Tca.

I will always try to be the best mother for you, love you forever and always.

ABSTRACT

This thesis is concerned with efficient uncertainty identification (UI) – namely the nonlinear inverse problem of establishing specific statistical properties of an uncertain structure from a practically-limited supply of low-frequency dynamic response information. An established UI approach (published in 2005) which uses Maximum Likelihood Estimation (MLE) and the Perturbation Method of uncertainty propagation is adopted for the study using (for the first time) mode shape information rather than just natural or resonant frequencies. The thesis develops a method based on the use of selected coefficients in a generalized displacement model i.e. a weighted series of spatially-continuous multiply-differentiable base functions to approximate the structural free-vibration response of an uncertain structure. The focus is placed on the estimation (from relatively small data sets) of the statistical properties of the location of an attached point-mass with normally-distributed position.

Simulated data for uncertain point-mass-loaded linear beam and plate structures is initially used to test the method making use of as much exact or closed-form differentiable information as possible to obtain frequencies and mode shapes. In the case of plate structures, extensive use is made of the Rayleigh Ritz method to generate the required response coefficients. This is shown to have significant advantages over alternatives such as the Finite Element method. The approach developed for use with free vibration information is then tested on measured experimental data obtained from an acoustically-forced clamped plate. Structural displacement measurements are taken from the plate using Vibromap 1000, a commercially-available ESPI-based holomodal measurement system capable of wide-field vibration response observation in real-time, or quantitative displacement response measurement.

The thesis shows that the developed uncertainty identification method works well for beams and plates using simulated free-vibration data.

Contents

NOMENCLATURE

$f(.)$: probability density function

f(.) : system function

J : Jacobian matrix

$l(.)$: log likelihood

$L(.)$: likelihood

m : number of response variables

n : number of uncertain parameters/variables

N : number of samples/measurement

N(.) : normal probability distribution

M : total number of parameters associated with a distribution

x : uncertain parameter

x_i : i-th uncertain parameter

x : uncertain parameter vector

x_i : i-th sample of the parameter vector

y : response

y_i : i-th response variable

Y : response vector

Y_i : i-th sample of the response vector

μ : mean vector

Σ : covariance matrix

σ_x : standard deviation

θ_x : parameters of the uncertain parameters distribution

CHAPTER 1

INTRODUCTION

Real structures (of nominally identical type) differ from each other owing mainly to variations in material properties, manufacture, and operational conditions. The dynamic modelling of real structures is normally based on the assumption that the parameters are known with certainty in all stages of the design process. In particular, mobile engineering structures are designed to be lightweight, often resulting in complex geometry and form, with great potential for variability such as those to be found in vehicle bodies, engine blocks, satellite structures, spacecraft, aircraft, and ship structures. And yet, in all of these examples, significant uncertainties naturally occur during manufacture and assembly. For such structures to operate economically, it is necessary for the safety factors embedded in the design process not to lead to over-conservative design.

Avoiding the problem of over-design, in the presence of uncertainty, is a major challenge. But to solve this problem two things are required. First, the properties of all the uncertainty must be defined in its entirety, either in statistical terms or otherwise. And second, the problem is to study the effect this uncertainty has on key design variables as the uncertainty is propagated. Such propagation may relate to mass variability, dimension variability, boundary conditions, or damping uncertainty. In most studies to date, attention has largely focused on propagating the uncertainty by making assumptions about the properties of the uncertainty. In general the issues associated with the number-of-degrees-of-freedom, whether the structure is linear or nonlinear, and operating amplitude and frequency range are all factors which may complicate the analysis. But the particular challenge for the first task, namely the uncertainty identification (especially if an ensemble of real structures is used to obtain data) is to develop a method that, for practical reasons, keeps the sample sizes to an absolute minimum. In this thesis the focus is on the problem of determining the properties of the uncertainty.

Modelling of structures can be considered both at the initial stages of design, where for engineering problems the task is to find a good solution early on,

whereas a later task is one of refinement. Sources of noise, vibration and harshness (NVH), in particular unfavourable responses, need to be identified and removed so that the design will ultimately be acceptable both in technical and economic terms. This process requires efficient structural dynamic modelling methods. But it also needs accurate data on the sources of uncertainty. At low frequency, the finite element method is often a very good approach to generate accurate solutions to engineering structural analysis problems. Making a model mesh finer should allow higher frequency behaviour to be predicted, but in fact it cannot resolve the uncertainty problem present in the modelling at low frequency, and only makes the problem more obvious as frequencies increase. In cases where the uncertainty is known be statistical, estimation of the properties of the model uncertainties associated with discrete parameters, such as mean values, standard deviations, and probability distributions, will ultimately enable a high level of confidence in prediction approach via a suitable uncertainty propagation method. It will also massively reduce time and cost by not having to test an ensemble of structures to validate the accuracy of predictions. In practice it is unfortunately rare that uncertainty can be quantified in an absolute sense, and the designer has to accept that the actual structural parameters will be uncertain when the structure is built.

Lin [1967] states that: "*the main approach to evaluate the reliability of a structure that has been designed to resist random excitations is using stochastic-process (probability) theory in a structural response analysis*". According to Lin [1967], reliability means the probability of success. The term reliability is usually defined as the complement of the probability of failure, or the probability of safety of the structure over a given period of time, Melchers [1999]. The design procedures for a structural product take aspects of both uncertainty and variability parameters. The terms uncertainty and variability are not explicit. Individual researchers might have applied the same terminology but the meaning is subjective. Gersem and Hilde et al [2005] for example, describes an overview of the definitions of variability and uncertainty in the context of finite element method.

Since there can in general be many different ways of defining uncertainty in what follows, an initial attempt is made to classify uncertainty using different definitions. Then, to undertake analysis (and indeed to understand the methods of structural uncertainty identification), it is appropriate to outline available uncertainty propagation methods, which is naturally followed by an overview of uncertainty identification and the available approaches. A literature review of structural uncertainty modelling and identification then follows, leading to the objectives of the thesis.

1.1 Classification of Structural Uncertainty

Uncertainty can be classified as variability (*aleatoric* uncertainty), or (*epistemic* uncertainty) or prejudicial uncertainty (error) [Anderson, 2001]. The main characteristics of variability correspond to a difference that occurs in the physical design of a model property which is irreducible, and ranges over time, or from unit to unit. Characteristic examples of variability are a design property as a result of manufacturing process, installation, environmental effects on a model (temperature, humidity, etc), non-uniform materials properties, and specific instability in operating conditions.

The main characteristics of uncertainty correspond to any model property that cannot be quantified accurately (potential deficiency), reducible during increasing data, and representing a lack of knowledge. Characteristic examples of uncertainty are non-rigid models for boundary conditions, simplified models for joints, models for material damping, and random model changes due to ageing, loading, etc. Most uncertainties in a structure (which influence the structural dynamic characteristics) are caused by an uncertainty level in such parameters as the material properties, dimensions, temperature change, or loading conditions. These factors result in uncertain frequency response functions (FRFs) of the component models. Vehicles rolling-off assembly lines for example, show significant differences in measured acoustic responses (NVH characteristics). These differences can be classed as uncertainty, which can create problems for modelling and prediction of the NVH characteristic, particularly the NVH response of vehicle bodies.

The main characteristic of prejudicial uncertainty (error) is recognised as bias and reducibility during the modelling process. Characteristic examples of error are simplified modelling assumptions. For example finite grid resolution in model discretisation will cause numerical errors, whereas some errors in structural analysis are caused by inaccurate computation or measurement errors in obtaining the data for model calibration.

The analysis of the vibration characteristics of linear structural dynamic behaviour will depend on the nominal properties of the structure such as the mass, damping, and stiffness. The nominal model for a force-damped structural dynamic system is [Langley, 2000]:

$$[\mathbf{M}]\ddot{z}+[\mathbf{C}]\dot{z}+[\mathbf{K}]z=\mathbf{F}(t) \tag{1.1}$$

where z is a displacement vector, **M**, **C**, and **K** are N x N mass, damping, and stiffness matrices, and **F** is a vector of loads. To analyse the structural dynamic characteristics of the system described by equation (1.1) the condition of the structure will be needed, such as whether free or forced, damped or undamped. Equation (1.1) is a system of differential equations for a force-damped structure which in general could result from discretisation using a finite element model of the system, or from the use of a Lagrange-Rayleigh-Ritz approach. Analysis can immediately proceed if there is no uncertainty in the parameters.

The uncertainty in the mass damping and stiffness matrices will contribute to uncertainty in the structural response but relating this to the known physical sources can be a major challenge. The validation and uncertainty qualification phases of a modelling process, such as appropriate for the model of equation (1.1), in general involves the observation of nature, conceptual modelling, mathematical modelling, numerical modelling, numerical implementation, numerical evaluation, surrogate modelling, surrogate implementation and surrogate evaluation [Anderson, 2000]. Despite all of these aspects for a complete analysis, the application of uncertainty in simple structural dynamics can be achieved in an academic environment since much can be learned of

relevance to real structures. Typically these include beam and plate structures with mass variability (e.g. with attached point masses placed in random positions), weight variations of a point mass, multiple attached point masses, variable geometry, and possibly variable material properties. When this information is known then uncertainty propagation methods can be applied. It will indeed be appropriate shortly to explain what is involved in uncertainty propagation since it will be seen that these methods also form part of uncertainty identification. Before then, it is useful to briefly explain the different ways structural uncertainty is modelled.

1.2 Methods of Structural Uncertainty Modelling

There are two approaches to modelling dynamic analysis of structures with uncertain properties: probability (statistical) and possibility approaches. Statistical approaches model the variability in the structure as random variables and then attempt to construct probabilistic descriptions of the response. The probabilistic approaches work well when the defining fundamental input distribution has adequate information. Possibilistic approaches are deterministic (i.e. no randomness, producing the same output for a given starting condition) by trying to find the worst possible case by examining the response when variables are bounded. Langley [2000] has reviewed the dynamic analysis with uncertain properties using probabilistic methods: including Monte Carlo simulation; the stochastic Finite Element method; and the First Order Reliability Method (FORM). And for possibilistic methods: Interval Analysis; Convex Modelling and Fuzzy Analysis are described. Analysing uncertainty at low frequencies involves using the probability methods, at mid- frequencies is using Statistical Energy Analysis (SEA) and Finite Element Analysis (FEA); and at high frequencies using Statistical Energy Analysis (SEA). SEA is a method to predict vibration behaviour and noise at high and mid-frequency. This method is based on power flow (vibrational energy flow) and can predict the mean value and standard deviation of the vibrational energy flow of the structure. But the disadvantage of SEA at low frequency is in neglecting many structural details.

An important part of modelling uncertainty is the task of combining different aspects involving estimation or calibration [Onatski, 2011]. Rabbiolo [2003]

stated that for design purposes, it is valuable to be able to quantity the limit of predictability in order to make predictions in the different frequency ranges using appropriate techniques. Traditionally, the limit of predictability, together with the corresponding definition of the frequency bands where statistical methods are appropriate, has been determined based on some statistics of a single implementation of a system. The following qualitative definitions of low, mid, and high frequency are proposed: Low frequency (where response spectra exhibit strong modal behaviour); Middle frequency (the response spectra exhibit high irregularities, indicating irregular modal density; boundary conditions, geometry and materials play an important role); and High frequency (The response spectra are “smooth”, indicating high modal density; boundary conditions, geometry, and material are not important for the average response properties).

Finite Element Analysis (FEA) or Finite Element Method is a way of obtaining a numerical solution to field problems. Mathematically, a problem can be expressed by a system of differential equations. The Finite Element Method puts a continuous structure into discrete elements, which are connected by nodes. There is much software available for FEA such as Nastran, and Ansys. The modelling software and post processing tools that are used in this research are Patran and Nastran. (Both are tools particularly for Monte Carlo simulation to enable validation to confirm how good a prediction is). On a real system, experimental mesurements are needed. To measure frequencies and mode shapes various measurement systems can be used. In this study, the VibroMap 1000 holographic laser system is used which is a tool that can observe a vibrating mode and then proceed to make quantitative measurements.

1.3 Uncertainty Propagation in Structural Dynamics

“Incorporating uncertainty in a deterministic analysis by having it’s input as uncertain and quantifying the consequent uncertainty in the outputs is commonly referred as uncertainty propagation” [Fonseca, 2005c]. The three most common uncertainty propagation methods are the Monte Carlo simulation method, the perturbation method, and the fuzzy method [Fonseca, 2005c]. Monte Carlo simulation gives approximate solutions via a statistical sampling

approach but it takes considerable time to reach convergence. The perturbation method usually proceeds by computing only the linear terms in a Taylor series approximation by perturbing each parameter and adding a small term into the system. For the fuzzy method, the normalised probability density function is taken as the function for the parameters, and vice-versa for the response. And analysis of a fuzzy system is to quantify indefinite and uncertain parameters.

1.4 Uncertainty Identification in Structural Dynamics

The inverse problem of estimating the distribution of parameters in a structure with parameter variability is known as uncertainty identification. This inverse problem attempts to measure the distribution of parameters from response measurement, i.e. to either explicitly obtain the distribution in the mass, damping, and stiffness matrices from measured frequency response information or to explicitly obtain the distribution of some particular source of uncertainty such as the distribution of an unknown mass or its location. “Uncertainty is quantified relative to measured quantities” (i.e., experimentally obtained modal frequencies, frequency response functions, displacements, and mode shapes [Haselman, 2001]).

1.5 A Review of Structural Uncertainty Modelling and Identification

There are obviously a huge number of publications in the literature that relate to the vibration analysis of simple (academic) and real structures. In reviewing the literature from a point of view of uncertainty identification, the focus has been placed on three areas: i) analytical uncertainty Identification tools, ii) deterministic computation tools (particularly for beam and plate structures) to enable fast Monte Carlo simulation, and iii) on experimental approaches to validate methods for identifying information about of structures with uncertainty.

Analytical Uncertainty Identification tools

Shiryayev and Page et al [2007] obtained mean values of uncertain parameters of a bolted-joint by applying the adjusted Iwan Beam (AIB) to model the response of a joined structure. Evidence theory by McGill and Ayyub [2008] has been used to obtain the estimation of model parameter distributions. Parametric

and non-parametric probabilistic approaches are used in complex systems in aerospace engineering, comprising a satellite coupled to its launcher [Capiez-Lernout et al, 2006]. Fraccone and Ruzzene et al [2008] developed a procedure for maximization and quantification of any remaining uncertainty related to an estimation technique. Uncertainty of bladed discs in gas-turbine engines has been tested experimentally and then used together with predictive model.

Fonseca, et al [2005b] presented an efficient technique to identify and quantify variability in the parameters from experimental data by maximising the likelihood of the measurement, using the well-established Monte-Carlo simulation or perturbation methods for the likelihood computation. The Monte-Carlo approach works well but is slow, whereas the perturbation approach has problems when the linear approximation to the response is less accurate. Fonseca [2005a] showed via an experimental method, the benefits of an uncertainty quantification method applied to a cantilever beam with uncertain point-mass position along the beam (this will be discussed in Chapter 3 also using other theoretical methods for obtaining the frequencies and mode shapes to identify uncertainties).

Dunne and Riefelyna [2009] applied a maximum likelihood estimation (MLE) approach of [Fonseca, 2005c] using the perturbation method for both beam and simply-supported-plate structures with an attached point-mass of unknown position. The method was adapted to use both frequency and mode shape information which was tested on simulated data (the present study extends this work to identification involving a clamped plate which is validated using both Monte Carlo simulation and experimental data). Because the analysis of beam and plate structures imposes certain computational requirements which are not easily met with tools such as the FEM, alternative deterministic computation tools for beam and plate structures are now reviewed.

Deterministic computation tools for beam and plate structures

Many researchers have focused on developing new techniques to enable very efficient vibration analysis of beam and plate structures. These can be especially useful for Monte Carlo simulation, in some cases totally avoiding

approximations and spatial limitations that arise in other methods (such as restriction of mass location variability to node points in the FEM). These methods can also form part of an uncertainty identification method however, they are generally computationally very demanding. Arenas [2003] summarised the Virtual Work principle that has been implemented for analysing the vibration of a clamped rectangular plate like the approach by Sung [1997]. The Virtual Work method gives good comparison between numerical and experimental results. The method of superposition has been used on rectangular clamped- and cantilever-plates by Gorman [1976] and also Gorman and Sharma [1976] to analyse the free vibration problem. This showed the accuracy of frequency and mode shape information obtained using this method. The Ritz method has been used to solve plate vibration problems by Young [1950], Leissa [1969, 1973] and Low [1997]. Leissa's book [1969] contained information about the vibration analysis of plates, not only of rectangular geometry but also circular plates with varying boundary conditions. The Ritz method is one of the possible methods for easily getting approximate solutions for plate frequencies and mode shapes [Nieves, 2004]. Low [1997] compared natural frequencies for both loaded fully clamped plates and clamped-simply-supported boundary conditions between a Rayleigh-Ritz method and shaker-driven experimental measurement. (The method used by Low will be discussed further in Chapter 4 for initial stage work on identifying the uncertainty properties of uncertain plate structures).

Chen et al [2004] presented an interval optimization method to solve the uncertain problems of the vibration systems with multi-degrees-of-freedom, where the structural characteristics are assumed to depend on specified parameter intervals. They combined an interval extension method with the first-order Taylor series expansions of system functions. Previous work by Chen and Wu [2004] had shown numerically that the method was effective. The interval optimization method to obtain the dynamic response of uncertain structures with natural frequency constraints is derived by combining the interval extension of the system function with the perturbation theory of dynamic response and eigenvalue analysis. Plunt [2003] showed a number of examples where statistical energy analysis (SEA) has been applied successfully in different product design phases even using small and simplified models. Energy

methods of prediction are a natural alternative for obtaining the dynamic response for the high frequency range. However SEA makes no attempt at explicitly identifying uncertainty, and at high frequency neither does it need to.

Experimental Approaches

Laser interferometer has been accurately used to detect the displacement or mode shapes of a vibrating cylinder. Low's previous work [1997] used a TV holographic system as a detector of the vibration and Ritz's method with unidirectional displacements for non-free boundary condition plates. The establishment of a method to estimate the error of experimental measurements permits the calculation of systematic uncertainties of the elastic constant and frequencies. In the Ritz's method, a solution for the displacements is an approximation of an appropriate set of base functions which satisfy the boundary conditions for the displacements, if these are predetermined.

Papadimitriou [2004] introduced the information entropy norm as the measure that best corresponds to the objective of structural testing, which is to minimize the uncertainty in the model parameter estimates. Specifically, optimal sensor configuration is selected as the one measure that minimizes the information entropy measure since it gives a direct measure of uncertainty. An important advantage of the information entropy measure is that it allows a comparison to be made between sensor configurations involving a different number of sensors in each configuration.

Hazell and Mitchell [1986] undertook experimental eigenvalue and mode shape analysis for flat clamped plates using holographic interferometry, and compared the results with theoretical predictions. First, he recorded holographically, more than 25 modes for a square plate, and 16 modes for a rectangular plate. And then, using the selected recorded mode shapes, compared the results with beam mode shapes and modified Bolotin mode shapes that are both very popularly assumed mode shapes in term of numerical techniques. These assumed mode shapes are shown to have good agreement with the experimental results.

Vijayakumar and Ramaiah [1978] also used a modified Bolotin method as an asymptotic solution for the Rayleigh-Ritz method to analyse the vibration of a clamped square plate. The initial data for the first few eigenvalues obtained by Bolotin, Rayleigh, and Rayleigh Ritz method. Later these mode shapes were used as acceptable functions in the Rayleigh-Ritz method. It showed that using these asymptotic solutions in the Rayleigh-Ritz method is much more appropriate than the use of the conventional beam-type mode shapes.

Wu [2007] used a novel Bessel function method to achieve the exact solution for frequencies and mode shapes of a rectangular plate with three boundary conditions: first a fully-simply-supported, second a fully-clamped plate, and third, two opposite edges simply-supported and the other two edges clamped. It is shown that the proposed method provides simple, direct and highly-accurate solutions for rectangular thin plates.

1.6 Objectives of the thesis

The literature available on the subject of uncertainty identification clearly shows that some progress has been made in developing new techniques which exploit dynamic response information which is largely unspecified. When these methods only use frequency information the scope is however limited. Other types of response information can therefore in principle be used, in particular, mode shapes which appears not to have been examined at all. Moreover there is no evidence of these methods being tested using mode shape information on real structures under experimental conditions or otherwise. In general, experimental testing of uncertain identification is difficult because this requires testing of an ensemble of controlled structures with appropriate known variability. This requirement severely restricts the scope of what can be done experimentally since most non-trivial structures have some degree of uncertainty. Taking these factors together the following objectives emerge as appropriate questions to ask. The objectives of the research undertaken in this thesis are stated as follows:

i) to extend an uncertainty identification method which makes use of free-vibration dynamic response information in particular, a method that

makes use of both natural frequency and free-vibration mode shape information suitable for lightly-damped structures random uncertainty. As part of this objective, an appropriate matrix will be constructed to allow the merit of using mode shape information over on frequency to be assessed quantitatively.

ii) to test the developed method on simulated free-vibration data corresponding to a representative structure

iii) to test the method experimentally on a real, lightly-structure damped structure (under forced-vibration conditions) to confirm the use of a free-vibration-based method.

1.7 Layout of the thesis

The thesis has 7 chapters; Chapter 1 (as seen) gives an introduction and background literature, Chapter 2 develops an efficient uncertainty estimation method, Chapter 3 gives an application of uncertainty estimation using theoretical frequencies and mode shapes to uncertain beam structures. Chapter 4 gives an application of uncertainty estimation using theoretical mode shapes to uncertain plate structures, Chapter 5 describes experimental facilities used in the project, and describes the procedures of mode shapes measurement for a clamped all-sides rectangular plate using holographic laser based VibroMap 1000. Chapter 6 shows attempts at experimental verification of the efficient uncertainty estimation method on plate structures, and Chapter 7 gives conclusions and recommendations for further work. The content of the chapters is now explained in terms of the scope of the work.

The Scope of the thesis

Chapter 1, as already shown presents an introduction and background of the research. Many researchers have already related their work within this area to other topics. But for the first time uncertainty identification and the problem of accurate mode shape computation on clamped-plate structures have been set side-by-side.

Chapter 2 deals with development of an efficient uncertainty estimation method. The most important existing method is fully explained and the prepared development discussed.

In Chapter 3, implementation proceeds so that the uncertainty estimation method is extended to uncertain beam structures by using frequency and mode shape information. Several methods to obtain frequency and mode shape data are also presented such as; the Receptance method, the Finite element method, Rayleigh's quotient and the Rayleigh-Ritz method.

Chapter 4 shows the effect of maximizing the likelihood estimation for plate structures using mode shape information to identify the uncertainty. The method to obtain mode shape information is by using the Rayleigh-Ritz method. To validate the accuracy of the Rayleigh-Ritz method, the Finite Element Method (FEM) has been used for certain plate structures. The Virtual Work principal also has been presented for the certain plate structures as a comparison tool with the two methods (i.e. the FEM and Rayleigh-Ritz).

Chapter 5 is all about the experimental facilities and procedures on how to obtain and collect mode shapes information for uncertain plate structures. Details on holographic laser based VibroMap 1000, how it works and the specifications. There is very little published on the practical use of the VibroMap system – hopefully this thesis bridges this gap.

In chapter 6 experimental verification of efficient uncertainty estimation method on plate structures is attempted. Comparisons are shown between the prediction methods, and the measured data from the VibroMap 1000, which is implemented to identify the uncertainty.

Chapter 7 contains the main conclusions of the research with the future work in this area identified.

CHAPTER 2

DEVELOPMENT OF AN EFFICIENT UNCERTAINTY IDENTIFICATION METHOD

The problem of uncertainty identification is how to determine the properties of an uncertain structure from response measurements. Here the response measurement could be static displacements, static strains, or some other static displacement information. However, it is well known that dynamic responses are more likely to contain a richer source of information. One particular requirement in general is to keep the amount of measured response information to a minimum. This is a practical requirement since the data would normally have to be obtained from an ensemble of built structures. Clearly, under experimental conditions this requires duplication of the experiment which would be extremely costly for all but the simplest of products. Even if the product existed in large batches, the experimental effort to measure responses from numerous products is not a simple task.

The purpose of this chapter is to adapt an existing uncertainty identification method to enable it to be used with vibration mode shape information. The literature review in Chapter 1 showed that there was very limited previous work on this topic. However, in studying the relevant literature it is apparent that existing methods can be further extended beyond the scope originally intended. In particular, this chapter adapts and extends the maximum likelihood uncertainty estimation method proposed by Fonseca et al [2005b]. As mentioned in Chapter 1, this approximate method has been successfully applied to low frequency uncertainty identification of beam structures with uncertainty introduced by randomly positioning point masses along the beam. The method was used to estimate the standard deviation of the position of a point mass from measured natural frequencies. But the method is in principle sufficiently general to be used for uncertainty estimation of any structure using any type of response, not just natural frequencies. Assuming the source of uncertainty is described by a multi-variate normal distribution, the only source of approximation is the necessary linearization of the response function. In

general, the greater the level of uncertainty the larger the approximation error is expected to be.

Shortly an overview of the uncertainty identification method proposed by Foncesa *et al* [2005b] will be presented. This is followed by the particular adaptation of the method for use with free vibration mode shapes of structures in general involving a non-obvious step, since a mode shape is a response surface which needs to be condensed from an infinite set, to a finite set of independent data. The adaptation is then specialised for use with beam and plate structures, in both cases rendered uncertain by positioning point masses with random locations (normally distributed). This latter adaptation provides the basic approaches needed for application to beam structure using various theoretical and Monte Carlo simulation based methods in Chapter 3, and for application, using simulated data, to plate structures in Chapter 4. Before discussion of the Foncesa *et al* uncertainty identification method it is appropriate to very briefly review in very general terms, the general uncertainty identification problem, the Monte Carlo simulation method, plus two methods that are used within the uncertainty identification method, namely the perturbation method, and the maximum likelihood estimation method.

The uncertainty identification problem revisited

As mentioned in Chapter 1, the (vector) response equation:

$$y = f(x) \tag{2.1}$$

describes the main problem with parametric uncertainty identification where the statistical properties of the vector x = $[x_1\ x_2\ \ldots\ x_n]^{\mathrm{T}}$ is a set of *n* uncertain parameters such as used to define material or geometric properties, dimensions, mass distribution and so on, that are to be obtained from a set of samples of *m* measured response variables y = $[y_1\ y_2\ \ldots\ y_m]^{\mathrm{T}}$, which could include measured natural frequency data, measured frequency response functions (FRFs), mode shapes, and so on. In general the function f in equation (2.1) will obviously be an m-dimensional vector function.

Monte Carlo Simulation

One method which is used to estimate the uncertain parameters in structural dynamics is the conventional uncertainty estimation based on Monte Carlo simulation. The conventional uncertainty analysis by the Root Sum Square (RSS) method is often difficult in complex systems and requires approximation at each stage of processing placing serious doubts on the validity of the results [Basil, 2001]. Monte Carlo simulation was devised as an experimental deterministic method to solve difficult probabilistic problems since computers can easily simulate a large number of experimental trials that have random outcomes. When applied to uncertainty estimation, random numbers are used to randomly sample parameters in the uncertainty space instead of point calculations carried out by conventional methods. Such an analysis is closer to the underlying physics of actual measurement processes that are probabilistic in nature. There are many advanced variants on the Monte Carlo simulation method which allow the process to be optimised or accelerated such as using *Latin Hypercube* data sampling strategy or the method of *Importance Sampling* to select a distribution to reduce the number of simulation runs.

The Perturbation Method

Perturbation theory comprises a set of mathematical methods that are used to find an approximate solution to a problem which cannot be solved exactly, by starting from the exact solution of a related problem. Perturbation theory is applicable if the problem at hand can be formulated by adding a "small" term to the mathematical description of the exactly solvable problem. The general procedure of the perturbation method is to identify a small parameter, which when this parameter is set to zero, the problem become solvable. The perturbation method generates the solution in terms of a power series in the small parameter. The leading term of this power series is the solution of the problem.

Maximum Likelihood Estimation

Here, to help with an understanding of the uncertainty estimation method discussed shortly, the general approach to the Maximum likelihood estimation

(MLE) of parameters is discussed. The MLE method is a statistical method to estimate the parameters in a probability density function from a given set of data. It is based on the principle that was originally developed by Sir R. A. Fisher in 1912 [Myung, 2003]. In its simplest form, this can be best explained for a one-dimensional random variable *X* with a single unknown parameter θ associated with the PDF of *X.* The principle states that having selected a random sample of N observations $x_1, x_2, \dots, x_N$ of a continuous random variable x, where the probability density function $f(x)$ is a function of a single parameter θ, then the probability density function of observing these N independent values of x can be expressed as a multiplication of the PDFs for individual observations [Mendelhall, 2007] :

$$f(x_1, x_2, \dots, x_N|\theta) = f(x_1|\theta)f(x_2|\theta) \dots f(x_N|\theta) \tag{2.2}$$

Here f, the probability density function, becomes a function of θ for fixed values of the samples $x_1, x_2, \dots, x_N$. The likelihood function is then defined as:

$$L(\theta) = f(x_1, x_2, \dots, x_N|\theta) = f(x_1|\theta)f(x_2|\theta) \dots f(x_N|\theta) \tag{2.3}$$

where L is the likelihood of a sample. When the PDF is a function of a number of parameters, the likelihood function can be defined in terms of a vector of parameters $\theta_1, \theta_2, \dots, \theta_M$. Then the MLEs of $\theta_1, \theta_2, \dots, \theta_M$ are the values of $\theta_1, \theta_2, \dots, \theta_M$ that maximize L [Mendelhall, 2007]. In practice rather than use the likelihood function in its new state, the log of the likelihood function is computationally more attractive.

For a density function with one parameter θ, the MLE of the parameter is obtained by maximizing the log-likelihood function with respect to the parameter by calculating $\frac{dL}{d\theta} = 0$. This will give the equation required to estimate the value of θ based on the MLE method. For a PDF with *M* multiple unknown parameters, these can be estimated using the available data by solving the

systems of equations generated by setting the partial derivatives of the likelihood function to zero with respect to each of them [Haldar, 2000].

As an example, an application of MLE to parameter estimation for a one-dimensional normal random variable is initially helpful. The PDF for a one-dimensional normal random variable is:

$$f_x(x) = \frac{1}{\sigma_x\sqrt{2\pi}} exp^{\left[-\frac{1}{2}\left(\frac{x-\mu_x}{\sigma_x}\right)^2\right]} \tag{2.4}$$

where μ_x is the mean and σ_x is the standard deviation. This is a two parameter distribution where according to the definition $\theta_1=\mu_x$ and $\theta_1=\sigma_x$. The likelihood function for a given set of data with data samples x_i is:

$$L = \prod_{i=1}^{N} \frac{1}{\sqrt{2\pi}\sigma_x} e^{-\frac{1}{2}\left(\frac{x_i-\mu_x}{\sigma_x}\right)^2} \tag{2.5}$$

The log-likelihood function is:

$$\ln L = -N \ln\sqrt{2\pi} - N \ln \sigma_x - \frac{1}{2}\sum_{i=1}^{N}\left(\frac{x_i-\mu_x}{\sigma_x}\right)^2 \tag{2.6}$$

To obtain estimates for the two corresponding parameters, denoted as $\hat{\mu}_x$ and $S_x^2 = \hat{\sigma}_x$, the partial derivative of the logarithm of the likelihood function L with respect to the mean μ_x and the standard deviation σ_x is obtained and respectively set to zero. This gives the estimator for the mean as follows:

$$\frac{\partial \ln L}{\partial \mu_x} = \frac{1}{2}\sum_{i=0}^{N} 2\left(\frac{x_i-\hat{\mu}_x}{S_x^2}\right) = 0 \tag{2.7}$$

and

$$\sum_{i=1}^{N}(x_i - \hat{\mu}_x) = 0 \tag{2.8}$$

The equation to achieve the maximum likelihood estimate of the mean value parameter is thus:

$$\hat{\mu}_x = \frac{\sum_{i=1}^{N} x_i}{N} \tag{2.9}$$

And applying the same procedure for maximum likelihood estimated of the variance parameter S_x^2 is:

$$\frac{\partial \ln L}{\partial \sigma_x} = -\frac{N}{S_x} + \frac{1}{2}\sum_{i=1}^{N}(x_i - \hat{\mu}_x)^2 \frac{2}{S_x^3} = 0 \tag{2.10}$$

The ML estimate for the parameter S_x^2 thus becomes:

$$S_x^2 = \frac{\sum_{i=1}^{N}(x_i - \hat{\mu}_x)^2}{N} \tag{2.11}$$

2.1 Maximum Likelihood Estimation of Uncertain Structural Parameters

An important solution approach to obtain information about the statistical properties of uncertain parameters is to attempt to solve the inverse problem with parametric uncertainty. This involves attempting to invert equation (2.1):

$$x = f^{-1}(y) \tag{2.12}$$

Unfortunately, the inverse problem as given by equation (2.12) is usually either ill-conditioned, irreducible, or impossible. To overcome this problem an uncertainty propagation method is developed using equation (2.1). The first step is to linearise f(x) about some suitable point and then to make a simplifying assumption about the distribution of the unknown parameters. The maximum likelihood approach to estimating uncertain parameters proceeds by assuming the statistical distribution of random parameters is known such that $X \sim F_X(x; \theta_x)$, in which the vector of parameters θ_x is to be determined. In the

MLE approach, the log-likelihood function $l(\theta_x)$ is sought by considering the form:

$$l(\theta_x) = \log L(\theta_x) = \sum_{i=1}^{N} \log f\left(y'_{(i)}|\theta_x\right) \tag{2.13}$$

where $f\left(y'_{(i)}|\theta_x\right)$ is the conditional density function associated with y' (the set of N response measurements $[y'_1\ y'_2\ \ldots\ y'_N]$) given the parameter vector $\hat{\theta}_x$. Here $L(\theta_x)$ is the measurement likelihood function, where using the response function equation (2.1) the response measurement y_i are implicit functions of x_i. By finding the response vector that maximizes $l(\theta_x)$, this provides a basis for generating the most likely parameter estimates.

The simplest solution to solve for the properties of the uncertainty parameters is by making two assumptions [Fonseca, 2005c] that the response function (2.1) can be linearised, and ii) that the uncertain parameters follow a normal distribution. This second assumption requires that the unknown (input) variables follow a multi-variate normal distribution:

$$\mathrm{X} \sim \mathrm{N}_n\ (\mu_x, \Sigma_x) \tag{2.14}$$

where n is the number of variables, μ_x is the mean vector, and Σ_x is the covariance matrix. The linearization assumption involves taking the first term in a Taylor series expansion of equation (2.1). In fact this linearization step effectively becomes the perturbation method approximation of uncertainty propagation associated with equation (2.1) [Foncesa, 2005c] derived from a Taylor series expansion of f(x) as follows:

$$y = \mathrm{f}(\mathrm{x}^0) + \sum_{i=1}^{n} \frac{\partial \mathrm{f}}{\partial x_i}(\mathrm{x}^0)(x_i - x_i^0) + \frac{1}{2}\sum_{i=1}^{n}\sum_{j=1}^{n} \frac{\partial^2 \mathrm{f}}{\partial x_i \partial x_j}(\mathrm{x}^0)(x_i - x_i^0)\left(x_j - x_j^0\right) + \cdots \tag{2.15}$$

where $x^0 = [x_0^0 x_1^0 \dots x_n^0]^T$ is assumed to be in the vicinity of the mean μ_x. This is assumed to give an accurate approximation to the response surface. Now by taking the first-order term only, equation (2.15) reduces to [Fonseca, 2005c]:

$$y = f^0 + J^0(x - x^0) \tag{2.16}$$

where f^0 and J^0 are the function and it's Jacobian, evaluated at the point x^0 (where in general the Jacobian is a matrix obtained by differentiating a vector function f(x) of vector x with respect to each component of x where $J = \left[\frac{\partial f}{\partial x_1} \quad \frac{\partial f}{\partial x_2} \quad \frac{\partial f}{\partial x_3} \dots \quad \frac{\partial f}{\partial x_n}\right]$).

Linearization about an assumed point x^0 (near to the mean) thus allows the response vector y to be correspondingly normal since a linear transformation of a Gaussian (normal) random variable remains normal.

Approximation of the probability distribution function of y from equations (2.14) and (2.16) is therefore:

$$Y \sim N_m(\mu_y, \Sigma_y) \tag{2.17}$$

and it's probability function is:

$$\hat{f}(y|\mu_x, \Sigma_x) = (2\pi)^{-m/2}\left|\Sigma_y\right|^{-1/2} e^{-(y-\mu_y)^T \Sigma_y^{-1}(y-\mu_y)/2} \tag{2.18}$$

The perturbation solution and the normal assumption therefore becomes a means of constructing the approximate log-likelihood function [Fonseca, 2005c]:

$$l(\mu_x, \Sigma_x) = -\frac{1}{2}\left[N\, m \log 2\pi + N \log\left|\Sigma_y\right| + \sum_{i=1}^{N}\left(y'_{(i)} - \mu_y\right)^T \Sigma_y^{-1}\left(y'_{(i)} - \mu_y\right)\right] \tag{2.19}$$

where N is number of samples, m is the number of response variables and y' is a vector of responses. The response mean (vector) and the covariance matrix are given approximately as:

$$\mu_y = f^0 + J^0(\mu_x - x^0) \tag{2.20}$$

and

$$\Sigma_y = J^0 \Sigma_x J^{0T} \tag{2.21}$$

and where $J=\left[\frac{\partial f}{\partial x_1} \quad \frac{\partial f}{\partial x_2} \quad \frac{\partial f}{\partial x_3} \ldots \frac{\partial f}{\partial x_n}\right]$ is the Jacobian matrix, evaluated at the expansion point x^0. Frequency information and mode shapes for example can be used as the response variable y. In [Fonseca, 2005c], in the maximum likelihood estimation of the uncertain parameters, only frequency information was used as the response for a beam structure. In Chapter 3, to calculate the likelihood function, some of the methods again use frequency information as response data, but one method also uses mode shape information as a response data.

Because uncertainty identification is potentially very important in several different application areas where information is needed about the distribution of unknown parameters in a structural dynamic model (which are assumed to be random) a general overview of the method is justified. This needs to summarise it's detailed implementation and it's general limitations which is particularly important for example where the method might be considered for example in wide range of applications perhaps for quality control manufacturing (such as in the production of vehicle bodies, aircraft, and small (multiple) ship structures. It is therefore appropriate at this stage to summarise in general terms the steps involved in the uncertainty identification method of Fonseca [2005c]. This is written in a way that could apply to application of the method to any structure, whether the response data is generated using experimental data or through Monte Carlo simulation. But since the numerical computation of the Jacobian is relatively complicated, a separate section is included.

Summarised steps in the adopted uncertainty identification method

The implementation of the uncertainty identification method (which itself uses the perturbation method) therefore always involves the following six steps:

1/ The first thing is to establish the uncertain vector of n parameters $\underline{x}$ that are assumed to follow a normal distribution with mean vector μ_x and covariance matrix Σ_x.

2/ Construct an acceptable dynamic model for the structural behaviour under consideration in order to construct a model for the response y=f(x) i.e. that is in principle capable of generating the response data (that would be measured if using experimental data or simulated if using Monte Carlo simulation).

3/ Obtain a set of N response measurements$[y_1^{'}\ y_2^{'}\ \ldots\ y_N^{'}]$) from experimental or simulated data for each of the m response variables.

4/ Calculate the function f and its Jacobian J at μ_x value and after the value of f and J are obtained, then calculate the response mean μ_y and the covariance matrix Σ_y.

5/ Solve the approximate log-likelihood function $l(\mu_x, \Sigma_x)$ with the variables and parameters previously obtained.

6/ Minimise the log-likelihood function to obtain the statistical properties of the unknown parameters.

Computation of the Jacobian

In step 4/ computation of the Jacobian is needed. There are two ways to compute the Jacobian: analytically and numerically. Only for very simple cases, is it possible (as demonstrated in Chapter 3) to obtain the Jacobian analytically. The numerical computation, which involves differentiation by finite differences, is unfortunately relatively complicated for multi-dimensional uncertain parameter cases – this will be explained in more detail shortly. In the analytical way, the Jacobian, that is imbedded in equation (2.21), is obtained by use of classical calculus to calculate the first derivative of the response function with respect to the uncertain parameters (this step is in fact can only be applied in closed form to a 1D case in Chapter 3 where the Jacobian for a cantilever beam with an

attached point mass is calculated analytically because the frequency equation can be obtained in closed form).

Obtaining the Jacobian numerically for scalar function f of a single uncertain variable is an example of 1D problem. This is achieved using simple finite differences for a scalar function of one variable. Finite differences for functions of 2 or more variables involves construction of partial differential approximations by finite differences generated by multi-dimensional Taylor series approximations involving function evaluation at selected grid points.

One-dimensional Jacobian evaluation via Finite Differences

First, consider an undamped beam vibration problem where the only variable is the position of an unknown point mass attached to the beam. In this case for simplicity consider the beam undamped natural frequency as the response function y=f(x) where x is the uncertain position of the point mass and y here is a natural frequency. This could be the natural frequency for the first mode, or any other mode. Numerical computation of the Jacobian involves numerical differentiation of the natural frequency function y=f(x) with respect to the position of the point mass. Generation of the function f(x) for real structures usually involves the use of a numerical approximation to obtain natural frequencies (and mode shapes). Therefore since f(x) is rarely available in closed form, the position of the mass is conveniently discretised and represented at a series of grid points. Figure 2.1 shows is an illustrative example of equi-spaced discrete point for this 1D problem.

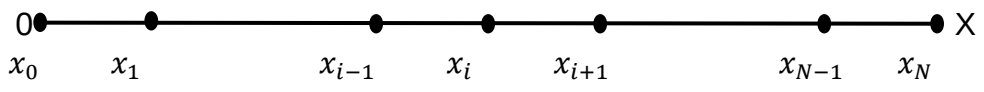

Figure 2.1 A Beam with length X and grid point x_i, where $i = 0, 1, \ldots, N$.

The equispaced discrete mass position point, between 0 and X is defined as:

$$x_i = i\,\Delta x \tag{2.22}$$

where the equi-spaced mesh size is defined as:

$$\Delta x = \frac{\mathrm{X}}{N} \tag{2.23}$$

The function f at the ith point f_i, can be evaluated as $\mathrm{f}(x_i)$ (in general approximately). The derivative at an arbitrary point x_i is in general needed. This can approximated using finite differences according to a number of different schemes, for example the first-derivative using a (forward) finite difference is:

$$\frac{d\mathrm{f}}{dx}(\overline{x}) = \frac{\mathrm{f}(\overline{x} + \Delta x) - \mathrm{f}(\overline{x})}{\Delta x} \tag{2.24}$$

or via a backward difference:

$$\frac{d\mathrm{f}}{dx}(\overline{x}) = \frac{\mathrm{f}(\overline{x}) - \mathrm{f}(\overline{x} - \Delta x)}{\Delta x} \tag{2.25}$$

or a central difference:

$$\frac{d\mathrm{f}}{dx}(\overline{x}) = \frac{\mathrm{f}(\overline{x} + \Delta x) - \mathrm{f}(\overline{x} - \Delta x)}{\Delta x} \tag{2.26}$$

In general, the difference Δx used in any of equations (2.24) – (2.26) need not be chosen to be the same as mesh size equation (2.23). But since function evaluations y=f(x) are needed for the finite difference it can be convenient to use the same difference Δx. In practice, with numerical differentiation if the finite difference is Δx is chosen too large the truncation error will be high. But if Δx is too small, any errors in the function f(x) approximation, or through noise on measurements (if experimentally derived) will be seriously magnified. In practice the value of Δx must be found through experimentation, and then will only apply to the particular application.

Two-dimensional Jacobian evaluation via Finite Differences

For a plate with a point mass located at an uncertain point on the x and y axis for example, this is a 2D case. This now involves multi-dimensional finite differences. In matrix form, the Jacobian J^0 near mean value μ, can be written:

$$J^0 = \begin{bmatrix} J^0_{11} & J^0_{12} \\ J^0_{21} & J^0_{22} \end{bmatrix} \tag{2.27}$$

Figure 2.2 shows a conveniently chosen equispaced discrete mesh (x_i, y_j) at which to evaluate the chosen response function.

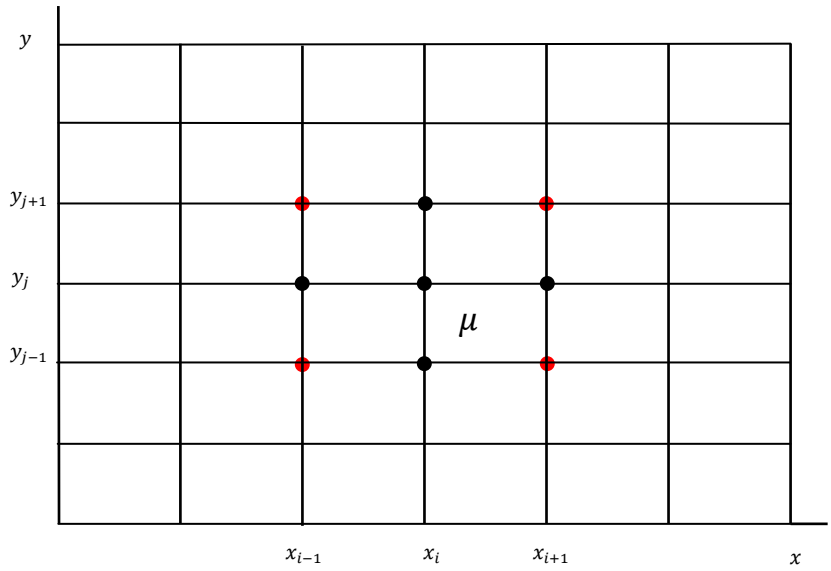

Figure 2.2 Geometric interpretation of small increments near mean value (μ) on x and y direction.

To evaluate the Jacobian at one of the mesh points partial derivatives at an arbitrary point (x_i, y_j) are in general needed. These can be approximated using finite differences, again according to a number of different schemes, with preference given to a central difference scheme as explained in the following steps to obtain the Jacobian:

1/ Create a small incremental (mesh) near the chosen point as shown on Figure (2.2). In this case the mesh is in the vicinity of mean value $\mu(x_i, y_j)$. The increment should be carefully chosen by using a 2-D trial and error method so that Jacobian will not have high errors or even singular values.

2/ Using finite differences replace the derivatives by difference approximations. The central difference scheme offers the easiest choice of approximation to obtain the following approximations to the partial derivatives:

$$J_{11}^{0} = \left(\frac{\partial f}{\partial x}\right)_i \approx \frac{f_{i+1} - f_{i-1}}{2\Delta x} \tag{2.28}$$

$$J_{12}^{0} = \left(\frac{\partial f}{\partial y}\right)_i \approx \frac{f_{i+1} - f_{i-1}}{2\Delta y} \tag{2.29}$$

$$J_{21}^{0} = \left(\frac{\partial f}{\partial x}\right)_j \approx \frac{f_{j+1} - f_{j-1}}{2\Delta x} \tag{2.30}$$

$$J_{22}^{0} = \left(\frac{\partial f}{\partial y}\right)_j \approx \frac{f_{j+1} - f_{j-1}}{2\Delta y} \tag{2.31}$$

When creating the finite differences Δx and Δy for grid point/mesh, the values should obviously not become too small (or zero) since this will lead to a singular Jacobian. But again neither should they be too big otherwise the truncation error will be unacceptable. Therefore a trial and error method is again used to find the right value for the increment size.

So far the discussion has been focused on the use of a response function y=f(x) involving natural frequencies. However, the emphasis is to exploit mode shape information. An assumption has been made that a method developed using free-vibration mode shapes can be used for structural uncertainty identification where the mode shape information is derived under forced-damped conditions. It is first necessary to discuss the particular extension of the method by [Fonseca et al, 2005b] to use with free vibration mode information. The question is exactly how will the mode shape information be summarised into a finite number of response variables since in general a surface requires an infinite number of variable to describe it.

2.2 MLE Uncertainty Identification using free vibration mode shapes

An objective of this study is to exploit more than just frequency information. There is however a need where possible to generate the Jacobian in equation (2.21) (which is generally quite difficult using for example approximate methods like the FEM). Therefore for the purposes of developing the method there is also a need to adopt some examples where a closed form Jacobian can be

constructed. The MLE method can, in principle, work with samples of any kind of response information. But given that for a continuous system, the vibration shape, in general, applies to a single mode, which is described by a surface rather than a single value (i.e. a number), an infinite amount of information is therefore contained within a mode shape. Moreover since there are an infinite number of free-vibration mode shapes for a linear system, each of the infinite number of modes has an infinite amount of information. However given that independent response measurements are required for the MLE, the arbitrary deflection point of a single mode is not completely independent even though the different modes are independent (because the eigenvectors are orthogonal). Indeed certain free-vibration mode shapes, such as for a simply supported square plate are described by a single function. In this situation, every displacement point for example, of a free-vibrating SSSS plate, is completely dependent on a single point. Clearly the use of parts of a mode shape would not guarantee independence. Some other measure of the mode shape is needed and how this should be normalised. Also the implications of the orthogonality vibration modes also need to be clarified. These points are now discussed in context.

Generalised displacement description of mode shapes

Consider a generalised displacement function in the form of a series expansion of basis function [Szilard, 1974] of the form:

$$w(x,y)=C_1f_1(x,y)+C_2f_2(x,y)+C_3f_3(x,y)+...+C_nf_n(x,y) \tag{2.32}$$

which reduces to:

$$w(x,y)=\sum_{k=0}^{n} C_i f_i\,(x,y) \tag{2.33}$$

where f_i (x,y), i = 1,2,3,…, are continuous base functions that satisfy the boundary conditions and assumption of the mode shapes for example for a plate surface. In general the base functions, which collectively from a basis, can be constructed as free vibration mode shapes of the nominal structure. The

coefficients C_1, C_2, C_3,…,C_n are the unknown constants (weights) that need to be determined from the minimum potential energy principle. If equation (2.33) can be adequately be truncated leaving only small error then this provides a means by which a structural mode shape can be summarised. The individual coefficients C_1, C_2, C_3,…,C_n in equation (2.33) form the vector response function y=f(x) in equation (2.1), where each component of y is a single coefficient C_i. The Jacobian components needed in equation (2.21) are the partial rates of change of each coefficient C_i with respect to the change in the corresponding uncertain parameter values.

Since the coefficients of the series in equation (2.33) that are extracted, behave as response variables, it is a requirement of the adopted uncertainty identification method that the response information should be independent. This is precisely the reason why the chosen response is not just a few displacement values in a mode shape (i.e. a few components in one of the eigenvectors). This is because in some cases, a single value of an eigenvector for example, would be able to represent the mode shape W(x,y). Therefore the implications of orthogonality of vibration modes on MLE uncertainty identification should be mentioned. Equation (2.33) provides the basis to create an independent description of a mode shape especially if the base functions themselves are orthogonal. It is generally important in vibration analysis that mode shapes are orthogonal to each other with respect to mass and stiffness. This is achieved if proportional damping is appropriate. For continuous systems the definition of orthogonality is expressed in terms of continuous functions f(x) and g(x) defined on an interval $a \leq x \leq b$, by their inner product:

$$(f, g) \equiv \int_b^a f(x)g(x)dx \tag{2.34}$$

If f(x) and g(x) are orthogonal then (f, g) = 0. No function is orthogonal to itself except $f(x) \equiv 0$ [Strauss, 1992]. For free response, orthogonality is used to simplify the calculation of the response coefficients when integer $n \neq m$ in the weight functions.

In the Rayleigh-Ritz method (discussed later in respect of plate vibrations, and in more detail in Chapter 3), the base functions are actually not required to be orthogonal. But choosing base functions which are orthogonal will eliminate the terms when m ≠ n and make the calculation much easier. For the simply supported plate case [Dunne and Riefelyna, 2009], the chosen base functions were orthogonal providing a closed form solution. Indeed the idea behind the use of Rayleigh-Ritz method is precisely to generate a series to represent the mode shape of the form equation (2.33). This can be used to compute approximate theoretical mode shape coefficients for use in Monte Carlo simulation. The same series can be used to fit experimentally measured data. But in order to make a comparison between the predicted and measured mode shapes, a normalisation process must be used. This will now be discussed.

Normalisation of Mode Shapes

There are two approaches that can be used to compare mode shapes: a graphical approach and a numerical approach [Ewins, 1984]. Before comparing predicted and measured mode shapes, a consistent normalisation procedure has to be adopted. Normalisation is essentially a scaling of a mode shape either by insisting that the generalised is unity or by insisting that the largest component is set to some value, such as unity [Bies and Hansen, 2009]. Mass normalisation therefore involves scaling each eigenvector to a unit value of generalised mass i.e:

$$\Psi_N{}^{\mathrm{T}}[M]\Psi_N = 1 \tag{2.35}$$

where Ψ_N is the mass-normalised mode shape function (eigenvector) for the *N*th mode. When a normalised mode shape is achieved by scaling the largest component to unity this is called ‘unity scaling’. Each displacement value in a particular mode shape is scaled so that maximum displacement is 1 by dividing each value in the mode shape (eigenvector) by the maximum value in the mode shape.

Limitations of Uncertainty Estimation via the Perturbation Method and Normal Assumption

The perturbation method requires that the response function should be chosen in such a way that the response is almost linear. If the number of uncertain parameters is high, or if a high-order expansion were to be used, then the calculation would become prohibitive since the perturbation method requires the use of a first-order expansion only so that the normal transformation assumption is retained. It is also important [Dunne and Riefelyna, 2009] that the number of response variables should not have exceed the number of the uncertain parameters. When this happens, the method would not be applicable because the Jacobian becomes singular, and the equation (2.19) gets into difficulty. To be precise the number of response variables m, cannot exceed the number n of uncertain variables. If this happens then the Jacobian is singular and the method fails. This requires that the number of response variables used at any one time is at most the same as the number of uncertain variables, definitely no more. The implications of this are for example when using the mode shape approximation equation (2.32) with only two uncertain parameters then only a pair of the coefficients from C_1, C_2, C_3,…,C_n can be used in the method at any one time. However where many more than two coefficients are available then it is possible to make several independent estimates of the statistics of the unknown parameters. For example if 10 coefficients in equation (2.32) is found to be an adequate approximation of a mode shape then in principle 5 pairs of these 10 coefficients can be used to generate 5 independent estimates of the statistics of the unknown parameters.

Constraints imposed on the use of Uncertainty Identification

Given the central limitation of the method thus described above, several related limitations arise which can be identified as criteria which prevent the use of estimated parameters using the adopted method. The first limitation is related to the use because of a singular Jacobian, rather a limitation on the use of estimated parameter statistics where the determinant of the Jacobian is small and near singular. A second limitation arises even when Jacobian criterion is not violated. This is the on the use of estimated parameters when the Hessian Matrix has a large determinant.

An alternative form of the Taylor series equation (2.15) truncated after the quadratic term can be written as:

$$y = \mathrm{f}(x + \Delta x) \approx \mathrm{f}(x) + \mathrm{J}(x)\Delta x + \frac{1}{2}\Delta x^{\mathrm{T}}\mathrm{H}(x)\Delta x \tag{2.36}$$

where J(x) is the Jacobian and H(x) is Hessian matrix (of second partial derivatives). Since the magnitude of the Hessian gives an indication of the magnitude of the nonlinearity of the response function its magnitude can be used to indicate whether the linearity assumption in the perturbation method is being violated. The criterion to check this is to ensure that the determinant of H(x) is less than some specified value, i.e.

$$|\mathrm{H}(x)| < \epsilon_{\mathrm{H}} \tag{2.37}$$

Adaptation of MLE uncertainty identification to beams and plates

Before finishing this chapter it is appropriate to briefly discuss the adaptation of uncertainty identification to beams and plates to prepare for the applications in Chapters 3 - 6. Note that Ewins [2001] defines a mode of vibration “as a way of vibrating, or a pattern of vibration, when applied to a system or structure that has several points with different amplitudes of deflection”. Various methods are available to solve for natural frequencies and mode shapes on simple structures such as beams and plates. As previously mentioned in Chapter 1, one of the methods for solving this problem is Rayleigh-Ritz method. Leissa [2005] presents a detailed historical basis of the Rayleigh-Ritz method. In solving the problem with Rayleigh method, first a mode shape (deflected function) is assumed which satisfies the geometric boundary conditions of the problem, and from this, calculations of the maximum value of the potential and kinetic energy function for the motion are made and equated. The key step is the choice of generalised displacement description of the mode shape. One of the proposals in this study is to test this idea is with mass variability. The options are possible by varying the mass itself randomly, by varying the positions of the mass but keeping the mass itself fixed, or possibly by varying the material properties of

the mass. Application of the Rayleigh-Ritz method on beam and plate structures will be respectively presented in Chapters 3 and 4.

CHAPTER 3

APPLICATION OF UNCERTAINTY IDENTIFICATION TO BEAM STRUCTURES USING FREQUENCIES AND MODE SHAPES

The work follows on from the development in Chapter 2 in which the methods of uncertainty identification were outlined and one particular method [Fonseca et al, 2005b] was extended. Particular emphasis was placed on the use of free vibration mode shape information in addition to the use of natural frequencies. The extension focused on the use of summarised (and hopefully independent) mode shape response measures (such as a generalised displacement expansion). Here the extended uncertainty identification method is applied to beam structures with mass uncertainty, in which the challenge is to deduce the statistical properties of the mass location from a number of simulated responses. The same method could then be applied to measured responses for a real beam although that is not attempted here.

First, to compare uncertainty identification using the Rayleigh-Ritz method of simulation (as discussed in Chapter 2) three alternative approaches are adopted for comparison. The Finite Element method and its use on uncertainty identification for beam with mass position variability is initially discussed (using frequency information only) in context including the practical details of the implementation. Then the focus switches to a second approach, the Receptance method which has the advantage of being able to generate natural frequencies in closed form, also allowing a closed form Jacobian needed for the uncertainty identification with mass uncertainty for a beam structure. The third comparative method is based on Rayleigh's quotient. The Rayleigh-Ritz method is then applied over the remainder of the chapter allowing a comparison to be drawn between using the other methods, and the Rayleigh-Ritz method, when using frequency information only applied to a beam with mass position variability.

A uniform beam is one of the simplest structures to study in structural dynamics. Bending vibration of beams plays an important role in vibration analysis of structures even in such examples as ships, vehicle bodies, and spacecraft.

The basic model for a beam problem is the flexural vibration of a beam with flexural stiffness $EI(x)$, and mass per unit length $\bar{m}(x)$, both of which vary arbitrarily with position. The transverse-displacement response $v(x,t)$is governed by the free-vibration equation of motion for the system [Szilard, 1974]:

$$EI\frac{\partial^4 v(x,t)}{\partial x^2} + \bar{m}\frac{\partial^2 v(x,t)}{\partial t^2} = 0 \tag{3.1}$$

The natural frequencies and mode shapes which can be obtained from equation (3.1), play an important role in vibration theory and engineering applications. Various approximate methods can be used to obtain the natural frequencies and mode shapes, and as mentioned, three methods will be implemented to compare with the Rayleigh-Ritz method in implementing the uncertainty identification tools discussed in Chapter 2.

3.1 Natural frequencies of a point-mass loaded beam via the Finite Element method and the Receptance method

Of the three approximate methods, the Finite Element method is extensively used in the design and analysis of engineering structures. Here it is used on the uncertain beam problem with mass variability. The focus is initially on using frequency information only. Indeed to start with, a comparison is shown between the Finite Element method and the Receptance method in calculating natural frequencies of a mass-loaded beam.

Finite Element Based Uncertainty Identification

In general Finite Element Analysis (FEA) is a method for the numerical solution of field problems. A geometric model becomes a mathematical model when its behaviour is described, or approximated, by selected differential equations and boundary conditions. A mathematical model is discretized by dividing it into a mesh of finite elements. Solving a practical problem by Finite Element analysis involves learning about the problem, preparing a mathematical model,

discretizing it, having the computer do the calculations, and checking the results.

The steps of finite element analysis involve i) preprocessing ii) numerical analysis and iii) postprocessing. In structural terminology, there are elements that are used in finite element analysis: e.g. a bar element (can resist only axial loads), a beam element (can resist axial, lateral, and twisting loads), and plate elements (can resist axial, lateral, and twisting loads). A plate element has 6 dof (degree of freedom) at each node.

The advantages of finite element modelling is that it is often easy to develop a models, which can be used to simulate, so there may not be a need to build a prototype. On the other hand, finite element models have some disadvantages, such as difficulties in making model assumptions, assigning the damping, and choosing boundary condition. In the context of uncertainty identification, the Finite Element method has a particular disadvantage for randomly positioning masses in that these usually need to be positioned on nodes, and therefore cannot be arbitarary positioned. The Finite Element method is however useful to provide a benchmark – this is explained from a point of view of modelling a beam with variable point mass location.

Cantilever beam analysis with a point mass using Patran and Nastran

To analyse the problem using the finite element method (Nastran), a model of the problem is first created.

The detailed steps using Patran (the solid are modeller) given as follows:

1. The element type is chosen.
2. The geometry of the beam model is created.
3. The element is generated and boundary conditions are imposed.

The beam was meshed into 100 elements (see figure 3.1) and the boundary conditions applied at node 1. The boundary conditions were fixed (as there are no translations and rotations) at the nodes.

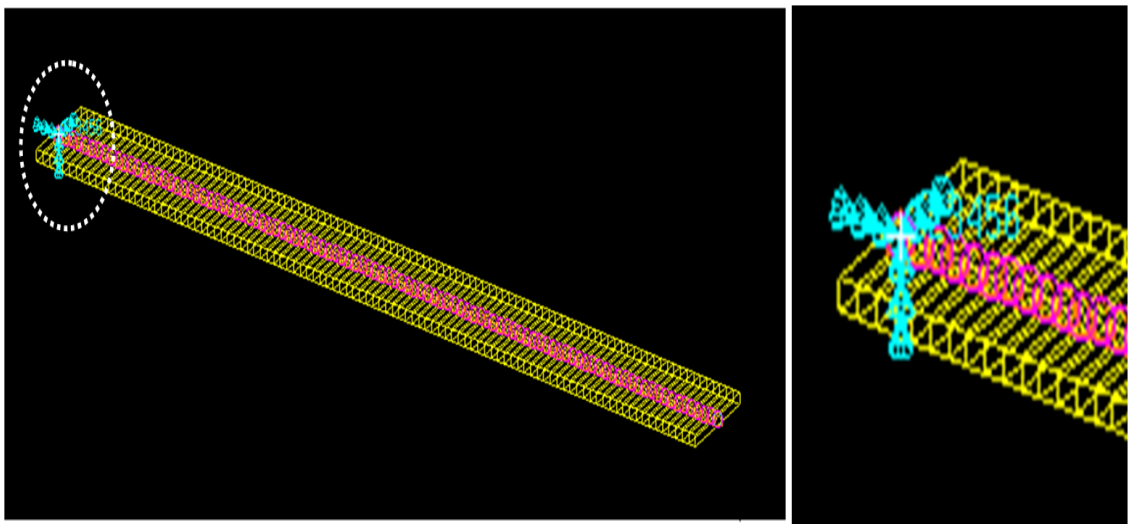

Figure 3.1 Cantilever beam with a point mass (Patran modelling).

The material properties selected for the rectangular beam are as follows:

	Unit	Value
L (beam length)	m	1
Young's modulus (steel)	N/m^2	210E+9
Poisson's ration (ν)		0.33
Density (ρ)	Kg/m^3	7800
A (cross sectional area)	m^2	0.001
I (moment of inertia)	m^4	$8.33*10^{-9}$
M (point mass)	kg	0.100

The point mass position is moved along the beam length at an element node and in only one position. These positions of the point mass are applied gradually along with a beam length. Nastran generated the natural and mode shapes, however only the mode shape which contained the deflection in the X-direction would be compared with those obtained using other methods. The natural frequencies (eigenvalues) of the cantilever beam with a point mass along the beam length, obtained via the FEM, are presented in figure 3.2

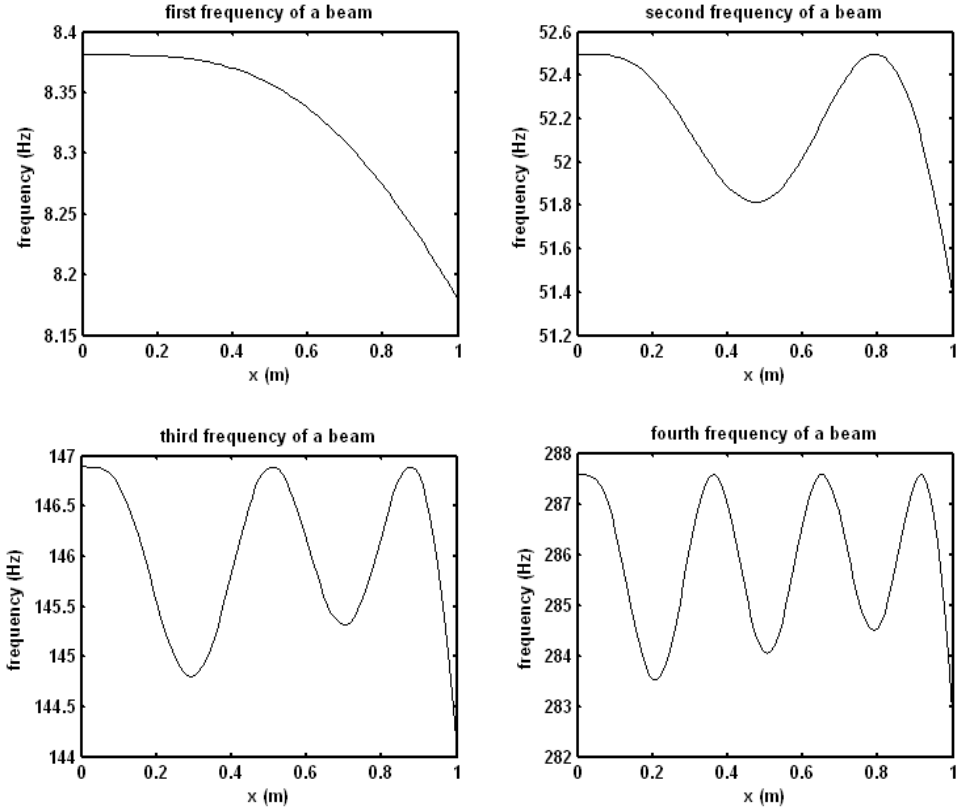

Figure 3.2 The first four frequencies of a cantilever beam with a point mass using the Finite Element method with Patran modelling and Nastran processing tools.

Note that these frequency predictions compare very well with the results in Fonseca et al [2005b] and also compare well with other methods.

Receptance method

The second approach adopted to generate natural frequencies for a beam with a point mass is the receptance method. This is an exact method that proves particularly useful.

A system with *n* degrees-of-freedom will have *n* simultaneous equations of motion. The equation of motion can be solved by trial solutions in which all the displacements vary harmonically. The receptance concept [Bishop and Johnson, 1960] is not restricted to translation displacements only, it can also be applied to rotations. A receptance gives information about the response of a system to a sinusoidal force loading, i.e. frequency response information. The

frequency at which a receptance becomes infinite is a natural frequency of the system. The Receptance method often saves much time and effort that is required for the determination of receptances by direct substitution into equations of motion.

Receptances of composite systems

A composite system can be written in terms of the receptance of it's sub-systems. These relations are shown in table 3 taken from [Bishop and Johnson, 1960] page 46. The method for finding the linear equation relations generated, are the result of application of principle of superposition.

The submodels used in the Receptance method [Gladwell and Bishop, 1960] are shown in figure 3.4. The combined system A in figure 3.4 is shown splitting into subsystems B and C in figure 3.5.

A Cantilever beam with a point mass using the Receptance method

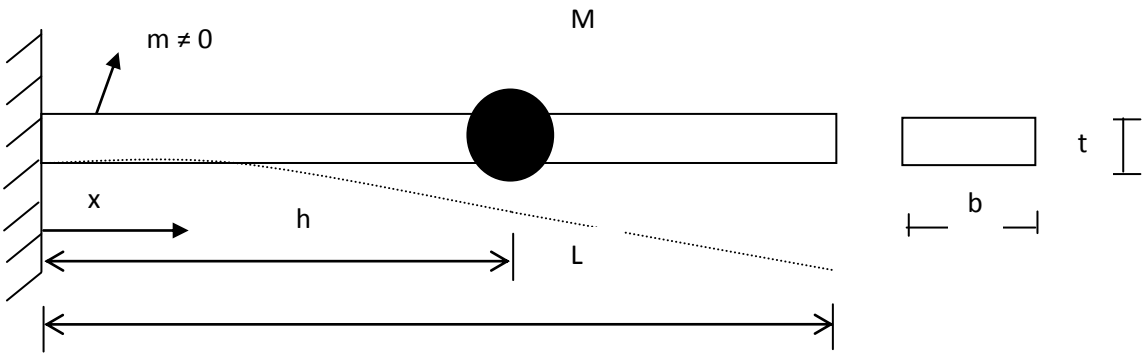

Figure 3.3 A cantilever beam with a point mass where the point mass is positioned at an uncertain location along the beam length (L).

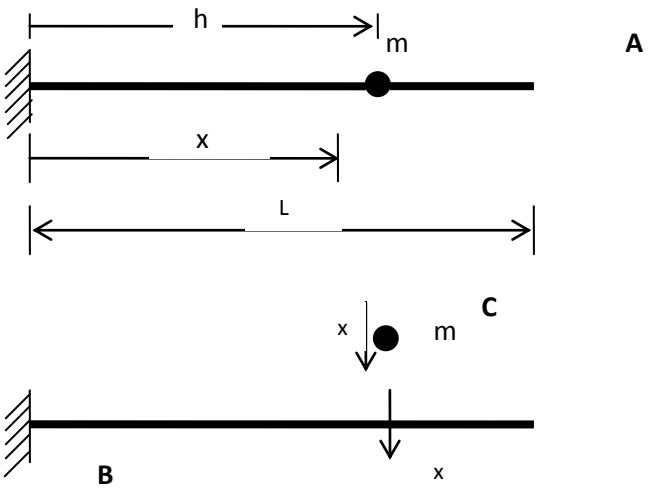

Figure 3.4 Schematic of receptance method applied for a cantilever beam with an attached point mass.

where h is the spatial distance from the reference where the force is applied, or the mass is attached on the beam, and x is the arbitrary spatial distance.

The Receptance method splits system A into subsystem B and C.

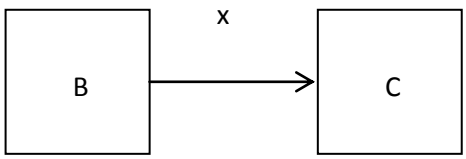

Figure 3.5 System A splitting into subsystem B and C as shown on table 3 taken from [Bishop and Johnson, 1960] page 46.

From table 3, [Bishop and Johnson,1960] page 46, the frequency equation for system A is:

$$\beta_{11} + \gamma_{11} = 0 \tag{3.2}$$

where for x = h

$$\alpha_{hh} = \beta_{11} \tag{3.3}$$

and

$$\gamma_{11} = -\frac{1}{m\omega^2} \tag{3.4}$$

and where m is the attached mass and ω^2 is a natural frequency.

From Table 2, taken from [Gladwell and Bishop, 1960] for a clamped-free beam, with ($0 \leq x \leq h$), the equation is

$$\alpha_{xh} = \frac{F_8F_8(\lambda x)F_7[\lambda(L-h)] + F_9F_{10}(\lambda x)F_7[\lambda(L-h)] + F_9F_8(\lambda x)F_9[\lambda(L-h)] - F_7F_{10}(\lambda x)F_9[\lambda(L-h)]}{4EI\lambda^3F_4} \tag{3.5}$$

The notation used in the expressions for the receptances of uniform beams from Table 1, [Gladwell and Bishop, 1960] are:

$$\left.\begin{aligned} F_4(\lambda x) &= \cos\lambda x \cosh\lambda x + 1 \\ F_7(\lambda x) &= \sin\lambda x + \sinh\lambda x \\ F_8(\lambda x) &= \sin\lambda x - \sinh\lambda x \\ F_9(\lambda x) &= \cos\lambda x + \cosh\lambda x \\ F_{10}(\lambda x) &= \cos\lambda x - \cosh\lambda x \end{aligned}\right\} \tag{3.6}$$

By substitution of equation (3.5) into equation (3.3), the frequency equation can be written in the form:

$$\frac{F_8F_8(\lambda x)F_7[\lambda(L-h)] + F_9F_{10}(\lambda x)F_7[\lambda(L-h)] + F_9F_8(\lambda x)F_9[\lambda(L-h)] - F_7F_{10}(\lambda x)F_9[\lambda(L-h)]}{4EI\lambda^3F_4} - \frac{1}{m\omega^2} = 0 \tag{3.7}$$

where the natural frequencies are:

$$\omega^2 = \frac{\lambda^4 EI}{A\rho} \tag{3.8}$$

finally substitution of equation (3.8) into equation (3.7), gives the frequency equation:

$$F_8(\lambda l)F_8(\lambda x)F_7[\lambda(L-h)] + F_9(\lambda l)F_{10}(\lambda x)F_7[\lambda(L-h)] + F_9(\lambda l)F_8(\lambda x)F_9[\lambda(L-h)] - F_7(\lambda l)F_{10}(\lambda x) F_9[\lambda(L-h)] - \frac{4A\rho l F_4}{\lambda l m} = 0 \tag{3.9}$$

where x = λ, and h = L– x. The natural frequencies can be obtained using the Receptance method by finding the roots of equation (3.9) and the results (frequencies) from equation (3.9) are shown in figure 3.6

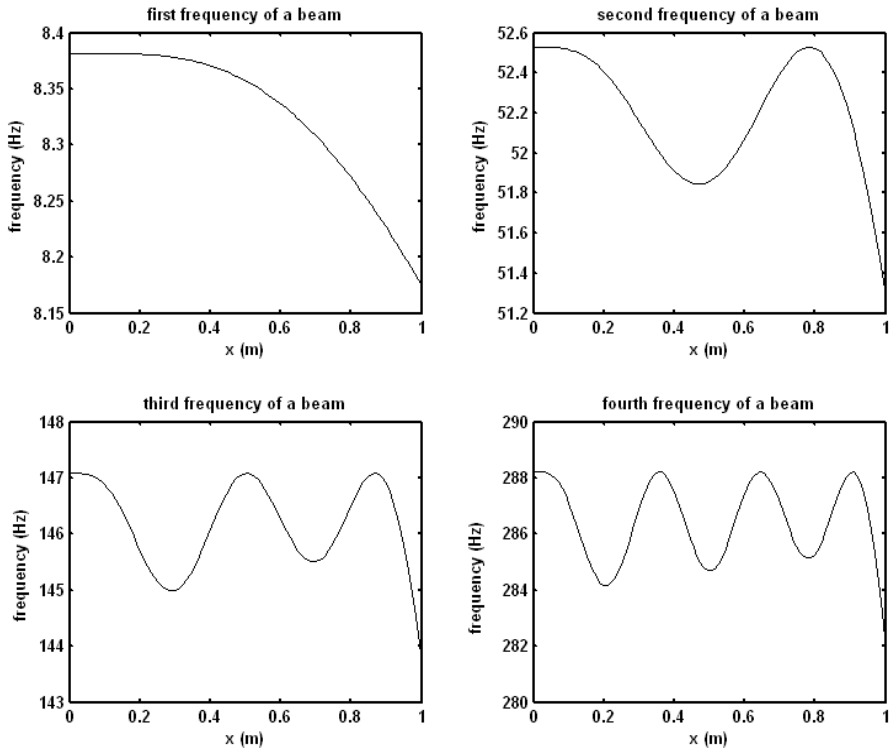

Figure 3.6 The first four frequencies of a cantilever beam with an attached mass using the Receptance method.

Figure 3.7 shows the first four natural frequencies of a cantilever beam with an attached mass as a function of point mass position obtain using both the Finite Element method and the Receptance method.

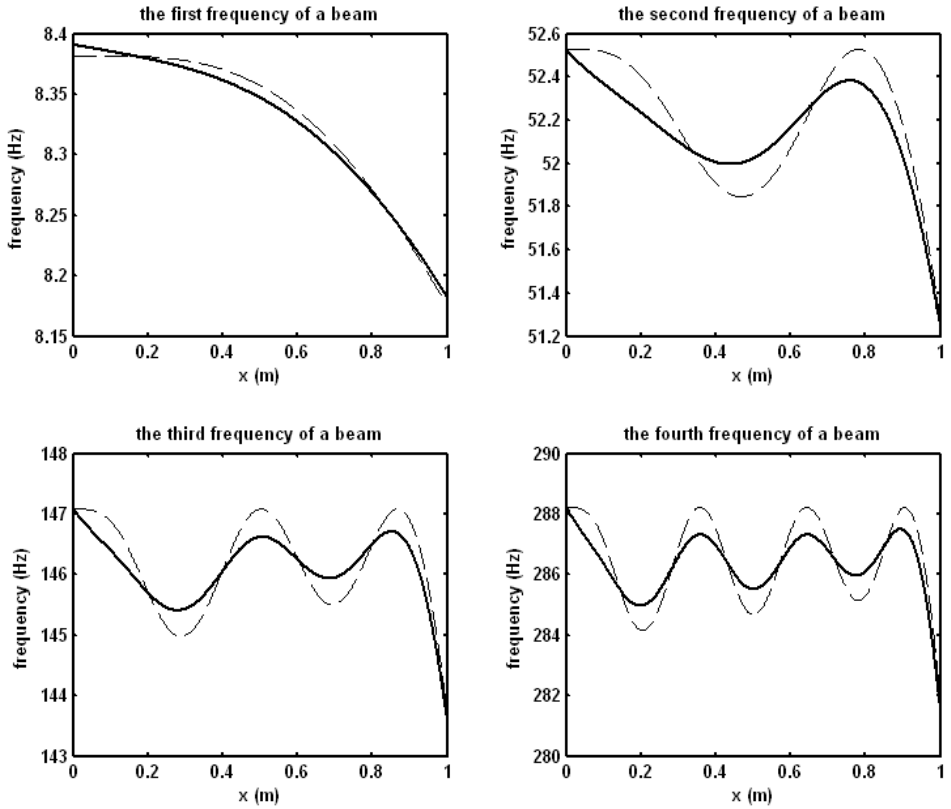

Figure 3.7 The first-four natural frequencies of a cantilever beam with an attached mass as a function of point-mass position: – the Finite Element method, and – the Receptance method.

A comparison between the calculation for the cantilever beam with a point mass using FEM and Receptances method is made by calculating the percentage error. The percentage is taken as the absolute value of the error (by subtracting the Receptance result from the FEM result) and dividing by the Receptance result.

The lowest percentage error for the first frequency is 0 % (for a point mass position of 0.93 m) and the largest value is 0.13 % (for a point mass position of 0.55 m). The percentage error shows that these are all below 1%. This means

that the prediction using the Receptance method (which is exact) and the Finite Element method are in agreement. But it is also clear that the FEM is in error at the higher frequencies – this can have an impact on uncertainty identification.

3.2 Maximum likelihood based uncertainty identification using frequencies obtained via the Finite Element method, the Receptance method, and the Rayleigh's quotient

The uncertainty identification method discussed in Chapter 2 is now applied using the frequency information generated using the Finite Element method and the Receptance method of section 3.1.

The problem case is the same cantilever beam with a point mass at an uncertain position along the beam length, shown in figure 3.1. The geometry and material properties of the beam are also the same as mentioned in section 3.1. The position of the point mass (x) follows a normal distribution with μ= 0.75 m and σ= 0.05 m.

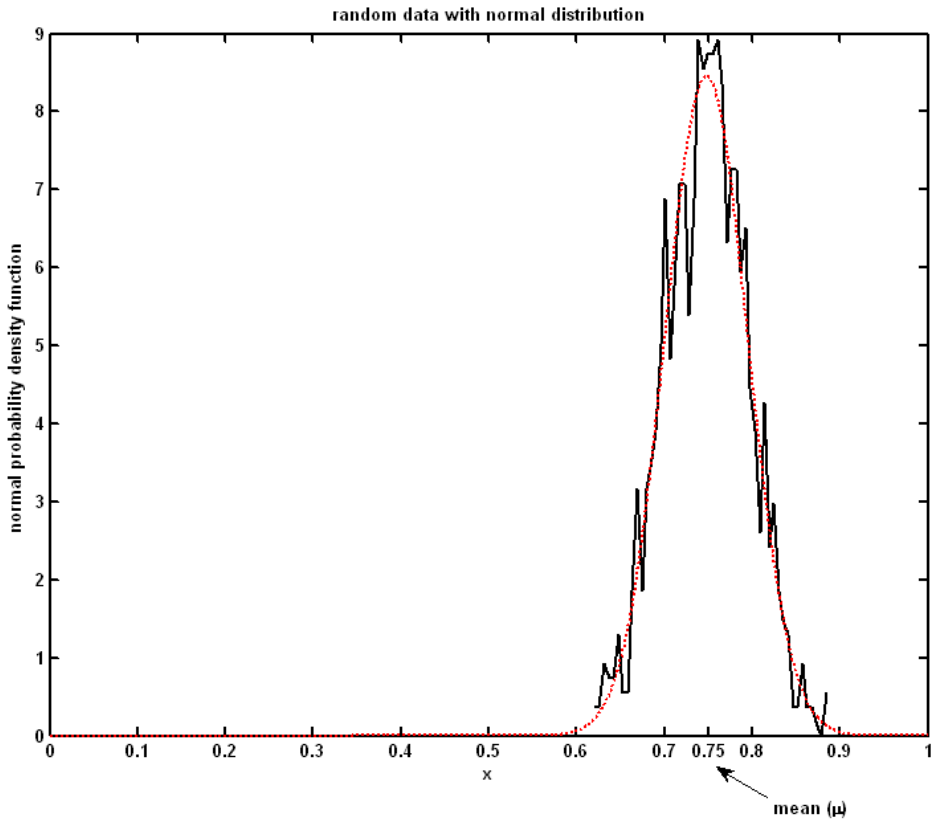

Figure 3.8 Position of a point mass along the beam length follows a normal distribution X ~ N.

Figure 3.8 shows an estimated histogram for the distribution of the mass position compared with the target normal distribution. Figure 3.9 shows the frequencies of the combined beam-mass system at the corresponding frequencies produced by the random positions.

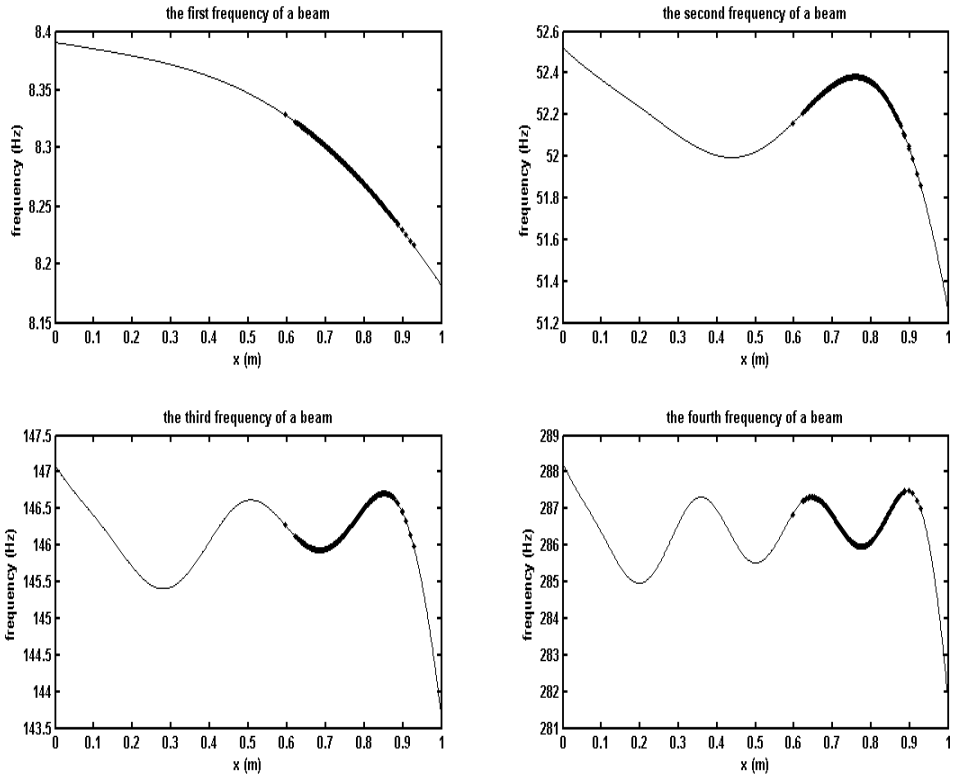

Figure 3.9 The first four frequencies for a beam with an attached mass at randomly varying position along the beam.

As previously mentioned in Chapter 2, the Maximum Likelihood Estimation method using the perturbation approach will need linearity on its response (in this case, the response is the natural frequency). For the first frequency of a cantilever beam with an attached mass shown on figure 3.9, the variation of the positions of the point mass along the beam are very small so that the natural frequency also vary almost linear. For higher frequencies (2^{nd}, 3^{rd} and 4^{th} frequency) the non-linearity has been introduced and increased as the frequencies become higher. When this condition happens then the method becomes prohibitive. Therefore the method only considers the use of the first natural frequencies.

The expansion point is chosen in the vicinity of the mean value because that gives the most likely place where the data is calculated, the best place to linearise the equation (on average).

The proposed approach is only applied one frequency at a time because this uncertainty identification is 1D problem that requires only used one response variable for one uncertain variable. As clearly stated in Chapter 2 page 34, the number of response variables should not exceed the number of uncertain variables. The method will fail if the opposite condition happens when inverting the covariance matrix in equation (2.19) because the Jacobian is singular.

Figure 3.10 and 3.11 show respective applications of the MLE based uncertainty identification via the FEM and the Receptance method.

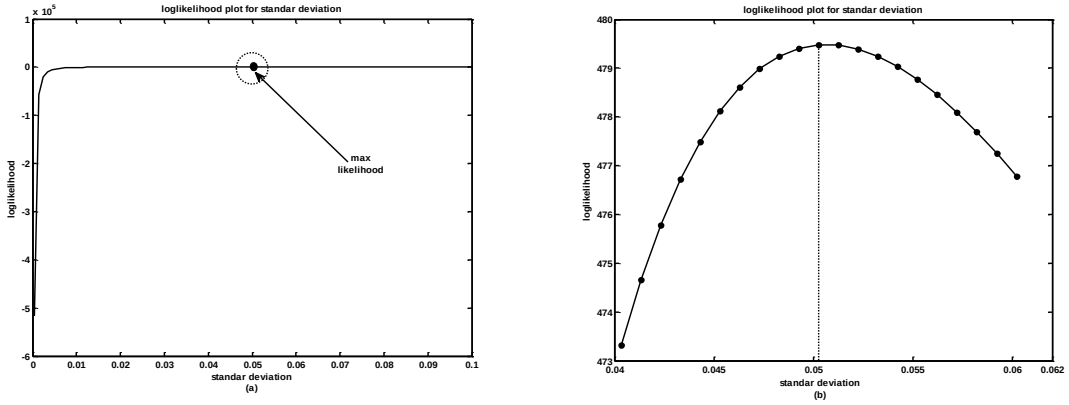

Figure 3.10. The Log-likelihood function for the standard deviation of a cantilever beam with an attached mass using natural frequency data obtained from finite element analysis using Patran and Nastran where (a) is the entire function and (b) is the zoomed version to indicate the maximum point in the figure 3.10 (a).

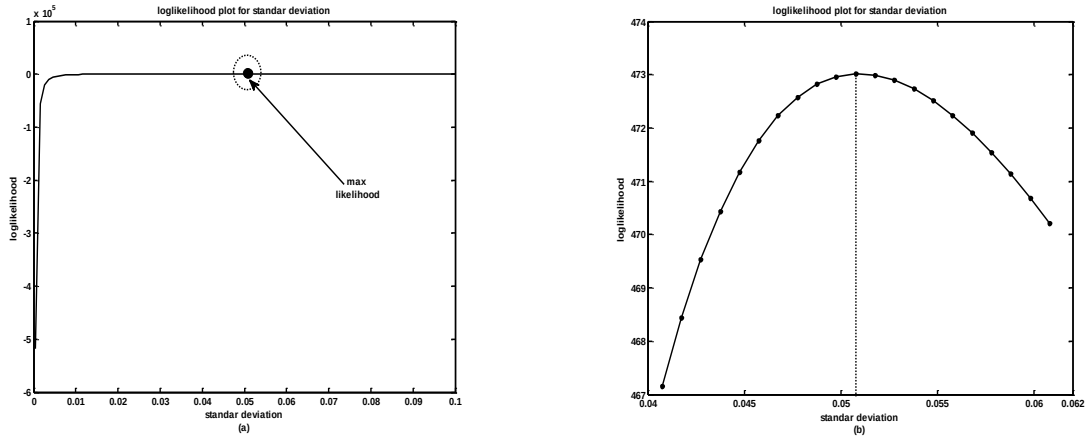

Figure 3.11 The Log-likelihood function for the standard deviation of a cantilever beam with an attached mass using natural frequency data obtained from the Receptance method where (a) is the entire function and (b) is the zoomed version to indicate the maximum point in the figure 3.11 (a).

The estimated standard deviation (at the maximum of the likelihood function shown in figure 3.10) using the Finite Element method via the Patran-Nastran software, is 0.0503. The percentage error between the target standard deviation (0.05) and the FEM is 0.59 %.

By contrast the standard deviation obtained from the Receptance method is 0.0508, and the percentage error between the target standard deviation (= 0.05) and from the Receptance method is 1.6 %.

Rayleigh's quotient

Rayleigh's quotient offers an alternative to the FEM and Receptance method for use in uncertainty identification on the beam problem. Here Rayleigh's quotient is applied directly to the beam problem. It's principal use is for approximate frequency analysis of a system having many degrees of freedom. Rayleigh's method is based on the assumed shape function of vibration. The basic concept of Rayleigh's method is based on the principle of conservation of energy and usually gives an accurate upper bound approximation. For the first natural frequency (note that Rayleigh's quotient is a special case of the Rayleigh-Ritz method applied shortly with only a one term base function. One big advantage

of the use of Rayleigh's quotient is that a closed form Jacobian needed in the application of the uncertainty identification method (Chapter 2) can be generated.

The Frequency equation obtained using the Rayleigh quotient is:

$$\omega^2 = \frac{3}{2\left[\frac{33}{140}\frac{mL}{2} + \frac{1}{8}\frac{M}{L^6}(9x^4L^2 - 6x^5L + x^6)\right]}\frac{EI}{L^3} \tag{3.10}$$

and the function for this cantilever beam with a point mass is:

$$F(x,\lambda) = \lambda^2 - \frac{1}{\left[\left(\frac{33}{140}\right)L + \frac{M(9x^4L^2 - 6x^5L + x^6)}{4mL^6}\right]^{\frac{1}{2}}} \tag{3.11}$$

therefore (from Chapter 2) the Jacobian for the function in this case is:

$$\frac{\partial y}{\partial x} = -\frac{0.00625M(36x^3L^2 - 30x^4L + 6x^5)}{\left[\left(\frac{33}{140}\right)L + \frac{1}{4}\frac{M(9x^4L^2 - 6x^5L + x^6)}{mL^6}\right]^{\frac{5}{4}} mL^6} \tag{3.12}$$

Rayleigh's quotient has a closed form solution to generate the eigenvalues of the system which will be compared later with a numerical approach.

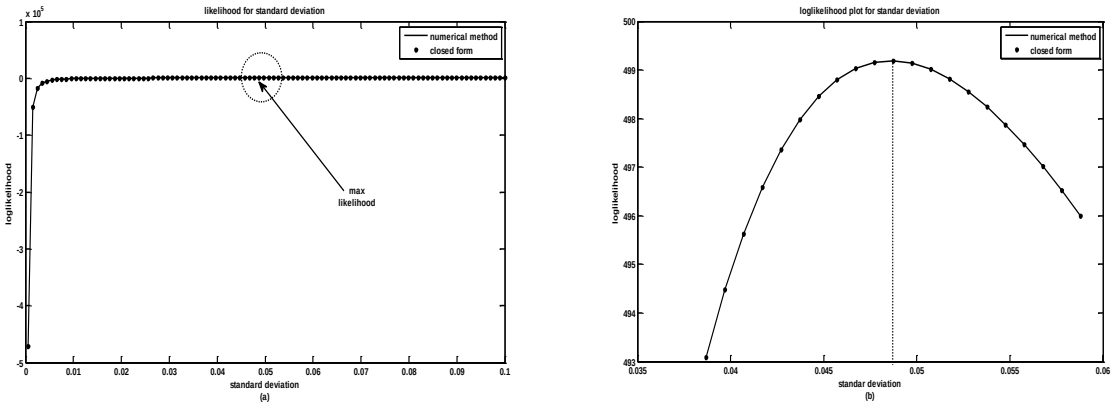

Figure 3.12 The Log-likelihood function for the standard deviation of mass position along the cantilever beam using Rayleigh's quotient where – is using a numerical method and • is using closed form solution. Figure 3.12 (a) is the entire function and (b) is the zoomed version to indicate the maximum point from the figure 3.12 (a).

Figure 3.12 shows the likelihood function needed in the application of the uncertainty identification method of Chapter 2.

The standard deviation at the maximum of the likelihood function using both the numerical approach and the close-form solution is 0.0487. The target standard deviation is 0.05 therefore the percentage error between the target standard deviation and standard deviation obtained from the numerical and close-form solution is 2.58%. this shows that the method works well on beam-type problems.

3.3 Rayleigh-Ritz based uncertainty identification using frequencies and mode shapes

The classical Rayleigh-Ritz method is commonly used for obtaining the first few natural frequencies and mode shapes of a linear multi-degree of freedom system.

The Rayleigh-Ritz method is now applied again to the cantilever beam with a point mass at an uncertain position that follows a normal distribution ($\mu = 0.75$, and $\sigma = 0.05$) to obtain fundamental frequencies and Rayleigh-Ritz coefficients.

There are two types of response when maximizing the likelihood function using

the perturbation method using: i) frequencies, and ii) mode shape information. The Rayleigh-Ritz coefficients were used in the Maximum Likelihood Estimation (MLE) approach with mode shape information. In this case, the method uses 4 terms in the base function expansion to get convergence in the Rayleigh-Ritz method. The Receptance method was used as a reference because it has an exact (close-form) solution.

The set of base functions for Rayleigh-Ritz method with 4 terms is as follows:

$$y(x) = C_n w_n(x) = C_1 w_1(x) + C_2 w_2(x) + C_3 w_3(x) + C_4 w_4(x) \tag{3.13}$$

where:

$$w_1(x) = \sin(1.875104x) - \sinh(1.875104x) + \left(\frac{\sin(1.875104L) + \sinh(1.875104L)}{\cos(1.875104L) + \cosh(1.875104L)}\right) + \cos(1.875104x) - \cosh(1.875104x) \tag{3.14}$$

$$w_2(x) = \sin(4.694091x) - \sinh(4.694091x) + \left(\frac{\sin(4.694091L) + \sinh(4.694091L)}{\cos(4.6940914L) + \cosh(4.694091L)}\right) + \cos(4.694091x) - \cosh(4.694091x) \tag{3.15}$$

$$w_3(x) = \sin(7.854757x) - \sinh(7.854757x) + \left(\frac{\sin(7.854757L) + \sinh(7.854757L)}{\cos(7.854757L) + \cosh(7.854757L)}\right) + \cos(7.854757x) - \cosh(7.854757x) \tag{3.16}$$

$$w_4(x) = \sin(10.995541x) - \sinh(10.995541x) + \left(\frac{\sin(10.995541L) + \sinh(10.995541L)}{\cos(10.995541L) + \cosh(10.995541L)}\right) + \cos(10.995541x) - \cosh(10.995541x) \tag{3.17}$$

The system natural frequencies (and Rayleigh-Ritz coefficients) can be generated by finding solutions using the Rayleigh-Ritz method with 4 terms, which are obtained by solving the eigenvalue and eigenvector problem.
Substitution of equation (3.14), (3.15), (3.16) and (3.17) into equation (3.13), gives equation (3.18):

$$
\begin{aligned}
y(x) = C_1 \Big[& \sin(1.875104x) \\
& - \sinh(1.875104x) + \left(\frac{\sin(1.875104L) + \sinh(1.875104L)}{\cos(1.875104L) + \cosh(1.875104L)} \right) \\
& + \cos(1.875104x) - \cosh(1.875104x) \Big] \\
& + C_2 \Big[\sin(4.694091x) - \sinh(4.694091x) \\
& + \left(\frac{\sin(4.694091L) + \sinh(4.694091L)}{\cos(4.6940914L) + \cosh(4.694091L)} \right) + \cos(4.694091x) \\
& - \cosh(4.694091x) \Big] \\
& + C_3 \Big[\sin(7.854757x) - \sinh(7.854757x) \\
& + \left(\frac{\sin(7.854757L) + \sinh(7.854757L)}{\cos(7.854757L) + \cosh(7.854757L)} \right) + \cos(7.854757x) \\
& - \cosh(7.854757x)] \Big] \\
& + C_4 \Big[\sin(10.995541x) - \sinh(10.995541x) \\
& + \left(\frac{\sin(10.995541L) + \sinh(10.995541L)}{\cos(10.995541L) + \cosh(10.995541L)} \right) + \cos(10.995541x) \\
& - \cosh(10.995541x) \Big]
\end{aligned}
\tag{3.18}
$$

Table 3.1 shows the magnitude of the first frequency for the cantilever beam with attached mass at x = L. As more terms are added, table 3.2 contains the

percentage errors between frequencies obtained by using the Receptance method, and by using the Rayleigh-Ritz method with 4 terms. Note the error becomes smaller when adding more terms into the function.

Receptance (Hz)	Rayleigh-Ritz 1 term (Hz)	Rayleigh-Ritz 2 terms (Hz)	Rayleigh-Ritz 3 terms (Hz)	Rayleigh-Ritz 4 terms (Hz)
8.1746096	8.1749100	8.1746559	8.1746241	8.1746159

Table 3.1 The magnitude of the 1st frequencies value of a cantilever beam with a point mass at x = L

Percentage Error (%)	Rayleigh-Ritz 1 term	Rayleigh-Ritz 2 terms	Rayleigh-Ritz 3 terms	Rayleigh-Ritz 4 terms
Receptance	0.0036	0.0005	0.0001	0.00008

Table 3.2 Percentage error between the Receptance method and the Rayleigh-Ritz method for the first frequencies of a cantilever beam with an attached mass.

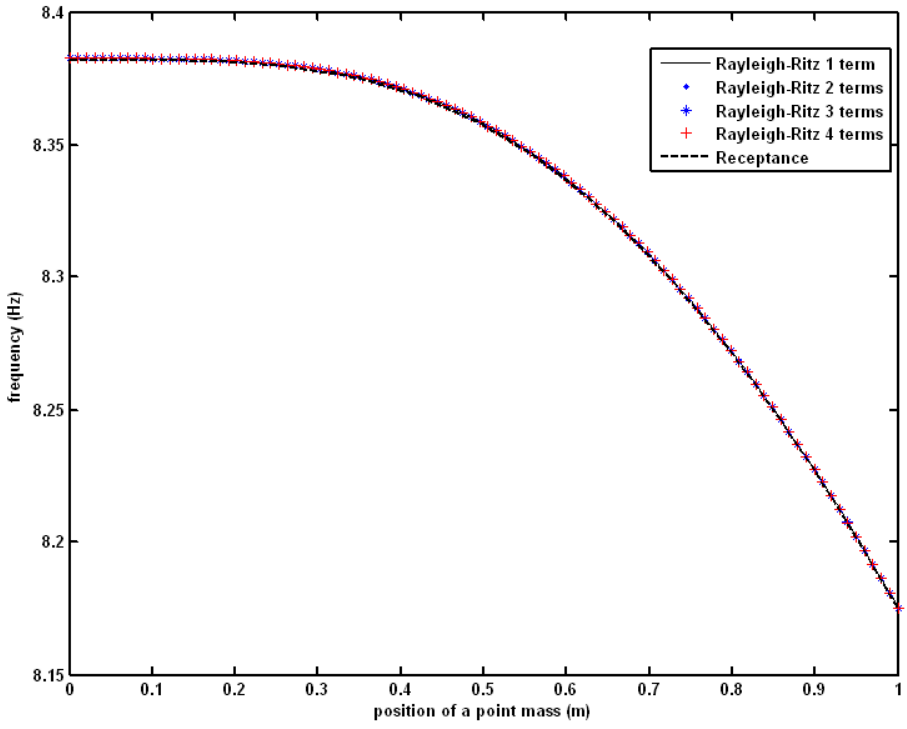

Figure 3.13 The first natural frequencies obtained for the mass-loaded cantilever beam comparing the Receptance method and the Rayleigh-Ritz method.

The response data for maximizing the likelihood function is a set of frequencies where the positions of an attached mass are random. Figure 3.14, 3.15, and 3.16 show the variations of the natural frequencies with attached mass at 10, 100, and 200 random positions that follow a normal distribution (μ = 0.75 m, and σ = 0.05 m).

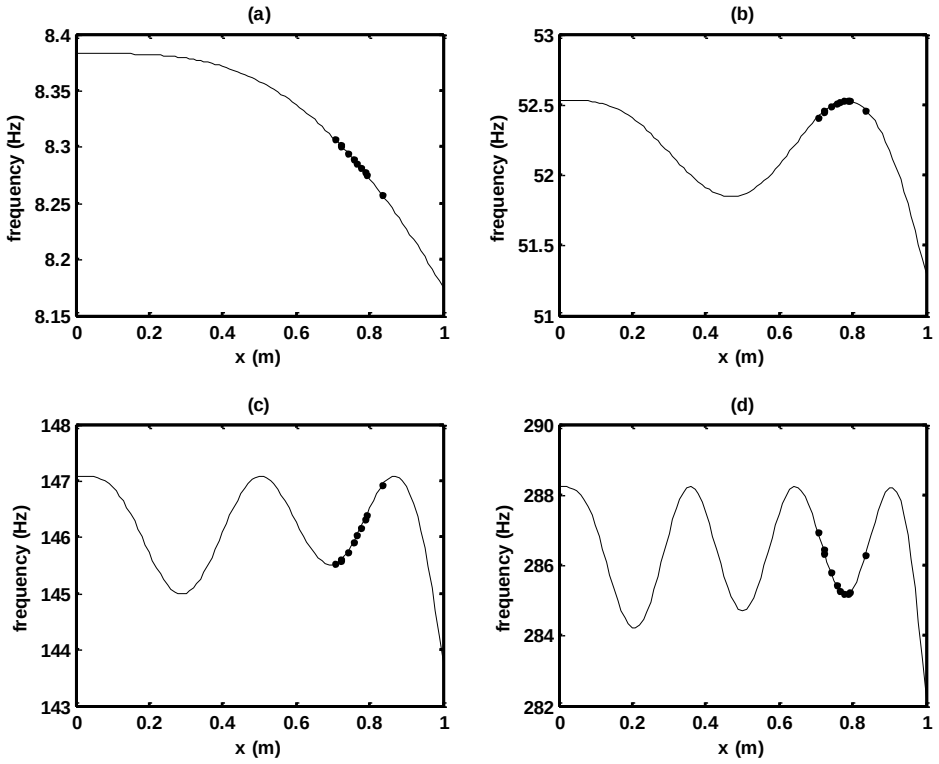

Figure 3.14 Frequencies calculated using the Rayleigh-Ritz method with 4 terms: (a) the first frequencies, (b) the second frequencies, (c) the third frequencies, and (d) the fourth frequencies where the symbol • corresponds to the 10 frequencies with the positions of a point mass being random.

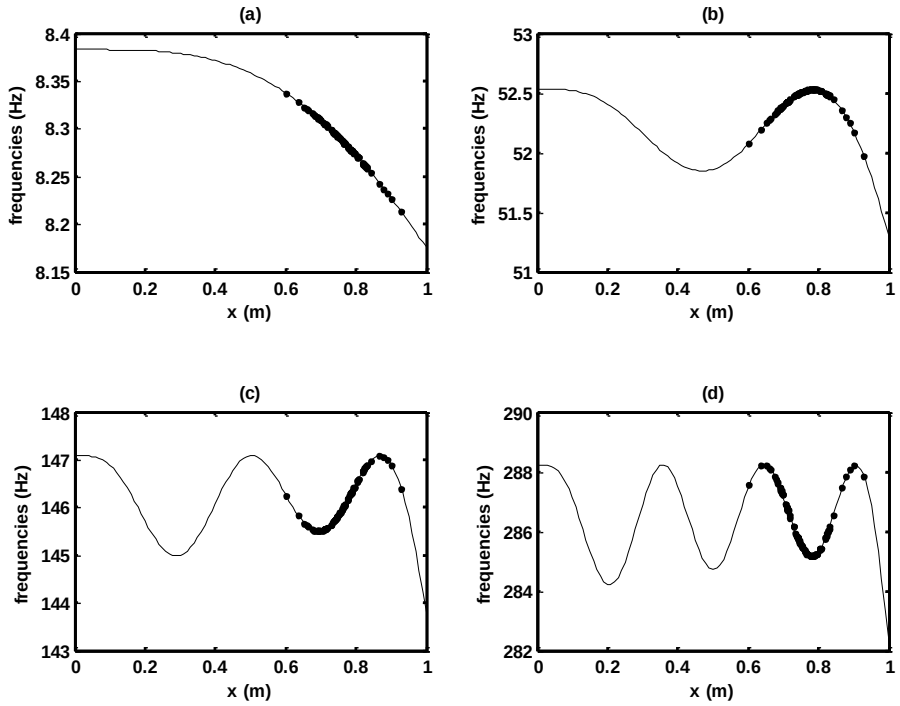

Figure 3.15 Frequencies calculated using the Rayleigh-Ritz method with 4 terms: (a) the first frequencies, (b) the second frequencies, (c) the third frequencies, and (d) the fourth frequencies where • are 100 frequencies with the positions of a point mass being random.

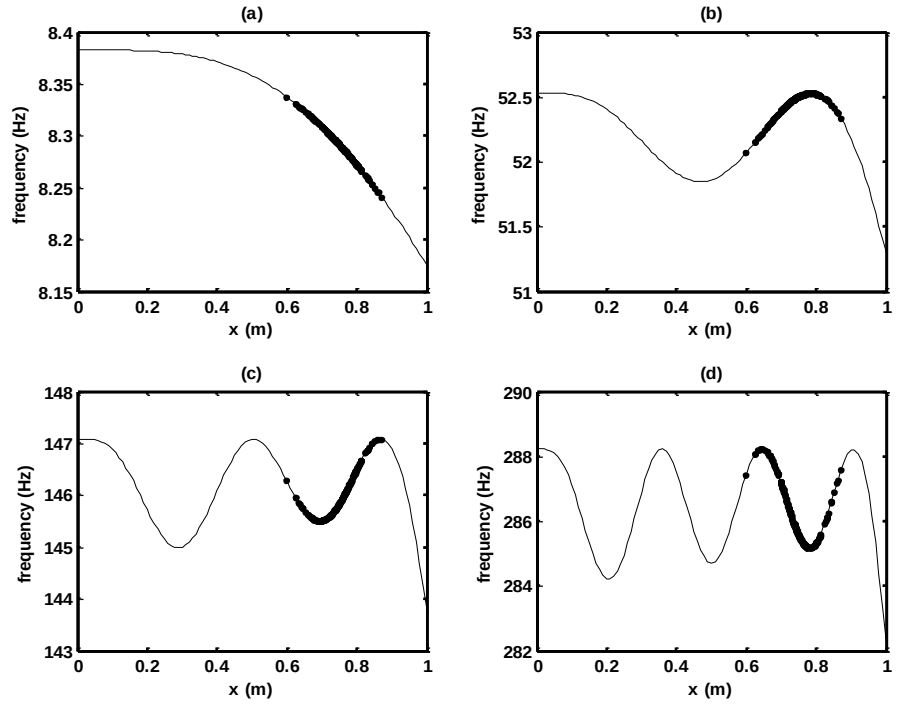

Figure 3.16. Frequencies calculated using the Rayleigh-Ritz method with 4 terms: (a) the first frequencies, (b) the second frequencies, (c) the third frequencies, and (d) the fourth frequencies where (•) are 200 frequencies with the positions of a point mass being random.

An example is now shown of maximizing the likelihood function using frequencies calculated using Rayleigh-Ritz method with 4 terms and fixed mean. And the results are shown in table 3.3.

	Using 10 random data	**Using 50 random data**	**Using 100 random data**	**Using 200 random data**	**Average**
	Estimated sigma x	**Estimated sigma x**	**Estimated sigma x**	**Estimated sigma x**	**Estimated sigma x**
First frequencies	0.0750	0.0550	0.0600	0.0500	0.0600
Second frequencies	0.0850	0.0750	0.0850	0.0700	0.0787
Third frequencies	0.0600	0.0410	0.0450	0.0400	0.0465
Fourth frequencies	0.0500	0.0550	0.0500	0.0500	0.0512

Table 3.3 Estimated standard deviation using the 1st frequencies, the 2nd frequencies, the 3rd frequencies, and the 4th frequencies calculated using the Rayleigh-Ritz method with 4 terms.

An example is now shown of maximizing the likelihood function using frequencies calculated using Rayleigh-Ritz method with 4 terms and fixed standard deviation. The results are shown in table 3.4.

	Using 10 random data	**Using 50 random data**	**Using 100 random data**	**Using 200 random data**	**Average**
	Mean (μ_x)	**Mean (μ_x)**	**Mean (μ_x)**	**Mean (μ_x)**	**Mean (μ_x)**
First frequencies	0.705	0.750	0.675	0.660	0.697
Second frequencies	0.115	1.000	0.115	0.105	0.333
Third frequencies	1.000	1.000	1.000	1.000	1.000
Fourth frequencies	0.745	1.000	0.740	0.745	0.807

Table 3.4 Mean calculated using the 1st frequencies, the 2nd frequencies, the 3rd frequencies, and the 4th frequencies calculated using the Rayleigh-Ritz method with 4 terms.

An example is now shown of maximizing the likelihood function using Rayleigh-Ritz 4 terms coefficients and fixed mean using the same set of random data. The results are shown in figure 3.15

The properties of mode shapes have been discussed on Chapter 2 page 29. Figures 3.16 until 3.19 showed that the generalised Rayleigh-Ritz coordinates for each mode vary with the position of a point mass along the beam.

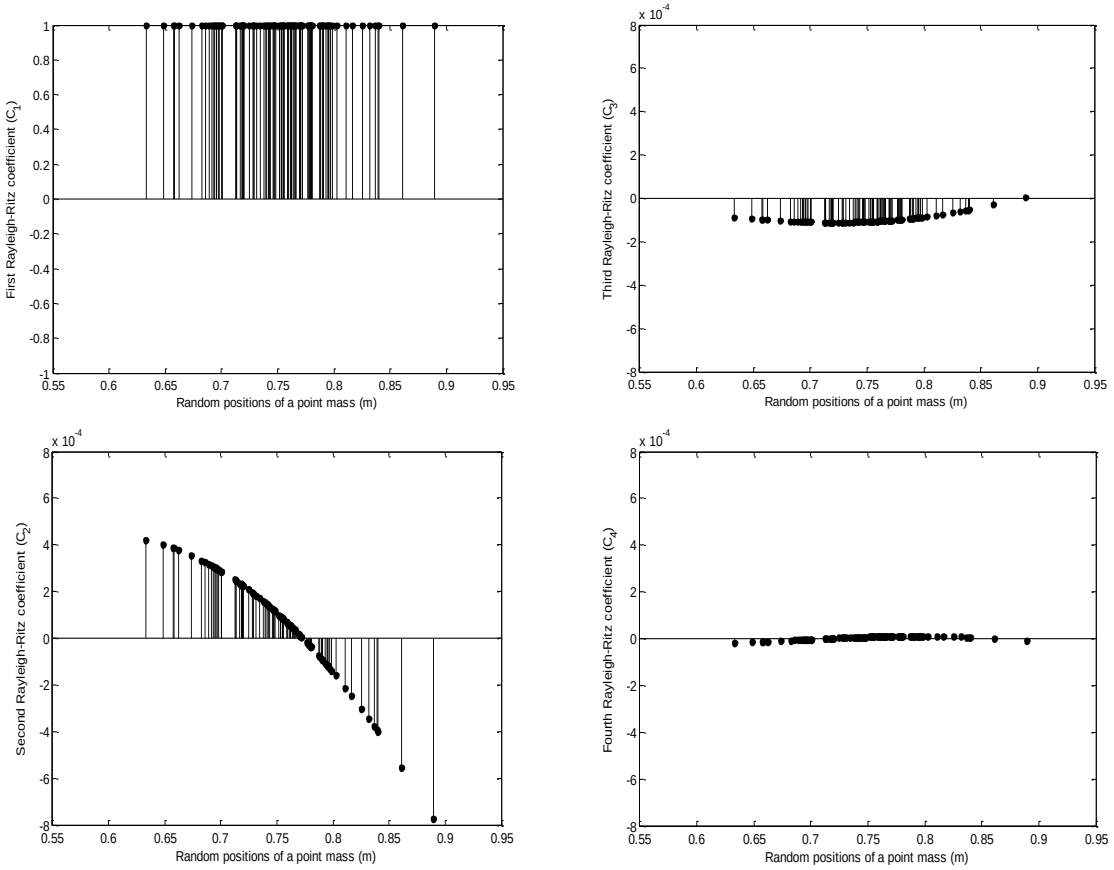

Figure 3.16 The generalised Rayleigh-Ritz coordinates vary with a 100 random positions of the point mass along beam for the first mode.

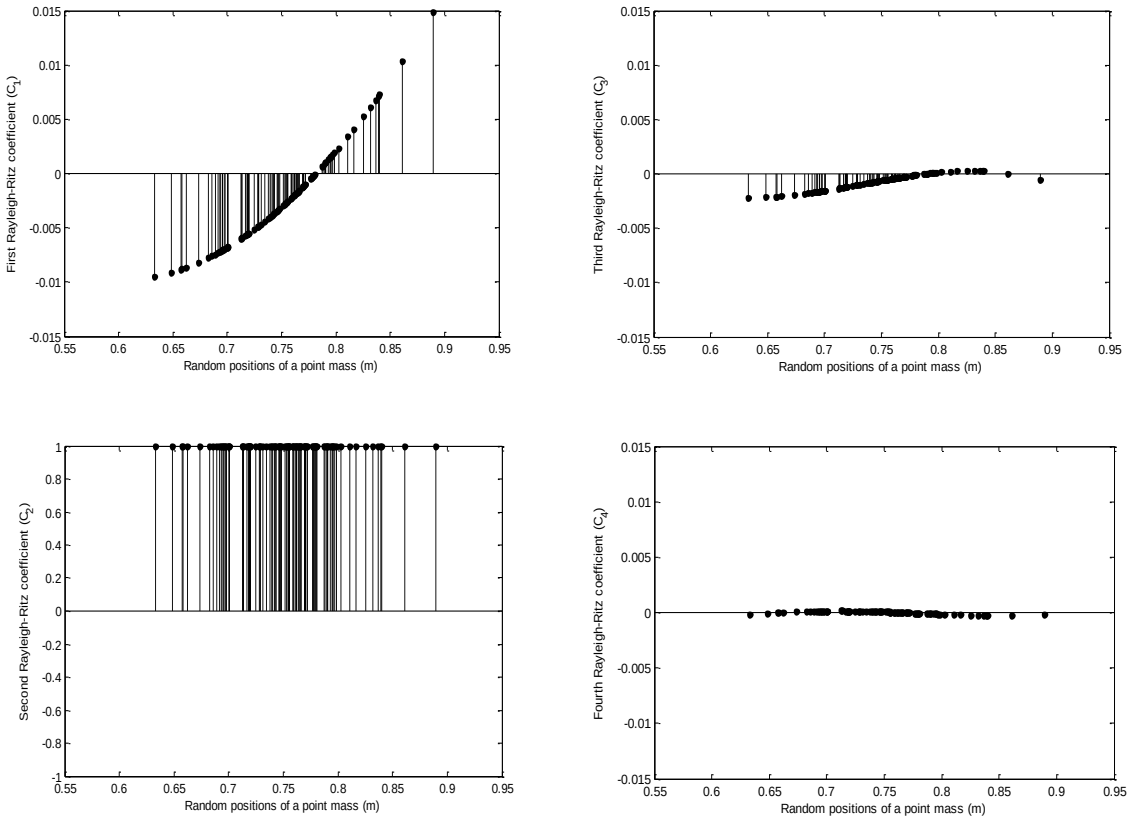

Figure 3.17 The generalised Rayleigh-Ritz coordinates vary with a 100 random positions of the point mass along beam for the second mode.

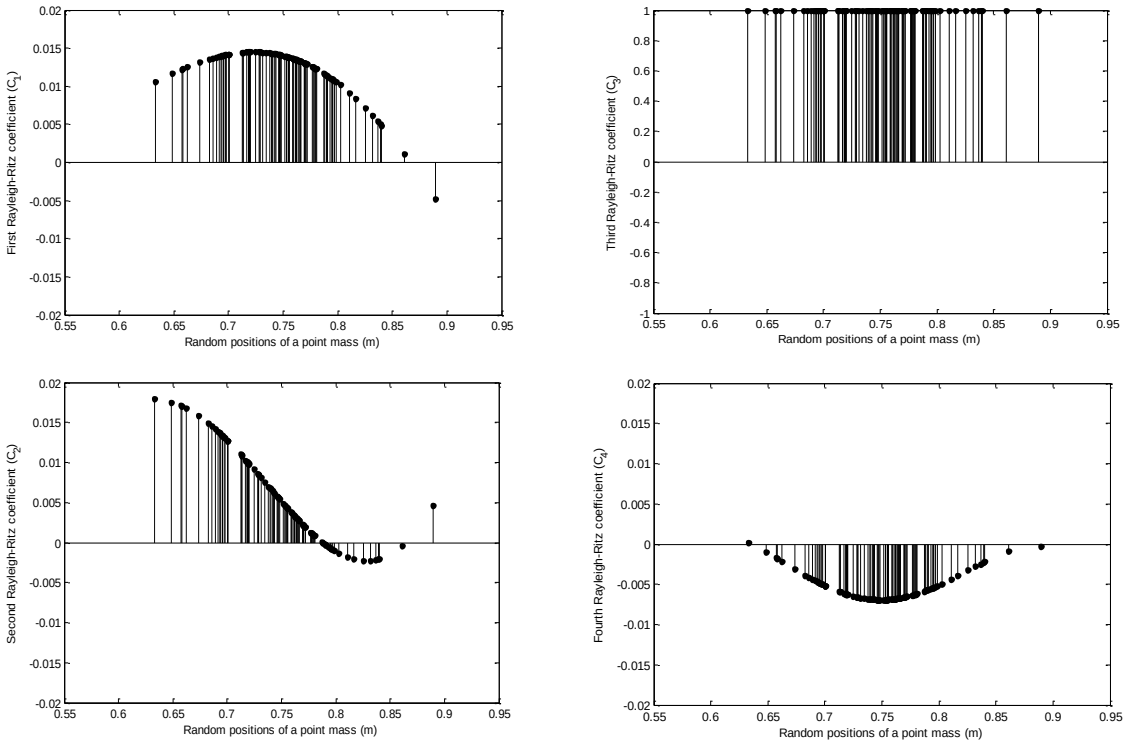

Figure 3.18 The generalised Rayleigh-Ritz coordinates vary with a 100 random positions of the point mass along beam for the third mode

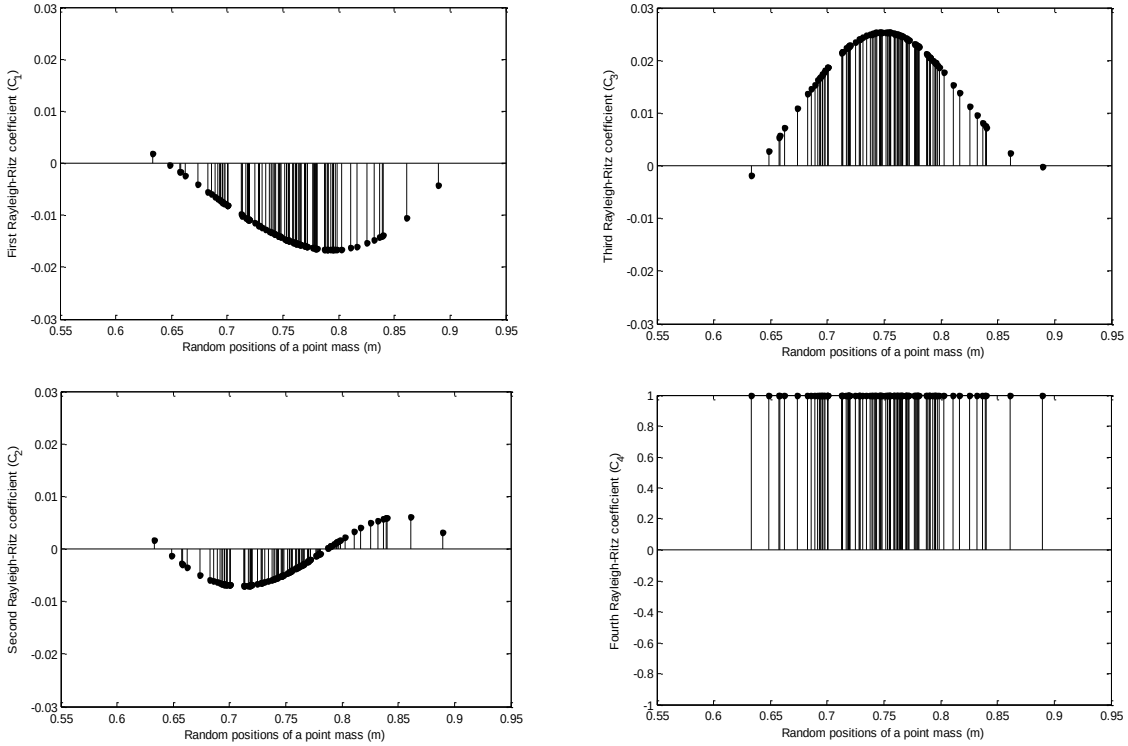

Figure 3.19 The generalised Rayleigh-Ritz coordinates vary with a 100 random positions of the point mass along beam for the fourth mode.

The first Rayleigh-Ritz coefficients (C_1) for the first mode have the same value (equal to one). These due to the normalisation process during the calculation. Therefore the C_1 cannot be used as a response in maximizing the log-likelihood function. For other Rayleigh-Ritz coefficients C_2, C_3 and C_4, these values are almost linear which are an important requirement to use the perturbation based MLE as previously mentioned in Chapter 2.

An example is also shown of maximizing the likelihood function using the Rayleigh-Ritz method with 4 terms using coefficients from mode 1. The results are shown in table 3.5.

N random data	Estimated sigma x (σ_x) Using C1	Estimated sigma x (σ_x) Using C2	Estimated sigma x (σ_x) Using C3	Estimated sigma x (σ_x) Using C4
100	N/A	0.050	0.090	0.115
200	N/A	0.065	0.110	0.125
Jacobian (J0)	N/A	-0.004337	0.000223	0.000146
Hessian value (S)	N/A	-0.029190	0.008070	-0.002761

Table 3.5 The maximum likelihood function using the Rayleigh-Ritz method with 4 terms using coefficients from mode 1 with 100 and 200 random responses.

A further example is shown of maximizing the likelihood function using the Rayleigh-Ritz method with 4 terms using coefficients from mode 2. The results are shown in table 3.6.

N random data	Estimated sigma x (σ_x) Using C1	Estimated sigma x (σ_x) Using C2	Estimated sigma x (σ_x) Using C3	Estimated sigma x (σ_x) Using C4
100	0.050	N/A	0.035	0.045
200	0.060	N/A	0.040	0.050
Jacobian (J0)	0.088831	N/A	0.018908	-0.003500
Hessian value (S)	0.595978	N/A	-0.067960	-0.063121

Table 3.6. Maximum likelihood function using Rayleigh-Ritz 4-term coefficients for mode 2 with 100 and 200 random responses.

Still a further example is shown of maximizing the likelihood function using the Rayleigh-Ritz method with 4 terms using coefficients from mode 3. The results are shown in table 3.7.

N random data	Estimated sigma x (σ_x) Using C1	Estimated sigma x (σ_x) Using C2	Estimated sigma x (σ_x) Using C3	Estimated sigma x (σ_x) Using C4
100	0.095	0.035	N/A	0.500
200	0.130	0.040	N/A	0.500
Jacobian (J0)	-0.035637	-0.154765	N/A	0.000768
Hessian value (S)	-1.402181	0.533440	N/A	1.565866

Table 3.7 Maximum likelihood function using Rayleigh-Ritz 4-term coefficients for mode 3 with 100 and 200 random responses.

And a final example is shown of maximizing the likelihood function using the Rayleigh-Ritz method with 4 terms using coefficients from mode 4. The results are shown in table 3.8.

N random data	Estimated sigma x (σ_x) Using C1	Estimated sigma x (σ_x) Using C2	Estimated sigma x (σ_x) Using C3	Estimated sigma x (σ_x) Using C4
100	0.050	0.035	0.500	N/A
200	0.060	0.040	0.500	N/A
Jacobian (J0)	-0.094618	0.105574	-0.003126	N/A
Hessian value (S)	1.649449	1.956872	-5.995352	N/A

Table 3.8 The maximum likelihood function using the Rayleigh-Ritz method with 4 terms using coefficients from mode 4 with 100 and 200 random responses.

Not all the generalised coordinate can be used to estimate the uncertain parameters because there existc same dependence. For example, the first generalised coordinates C_1 for maximizing the likelihood function using the first natural frequencies on table 3.5, are not applicable to use because all the values of C_1 are normalised to 1. This also applies to parameter C_2 when using the second natural frequencies in table 3.6; parameter C_3 for the third natural frequencies on table 3.7; and parameter C_4 for the fourth natural frequencies in table 3.8.

The magnitude of the Jacobian cannot be too small because it will lead to the singularity causing the method to fail. Large values of the Jacobian are clearly much better from an estimation viewpoint than small values.

The Hessian values are described in Chapter 2 on page 32 under the sub heading ‘constraints imposed on the use of uncertainty identification’. This Hessian value used as a second criterion, is needed when the Jacobian criterion fails to comply. The magnitude of the Hessian can be interpreted as the magnitude of the nonlinearity of the response function which plays an important role for using the perturbation based MLE. The specific value of the Hessian is

used to eliminate the generalised coordinates that will give poor estimations.

Discussion of the results

The maximum likelihood function using mode shape information for the cantilever beam with a point mass is presented in table 3.6 for each mode case. For mode 1, the second Rayleigh-Ritz coefficient gives better estimates than use of the other coefficients. The magnitude of the Jacobian for the third and fourth coefficients is much smaller than the first coefficient. The estimates of the second mode gave better estimates using the first, third and fourth coefficients. For the third mode, the second coefficient gave better estimates. The magnitude of Jacobian using the fourth coefficient is too small compared with use of the other coefficients. Using the first and second coefficients for mode 4, gave better estimates than using the third coefficient. Even though the magnitude of the Jacobian using the third coefficient is not too small, the estimate in the case are still not very good. The following tables also helps show the value of the method.

Rayleigh-Ritz eigenvector coefficients	**Mode 1**	**Mode 2**	**Mode 3**	**Mode 4**
	σ_x (m)	**σ_x (m)**	**σ_x (m)**	**σ_x (m)**
C1	excluded	0.0500	0.0950	0.0500
C2	0.0500	excluded	0.0350	0.0350
C3	excluded	0.0350	excluded	excluded
C4	excluded	0.0450	excluded	excluded
Average =	0.0500	0.0433	0.0625	0.0425
Frequencies	0.0600	0.0850	0.0450	0.0500
Average (from mode shape + frequencies) =	0.0550	0.0641	0.0537	0.0462
Average (from 4 modes) =	0.0547			

Table 3.9 The maximum likelihood function using the Rayleigh-Ritz method with 4 terms using coefficients with 100 random responses.

Rayleigh-Ritz eigenvector coefficients	Mode 1	Mode 2	Mode 3	Mode 4
	σ_x (m)	σ_x (m)	σ_x (m)	σ_x (m)
C1	excluded	0.0600	0.1300	0.0600
C2	0.0650	0.0400	0.0400	0.0400
C3	excluded	excluded	excluded	excluded
C4	excluded	0.0500	excluded	excluded
Average =	0.0650	0.0500	0.0850	0.0500
Frequencies	0.0500	0.0700	0.0400	0.0500
Average (from mode shape + frequencies) =	0.0575	0.0600	0.0625	0.0500
Average (from 4 modes)=	0.0575			

Table 3.10 Maximum likelihood function using Rayleigh-Ritz 4 terms coefficients with 200 random responses.

Tables 3.9 and 3.10 show individual estimates of the standard deviation for the cantilever beam with a point mass with 100 and 200 random positions of a point mass along the beam. Table 3.9 shows when 100 random sample are used to obtain estimates of the standard deviation via Rayleigh-Ritz coefficients. It is divided into 4 groups: Group 1 (mode 1) corresponds to use of the second and third coefficients; Group 2 (mode 2) corresponds to use of the first, third and fourth coefficients; Group 3 (mode 3) corresponds to use of the first and second coefficients, and Group 4 (mode 4) corresponds to use of the first and second coefficients. The estimate of the standard deviations for Group 2 and 4 are in the vicinity of the target value (σ_x = 0.05). Table 3.10 shows similar information as table 3.9. The estimate of standard deviation for Group 2 and 4 are the same as the target value. The criteria for excluding the standard deviation in the final estimate of the standard deviation are if the magnitude of the Jacobian values are less than 0.00300 ($|J0| < 0.00$), and the magnitude of the Hessian values are greater than 2.0 ($|S| > 2.0$).

Conclusions reached in Chapter 3

The application of the maximum the likelihod method using frequency and mode shape information on the beam with an attached mass produces confident results. Initially the first frequencies of a cantilever beam with an attached mass, obtained from Finite Element Method, Receptance, and Rayleigh's quotient, show reasonable agreement. These same frequencies have been implemented

in the Perturbation method for calculating the likelihood estimate for uncertain attached-mass positions on the beam. The coefficients (weights) of a set of base functions in the Rayleigh-Ritz method have been obtained and put it into the log-likelihood function as a set of response data. To create the randomness of response, the Monte Carlo simulation method had been used. The results using the coefficients of the Rayleigh-Ritz method show confident predictions in comparison with the target values.

Using mode shape information as a form of response variable for maximizing the likelihood function for 1D problems is evidentally successful. The advantages of using mode shapes in this case are: they contained more information than the frequencies that can be used to identify uncertainty. There are no problems in using higher modes since a high level of prediction confidence is maintained using only a small number of random positions of a point mass along the beam.

CHAPTER 4

APPLICATION OF UNCERTAINTY IDENTIFICATION TO UNCERTAIN PLATE STRUCTURES USING THEORETICAL MODE SHAPE INFORMATION

Like the previous chapter with the beam case, a plate is a good structure to test the extended method as described in Chapter 2.

The classical differential equation of motion for the transverse displacement of a plate is [Szilard, 1974] :

$$D\nabla^4 w + \gamma \frac{\partial^2 w}{\partial t^2} = 0 \tag{4.1}$$

where D is the flexural rigidity, and γ is the mass per-unit-area of the plate in which D is given by:

$$D = \frac{Eh^3}{12(1-\upsilon^2)} \tag{4.2}$$

and where is E is young modulus, h is plate thickness, and ν is Poisson's ratio.

If it is assumed that the plate is in free vibration then:

$$w = W \cos \omega t \tag{4.3}$$

Substitution of equation (4.3) into (4.1) gives:

$$(\nabla^4 - k^4)W = 0 \tag{4.4}$$

where $$k = \frac{\rho\omega^2}{D} \tag{4.5}$$

and

$$(\nabla^2 + \mathrm{k}^2)(\nabla^2 - k^2)W = 0 \tag{4.6}$$

For the rectangular plates, the deflection function used in Rayleigh's quotient is [Szilard, 1974]:

$$W(x,y)=X(x)Y(y) \tag{4.7}$$

Where X(x) and Y(y) are base functions for the approximate deflection that satisfies boundary conditions of the plate.

4.1 Approximate methods for calculating plate mode shapes

In this chapter the Rayleigh Ritz method is mainly used within the uncertainty identification method. Before then, some results using the Finite Element method to generate mode shapes are presented.

Finite element analysis of a plate structure

As previously mentioned in Chapter 3 the finite element method has been used to obtain the mode shapes for a clamped all-sides rectangular plate without an attached mass. The use of this method is only to compare the mode shapes with other methods such as the Virtual Work method and the Rayleigh-Ritz method.

The geometry and material properties of the rectangular plate are:

Unit	Value	
a (plate length)	m	0.25
b (plate width)	m	0.30
Young's modulus (mild steel)	N/m^2	210E+9
Poisson's ration (ν)		0.30
Density (ρ)	Kg/m^3	7873.3
T (thickness)	m	0.0019

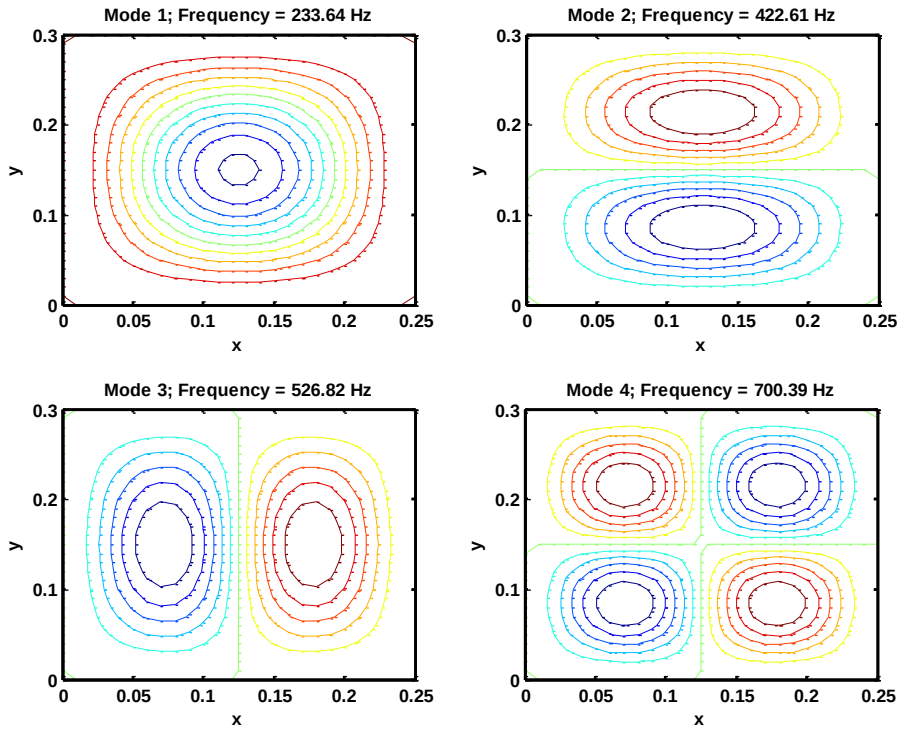

Figure 4.1 The first-four mode shapes for an all-sides clamped rectangular plate using the Finite Element method (Nastran).

Figure 4.1 shows the mode shapes obtained using the Nastran software. These results are merely to provide a benchmark for the Rayleigh Ritz method.

The Rayleigh Ritz method applied to plate structures without attached point masses

Many researchers have studied the vibration of rectangular plates using theoretical and experimental methods. Xing and Liu [2009a] have very recently published exact solutions for free vibrations of rectangular plates with various boundary conditions (including the case of fully clamped conditions). In fact, other exact developments have been reported for rectangular mindlin plates [Xing and Liu, 2009b], for thin orthotropic rectangular plates [Xing and Liu, 2009c], and for in-plane vibrations of rectangular plates [Liu and Xing, 2011]. It would be interesting to use these in, for example, a Rayleigh-Ritz solution of a plate with an attached mass (for which they are clearly are no longer exact) but the benefit of this is significantly reduced by noting that there is quite substantial amount of numerical work to get these mode shape in the first place. Therefore

it would be much simpler to use the approximate CC free-vibration mode shapes in the Rayleigh-Ritz method than the exact solution with Symplectic dual method by Xing and Liu [2009a].

Natural frequencies and mode shape of plates are calculated by an assumption of the vibration shape of the plate. A trigonometric series been used and satisfies the boundary conditions for plates [Low, 1997].

From [Low, 1997], the base functions that satisfy the boundary conditions for use in the Rayleigh-Ritz are given in table 4.1.

Two opposite ends	X_m (x)	Y_n (y)	m	n
S-S	$\sin\left(\frac{m\pi x}{a}\right)$	$\sin\left(\frac{n\pi y}{b}\right)$	1,2,3,…	1,2,3,…
C-C	$\sin\left(\frac{\pi x}{a}\right)\sin\left(\frac{m\pi x}{a}\right)$	$\sin\left(\frac{\pi y}{b}\right)\sin\left(\frac{n\pi y}{b}\right)$	1,2,3,…	1,2,3,…
C-S	$\sin\left(\frac{\pi x}{2a}\right)\sin\left(\frac{m\pi x}{2a}\right)$	$\sin\left(\frac{\pi y}{2b}\right)\sin\left(\frac{n\pi y}{2b}\right)$	2,4,6,…	2,4,6,…

Table 4.1 Assumed shape functions for use in the Rayleigh Ritz method where S means simply supported and C means clamped [Low, 1997].

The accuracy of the Rayleigh-Ritz method depends on choosing the correct approximate shape function. After implementing many shape functions such as polynomial, trigonometric etc, the base functions that satisfy the boundary condition are indeed the trigonometric series as presented in table 4.1.

The shape functions for an all-sides clamped plate are:

$$X_m(x)=\sin\left(\frac{\pi x}{a}\right)\sin\left(\frac{m\pi x}{a}\right) \tag{4.8}$$

and

$$Y_n(y)=\sin\left(\frac{\pi y}{b}\right)\sin\left(\frac{n\pi y}{b}\right) \tag{4.9}$$

Putting the series (4.8) and (4.9) into the deflection function equation (4.7) with 25 terms (5 terms in the x direction and another 5 terms in the y direction), the approximate solution is presented by equation 4.10.

$$W_{total}(x,y) = \mathrm{C}_{11}\sin^2\left(\frac{\pi x}{a}\right)\sin^2\left(\frac{\pi y}{b}\right) + \mathrm{C}_{12}\sin^2\left(\frac{\pi x}{a}\right)\sin\left(\frac{\pi y}{b}\right)\sin\left(\frac{2\pi y}{b}\right) + \mathrm{C}_{13}\sin^2\left(\frac{\pi x}{a}\right)\sin\left(\frac{\pi y}{b}\right)\sin\left(\frac{3\pi y}{b}\right) + C_{14}\sin^2\left(\frac{\pi x}{a}\right)\sin\left(\frac{\pi y}{b}\right)\sin\left(\frac{4\pi y}{b}\right) + \mathrm{C}_{15}\sin^2\left(\frac{\pi x}{a}\right)\sin\left(\frac{\pi y}{b}\right)\sin\left(\frac{5\pi y}{b}\right) + \mathrm{C}_{21}\sin\left(\frac{\pi x}{a}\right)\sin\left(\frac{2\pi x}{a}\right)\sin^2\left(\frac{\pi y}{b}\right) + \mathrm{C}_{22}\sin\left(\frac{\pi x}{a}\right)\sin\left(\frac{2\pi x}{a}\right)\sin\left(\frac{\pi y}{b}\right)\sin\left(\frac{2\pi y}{b}\right) + \mathrm{C}_{23}\sin\left(\frac{\pi x}{a}\right)\sin\left(\frac{2\pi x}{a}\right)\sin\left(\frac{\pi y}{b}\right)\sin\left(\frac{3\pi y}{b}\right) + \mathrm{C}_{24}\sin\left(\frac{\pi x}{a}\right)\sin\left(\frac{2\pi x}{a}\right)\sin\left(\frac{\pi y}{b}\right)\sin\left(\frac{4\pi y}{b}\right) + \mathrm{C}_{25}\sin\left(\frac{\pi x}{a}\right)\sin\left(\frac{2\pi x}{a}\right)\sin\left(\frac{\pi y}{b}\right)\sin\left(\frac{5\pi y}{b}\right) + \mathrm{C}_{31}\sin\left(\frac{\pi x}{a}\right)\sin\left(\frac{3\pi x}{a}\right)\sin^2\left(\frac{\pi y}{b}\right) + \mathrm{C}_{32}\sin\left(\frac{\pi x}{a}\right)\sin\left(\frac{3\pi x}{a}\right)\sin\left(\frac{\pi y}{b}\right)\sin\left(\frac{2\pi y}{b}\right) + \mathrm{C}_{33}\sin\left(\frac{\pi x}{a}\right)\sin\left(\frac{3\pi x}{a}\right)\sin\left(\frac{\pi y}{b}\right)\sin\left(\frac{3\pi y}{b}\right) + \mathrm{C}_{34}\sin\left(\frac{\pi x}{a}\right)\sin\left(\frac{3\pi x}{a}\right)\sin\left(\frac{\pi y}{b}\right)\sin\left(\frac{4\pi y}{b}\right) + \mathrm{C}_{35}\sin\left(\frac{\pi x}{a}\right)\sin\left(\frac{3\pi x}{a}\right)\sin\left(\frac{\pi y}{b}\right)\sin\left(\frac{5\pi y}{b}\right) + \mathrm{C}_{41}\sin\left(\frac{\pi x}{a}\right)\sin\left(\frac{4\pi x}{a}\right)\sin^2\left(\frac{\pi y}{b}\right) + \mathrm{C}_{42}\sin\left(\frac{\pi x}{a}\right)\sin\left(\frac{4\pi x}{a}\right)\sin\left(\frac{\pi y}{b}\right)\sin\left(\frac{2\pi y}{b}\right) + \mathrm{C}_{43}\sin\left(\frac{\pi x}{a}\right)\sin\left(\frac{4\pi x}{a}\right)\sin\left(\frac{\pi y}{b}\right)\sin\left(\frac{3\pi y}{b}\right) + \mathrm{C}_{44}\sin\left(\frac{\pi x}{a}\right)\sin\left(\frac{4\pi x}{a}\right)\sin\left(\frac{\pi y}{b}\right)\sin\left(\frac{4\pi y}{b}\right) + \mathrm{C}_{45}\sin\left(\frac{\pi x}{a}\right)\sin\left(\frac{4\pi x}{a}\right)\sin\left(\frac{\pi y}{b}\right)\sin\left(\frac{5\pi y}{b}\right) + \mathrm{C}_{51}\sin\left(\frac{\pi x}{a}\right)\sin\left(\frac{5\pi x}{a}\right)\sin^2\left(\frac{\pi y}{b}\right) + \mathrm{C}_{52}\sin\left(\frac{\pi x}{a}\right)\sin\left(\frac{5\pi x}{a}\right)\sin\left(\frac{\pi y}{b}\right)\sin\left(\frac{2\pi y}{b}\right) + \mathrm{C}_{53}\sin\left(\frac{\pi x}{a}\right)\sin\left(\frac{5\pi x}{a}\right)\sin\left(\frac{\pi y}{b}\right)\sin\left(\frac{3\pi y}{b}\right) + \mathrm{C}_{54}\sin\left(\frac{\pi x}{a}\right)\sin\left(\frac{5\pi x}{a}\right)\sin\left(\frac{\pi y}{b}\right)\sin\left(\frac{4\pi y}{b}\right) + \mathrm{C}_{55}\sin\left(\frac{\pi x}{a}\right)\sin\left(\frac{5\pi x}{a}\right)\sin\left(\frac{\pi y}{b}\right)\sin\left(\frac{5\pi y}{b}\right) \quad (4.10)$$

Verification of the convergence of the Rayleigh-Ritz method with an increasing number of terms (needed for agreement in frequencies and mode shapes) is shown by the error function in figure 4.2.

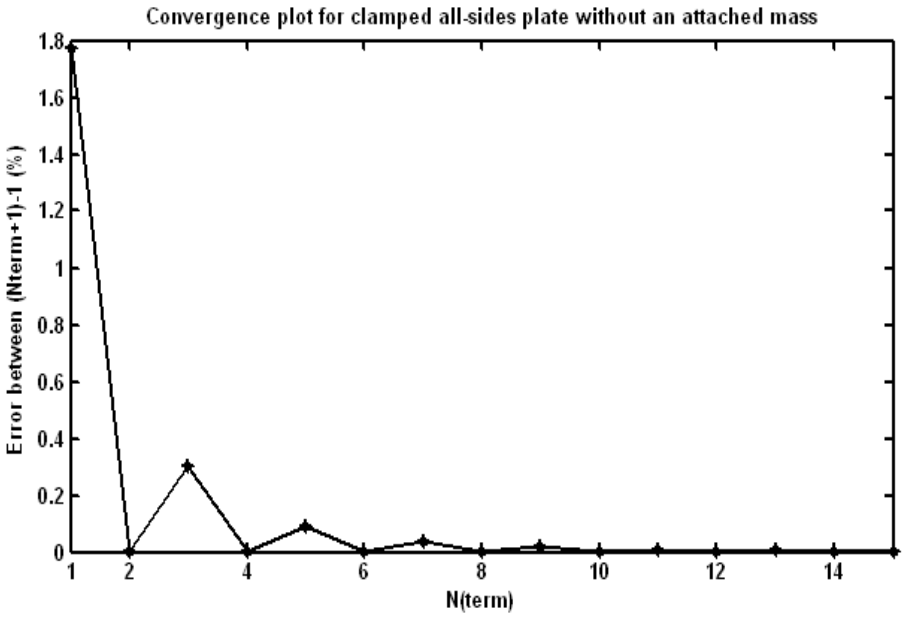

Figure 4.2 Error convergence of the Rayleigh-Ritz method as a function of the number of terms in each direction.

To briefly summarise the previous explanation, mode shapes of a plate using the Rayleigh-Ritz method not only can be represented by a set of basis functions but also depend on choosing the approximate shape function. The need to have a sufficient number of basis functions is very important for the Rayleigh-Ritz method to obtain the sufficiently accurate values needed to approximate the shape function. Adding additional terms into the basis function until convergence is reached is the best way to obtain an accurate shape function.

Figure 4.2 shows that at N(term) = 4, which represents the error between mode shape obtained using the Rayleigh-Ritz method, with 6 terms and 5 terms, is very small ($9.917E^{-15}$). Therefore the number of terms to be used during the calculation is 5 terms, each in the x and y directions. Using the number of terms = 5, the mode shape of an all-sides clamped rectangular plate without an attached mass can be calculated.

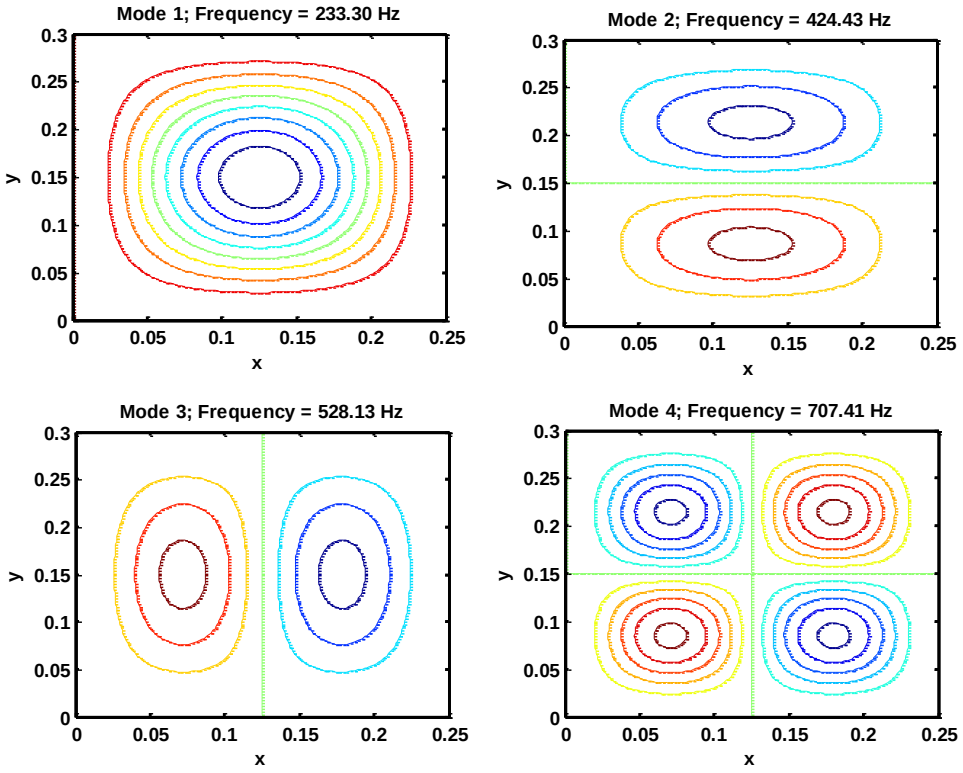

Figure 4.3 The first-four mode shapes of all-sides clamped rectangular plate using the Rayleigh-Ritz method with 25 terms.

A Virtual Work based method

As an alternative to generate approximate mode shape information, the Virtual Work principle has been used. The following result of an all-sides clamped rectangular plate without an attached mass is given shortly as a comparison with all the presented methods (i.e. Finite Element Method and Rayleigh Ritz method).

The approximate mode shape function for a bending plate with Virtual Work principle is [Arenas, 2003]:

$$\psi_{mn}(x,y)=\vartheta_m(x)\zeta_n(y) \tag{4.11}$$

where $\vartheta_m(x)$ and $\zeta_n(y)$ are eigenfunctions given as follows [Arenas, 2003]:

$$\vartheta_m(x)=J\left(\frac{\beta_m x}{a}\right)-\frac{J(\beta_m)}{H(\beta_m)}H\left(\frac{\beta_m x}{a}\right) \tag{4.12}$$

and

$$\zeta_n(y)=J\left(\frac{\beta_m y}{b}\right)-\frac{J(\beta_m)}{H(\beta_m)}H\left(\frac{\beta_m y}{b}\right) \tag{4.13}$$

where βm and βn are the roots of $\cosh(\beta)\cos(\beta) = 1$, and for clamped-clamped plate boundary conditions, $J(s) = \cosh(s) – \cos(s)$ and $H(s) = \sinh(s) - \sin(s)$.

The first four mode shapes of an all-sides clamped rectangular plate obtained by using the Virtual Work based method presented on contour plot (see figure 4.4).

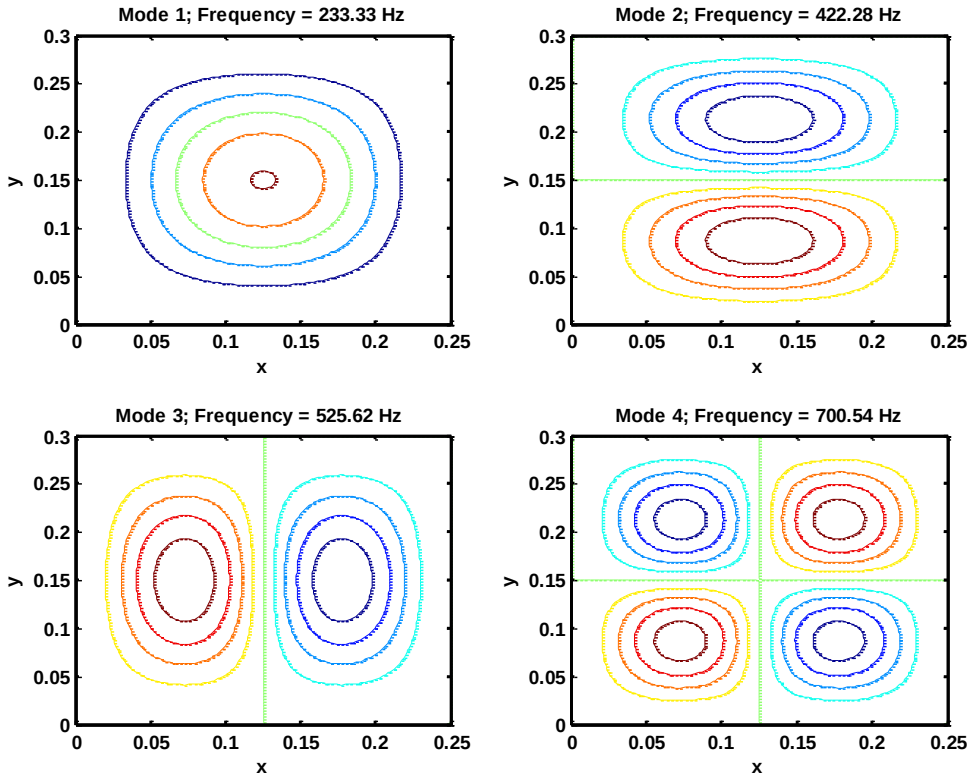

Figure 4.4 The first-four mode shapes for an all-sides clamped rectangular plate calculated using the Virtual Work method.

	Using FEM (Hz)	Using Rayleigh-Ritz (Hz)	Virtual work (Hz)
First Frequency	233.64	233.30	233.33
Second Frequency	442.61	424.43	422.48
Third Frequency	526.82	528.13	525.62
Fourth Frequency	700.39	707.41	700.54

Table 4.2 The first-four frequencies of all-sides clamped rectangular plate using the Finite Element method, the Rayleigh-Ritz method and the Virtual Work method.

Mode Shape	PE 1 (%)	PE 2 (%)	PE 3 (%)
First Mode	0.7666	0.5533	0.7694
Second Mode	1.7977	1.3291	2.3372
Third Mode	2.7437	1.7969	1.4798
Fourth Mode	2.1558	2.7309	1.9558

Table 4.3 Percentage error (PE) for mode shapes between the Rayleigh-Ritz method, the Finite Element method (FEM) and the Virtual Work method where PE 1: percentage error between the FEM and the Virtual Work method; PE 2: percentage error between the Rayleigh-Ritz method and the FEM; and PE 3: percentage error between the Rayleigh-Ritz method and the Virtual Work method.

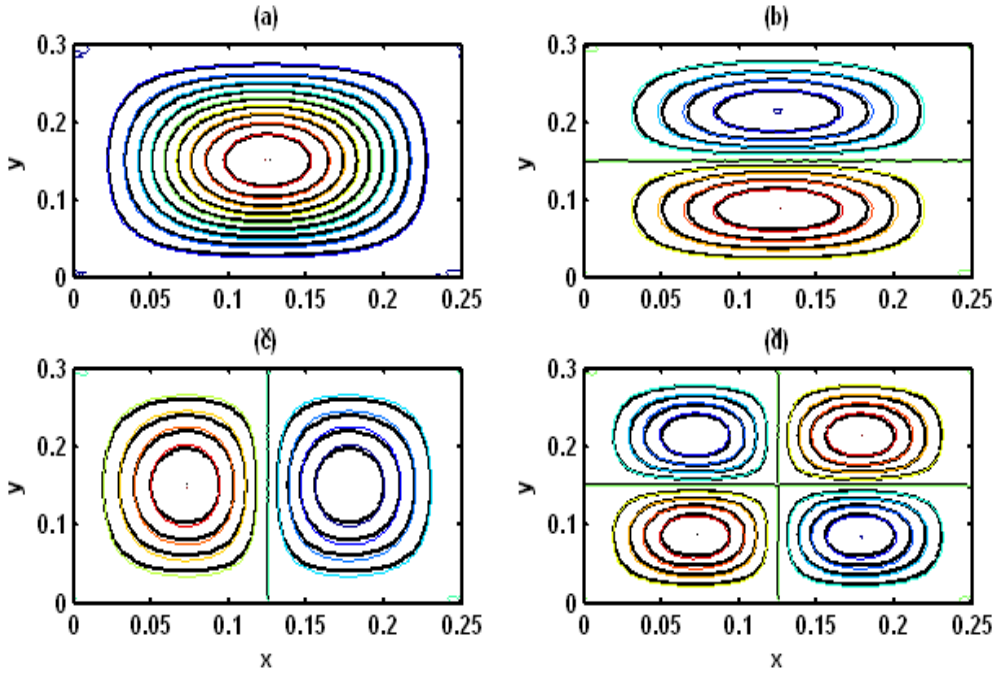

Figure 4.5 Comparison the mode shapes obtained using Finite Element method (presented in grey) and Virtual Work method (presented in colour): (a) first mode shape, (b) second mode shape, (c) third mode shape, and (d) fourth mode shape.

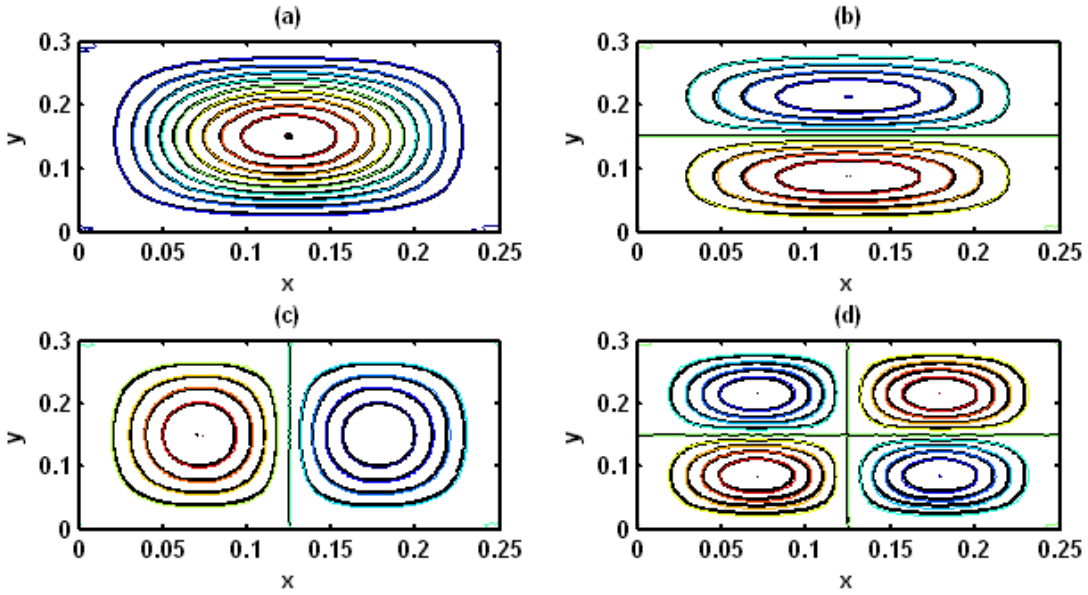

Figure 4.6 Comparison the mode shapes obtained using Rayleigh-Ritz method (presented in grey) and Finite Element method (presented in colour): (a) first mode shape, (b) second mode shape, (c) third mode shape, and (d) fourth mode shape.

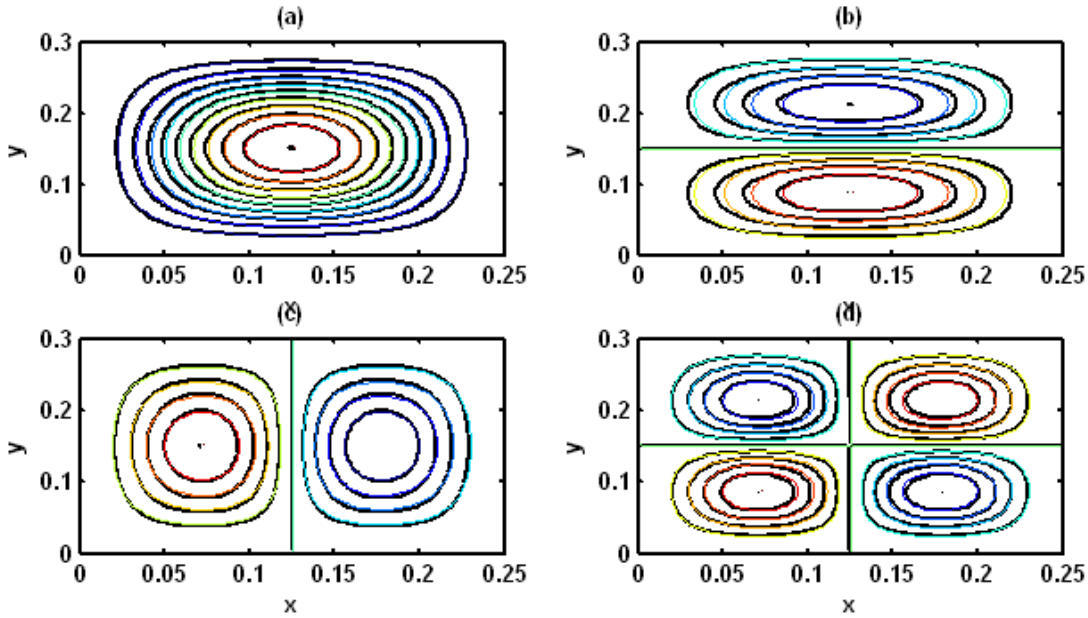

Figure 4.7 Comparison the mode shapes obtained using Rayleigh-Ritz method (presented in grey) and Virtual Work method (presented in colour): (a) first mode shape, (b) second mode shape, (c) third mode shape, and (d) fourth mode shape.

Application of the Rayleigh Ritz method to a CCCC rectangular plate with an attached point mass

Here mode shape information of an all-sides clamped rectangular plate is obtained by using the Rayleigh-Ritz method with 25 terms (m = n = 5).

To create the uncertainty in the plate, a point mass has been attached at uncertain locations. The Rayleigh-Ritz method, using the energy method and multi-term base function for assuming the mode shape or deflection function, has been adopted.

For the free vibration plate case, the maximum potential energy is [Low, 1997]:

$$U_{max} = \frac{D}{2}\int_0^a \int_0^b \left\{\left(\frac{\partial^2 w}{\partial x^2} + \frac{\partial^2 w}{\partial y^2}\right)^2 - 2(1-v)\left[\frac{\partial^2 w}{\partial x^2}\frac{\partial^2 w}{\partial y^2} - \left(\frac{\partial^2 w}{\partial x \partial y}\right)^2\right]\right\} dxdy \quad (4.14)$$

The maximum kinetic energy (neglecting the rotary inertia effect and having an attached mass on the plate) is [Low, 1997]:

$$T_{max} = \frac{\omega^2}{2}\left\{\int_0^b \int_0^a \gamma(x,y) w^2(x,y) dxdy + M(k,h) w^2(k,h)\right\} \quad (4.15)$$

where W(x,y) (equation 4.7) is an assumed mode shape, M (k,h) is a point mass at location k on x-axis and h on y-axis, and ω is the natural frequencies of the plate. In Rayleigh's quotient, the maximum potential energy is equal to maximum kinetic energy, and the result is [Low, 1997]:

$$\omega^2 = \frac{U_{max}}{T^*} \quad (4.16)$$

where $T^* = \frac{1}{2}\int_0^b \int_0^a \gamma(x,y) w^2(x,y) dxdy + \frac{1}{2} M(k,h) w^2(k,h)$

The assumed mode shape can be written as [Low, 1997]:

$$\mathrm{w(x,y)} = \sum_{\mathrm{m}}^{\mathrm{M}} \sum_{\mathrm{n}}^{\mathrm{N}} \mathrm{C_{mn}\, X_m(x) Y_n(y)} \tag{4.17}$$

where $X_m(x)$ and $Y_n(y)$ are base functions that satisfy the boundary condition of the plate, and C_{mn} is the coefficient of the functions.

Substituting equation (4.17) into equation (4.14) and equation (4.15), the maximum potential energy and maximum kinetic energy becomes:

$$U_{max} = \frac{1}{2} \sum_{m} \sum_{n} \sum_{p} \sum_{q} K_{mnpq} C_{mn} C_{pq} \tag{4.18}$$

and

$$T^* = \frac{1}{2} \sum_{\mathrm{m}} \sum_{\mathrm{n}} \sum_{\mathrm{p}} \sum_{\mathrm{q}} S_{mnpq}\, C_{mn} C_{pq} \tag{4.19}$$

where

$$K_{mnpq} = \iint \left\{ \left(\frac{\partial^2 X_m}{\partial x^2} Y_n + X_m \frac{\partial^2 Y_n}{\partial y^2} \right) \left(\frac{\partial^2 X_p}{\partial x^2} Y_q + X_p \frac{\partial^2 Y_q}{\partial y^2} \right) + 2(1-v) \left(X_m \frac{\partial^2 X_p}{\partial x^2} Y_n \frac{\partial^2 Y_q}{\partial y^2} - \frac{\partial X_m}{\partial x} \frac{\partial X_p}{\partial x} \frac{\partial Y_n}{\partial y} \frac{\partial Y_q}{\partial y} \right) \right\} dxdy \tag{4.20}$$

and

$$S_{mnpq} = \gamma \iint \left(X_m X_p Y_n Y_q \right) dxdy + M X_m(k) X_p(k) Y_n(h) Y_q \tag{4.21}$$

Solving the above eigenvalue problem gives the Rayleigh-Ritz solution [Low, 1997], which from equation (4.16) is given as:

$$\frac{\partial U_{max}}{\partial C_{mn}} - \left(\frac{U_{max}}{T^*} \right) \left(\frac{\partial T^*}{\partial C_{mn}} \right) = 0 \tag{4.22}$$

and

$$\frac{\partial U_{max}}{\partial C_{mn}} - \omega^2 \left(\frac{\partial T^*}{\partial C_{mn}}\right) = 0 \tag{4.23}$$

Equation (4.23) in matrix format is:

$$D[K]\{C\} = \omega^2[S]\{C\} \tag{4.24}$$

where [K] is the stiffness matrix, [S] is the mass matrix and {C} is a vector of unknown coefficients.

The Rayleigh-Ritz coefficients $C_{(i)}$ (eigenvectors), are obtained from equation (4.24), by using the eigenvector solution. The square matrices of [K] and [S] in equation (4.24) are obtained by converting the 4 dimensional matrices from equation (4.20) and (4.21) to 2 dimensional matrices by appropriate reassignment of the indices. Using the previous geometry and material properties of the rectangular plate with additional attached mass 0.023 kg at specific location in the x and y direction (k = 0.045 m and h = 0.042 m), the first-four mode shapes of an all-sides clamped rectangular plate is presented in figure 4.5.

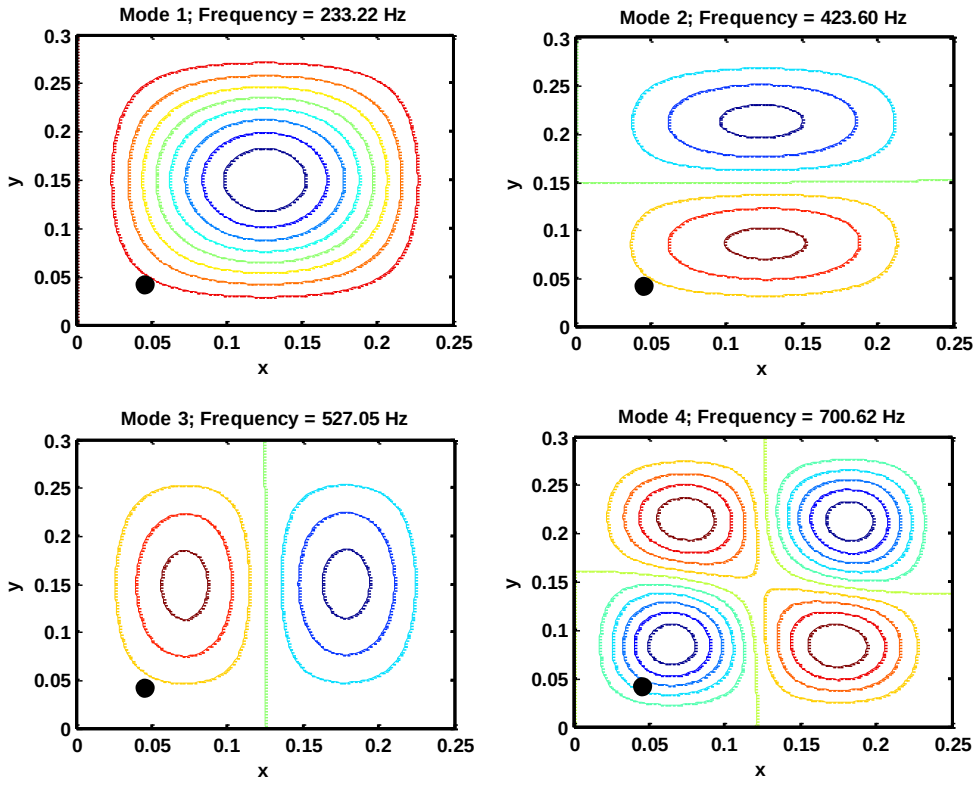

Figure 4.8 The first-four mode shapes of all-sides clamped rectangular plate with an attached mass 0.023 kg at location x = 0.045 m and y = 0.042 m obtained by using the Rayleigh-Ritz method with 25 terms (m = 5 and n = 5).

Eigenvalue (Frequency) of mode	Without an attached mass (Hz)	With an attached mass (Hz)
1	233.30	233.22
2	424.43	423.60
3	528.13	527.05
4	707.41	700.62

Table 4.4 The comparison of the first four frequencies of an all-sides-clamped rectangular plate without and with an attached mass.

The coefficients associated with the Rayleigh Ritz method are shown in Table 4.5. Putting the small point mass onto the plate does not produce significant changes (small decrease) in the eigenvalues and eigenvectors compared with the plate without an attached mass.

C	Mode 1		Mode 2		Mode 3		Mode 4	
	Without an attached mass	With attached mass	Without an attached mass	With attached mass	Without an attached mass	With attached mass	Without an attached mass	With attached mass
C1	-0.9953	-0.9952	0.0000	-0.0001	0.0000	0.0020	0.0000	-0.0475
C2	0.0000	-0.0011	0.9928	0.9922	0.0000	-0.0089	0.0000	0.0016
C3	-0.0736	-0.0741	0.0000	0.0047	0.0000	0.0098	0.0000	-0.1582
C4	0.0000	-0.0003	0.0769	0.0785	0.0000	0.0022	0.0000	-0.0114
C5	-0.0126	-0.0128	0.0000	0.0013	0.0000	0.0024	0.0000	-0.0196
C6	0.0000	-0.0007	0.0000	0.0086	0.9903	0.9889	0.0000	0.0062
C7	0.0000	-0.0008	0.0000	0.0067	0.0000	0.0146	0.9911	-0.9730
C8	0.0000	-0.0007	0.0000	0.0055	0.1172	0.1250	0.0000	-0.0344
C9	0.0000	-0.0004	0.0000	0.0027	0.0000	0.0048	0.1017	-0.1122
C10	0.0000	-0.0003	0.0000	0.0019	0.0236	0.0263	0.0000	-0.0103
C11	-0.0609	-0.0612	0.0000	0.0024	0.0000	0.0045	0.0000	-0.0230
C12	0.0000	-0.0006	0.0907	0.0937	0.0000	0.0045	0.0000	-0.0211
C13	0.0020	0.0014	0.0000	0.0038	0.0000	0.0066	0.0000	-0.0391
C14	0.0000	-0.0003	0.0034	0.0054	0.0000	0.0034	0.0000	-0.0127
C15	0.0016	0.0014	0.0000	0.0016	0.0000	0.0026	0.0000	-0.0104
C16	0.0000	-0.0002	0.0000	0.0015	0.0709	0.0722	0.0000	-0.0047
C17	0.0000	-0.0003	0.0000	0.0017	0.0000	0.0032	0.0862	-0.0914
C18	0.0000	-0.0003	0.0000	0.0019	0.0057	0.0088	0.0000	-0.0113
C19	0.0000	-0.0002	0.0000	0.0011	0.0000	0.0018	0.0070	-0.0129
C20	0.0000	-0.0001	0.0000	0.0009	0.0004	0.0018	0.0000	-0.0049
C21	-0.0101	-0.0102	0.0000	0.0006	0.0000	0.0010	0.0000	-0.0045
C22	0.0000	-0.0001	0.0166	0.0174	0.0000	0.0011	0.0000	-0.0047
C23	0.0011	0.0009	0.0000	0.0010	0.0000	0.0018	0.0000	-0.0092
C24	0.0000	-0.0001	0.0000	0.0006	0.0000	0.0010	0.0000	-0.0036
C25	0.0007	0.0006	0.0000	0.0005	0.0000	0.0009	0.0000	-0.0031

Table 4.5 The comparison of first-four sets of coefficients derived from mode shapes without and with an attached mass. C is the vector of Rayleigh-Ritz coefficients where $C1=C_{11}$, $C2=C_{21}$, $C3=C_{31}$, $C4=C_{41}$, $C5=C_{51}$, $C6=C_{12}$, $C7=C_{22}$, $C8=C_{32}$, $C9=C_{42}$, $C10=C_{52}$, $C11=C_{13}$, $C12=C_{23}$, $C13=C_{33}$, $C14=C_{43}$, $C15=C_{53}$, $C16=C_{14}$, $C17=C_{24}$, $C18=C_{34}$, $C19=C_{44}$, $C20=C_{54}$, $C21=C_{15}$, $C22=C_{25}$, $C23=C_{35}$, $C24=C_{45}$, and $C25=C_{55}$.

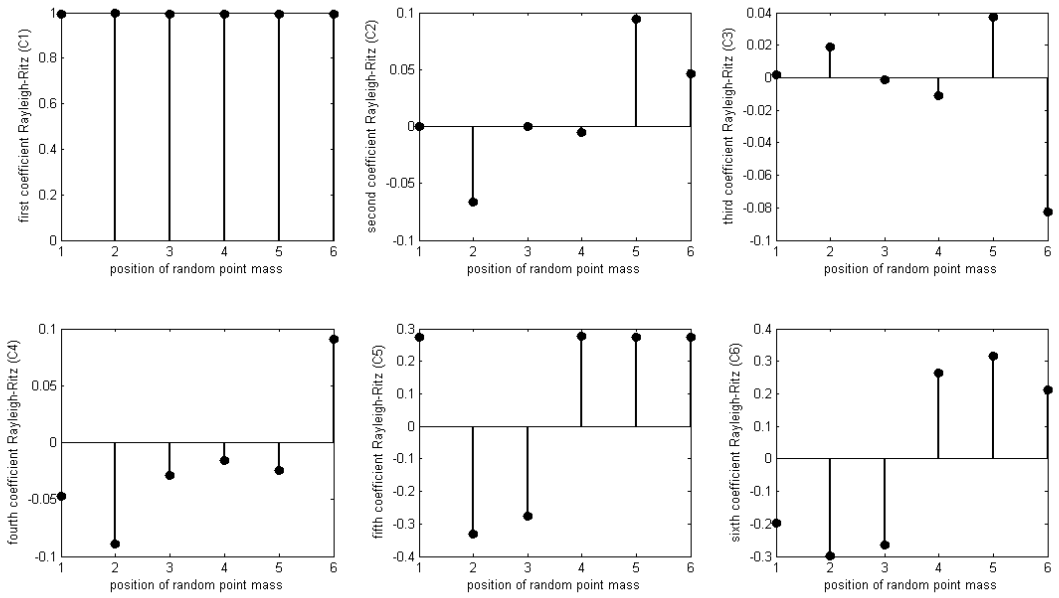

Figure 4.9 The generalised Rayleigh-Ritz coordinates (C1-C6) vary with 6 random positions of the point mass along the beam for the first mode.

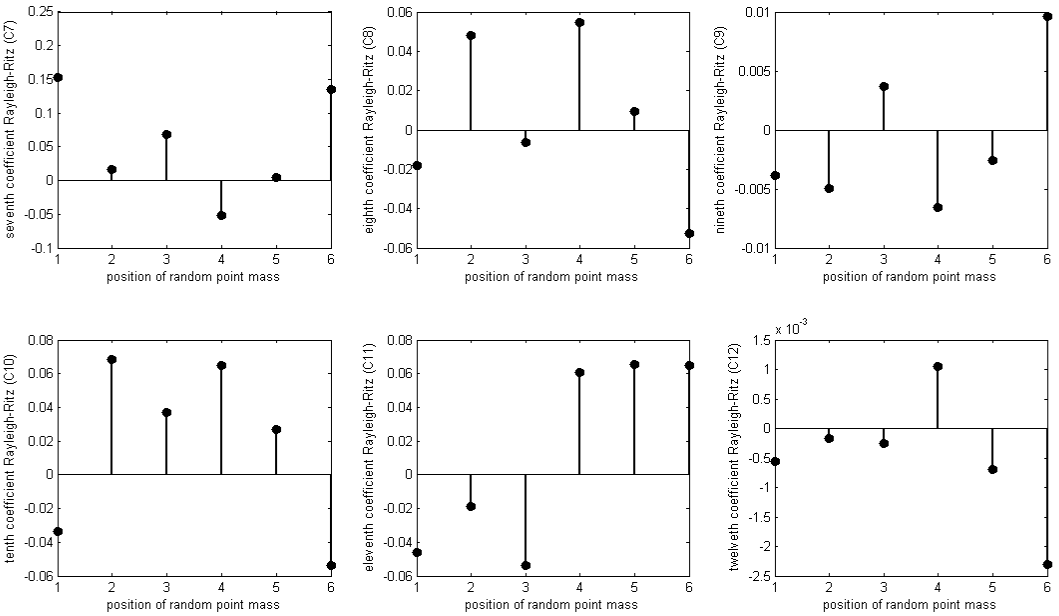

Figure 4.10 The generalised Rayleigh-Ritz coordinates (C7-C12) vary with 6 random positions of the point mass along the beam for the first mode.

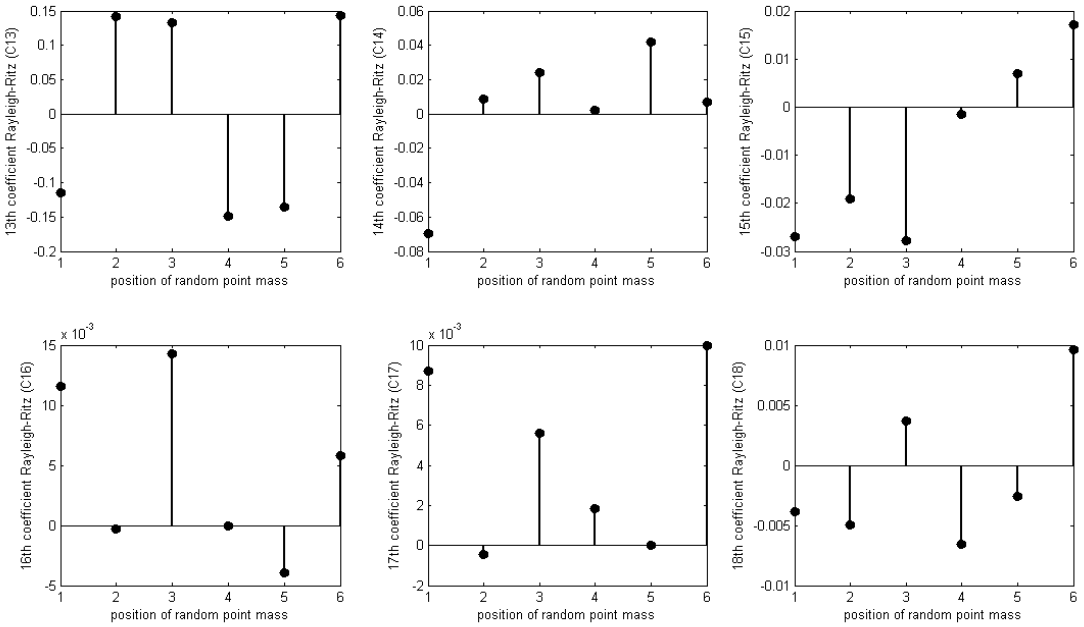

Figure 4.11 The generalised Rayleigh-Ritz coordinates (C13-C18) vary with 6 random positions of the point mass along the beam for the first mode.

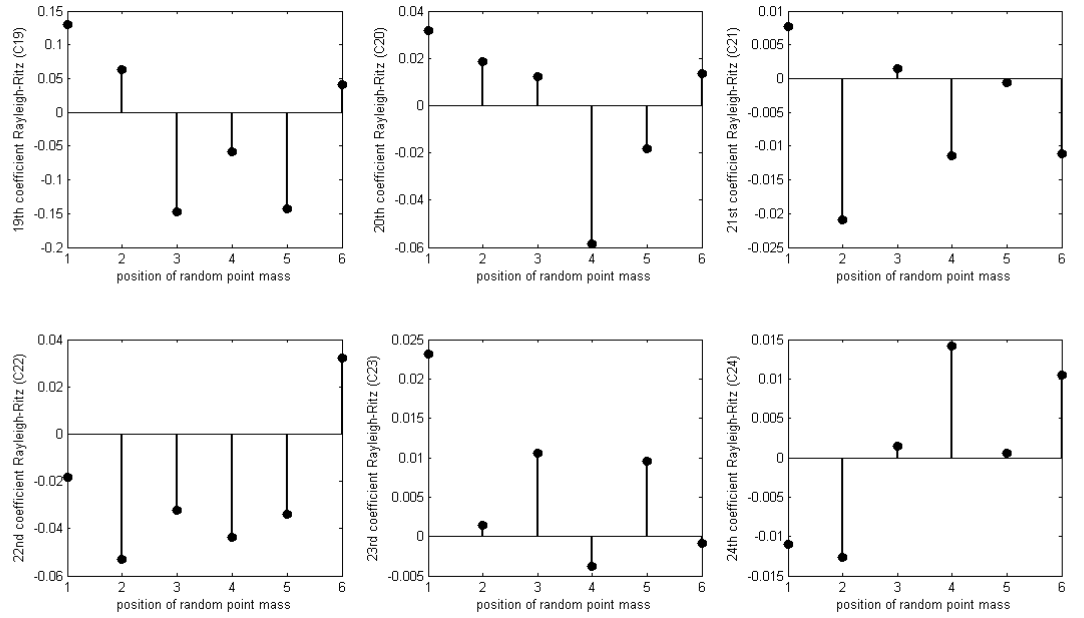

Figure 4.12 The generalised Rayleigh-Ritz coordinates (C19-C24) vary with 6 random positions of the point mass along the beam for the first mode.

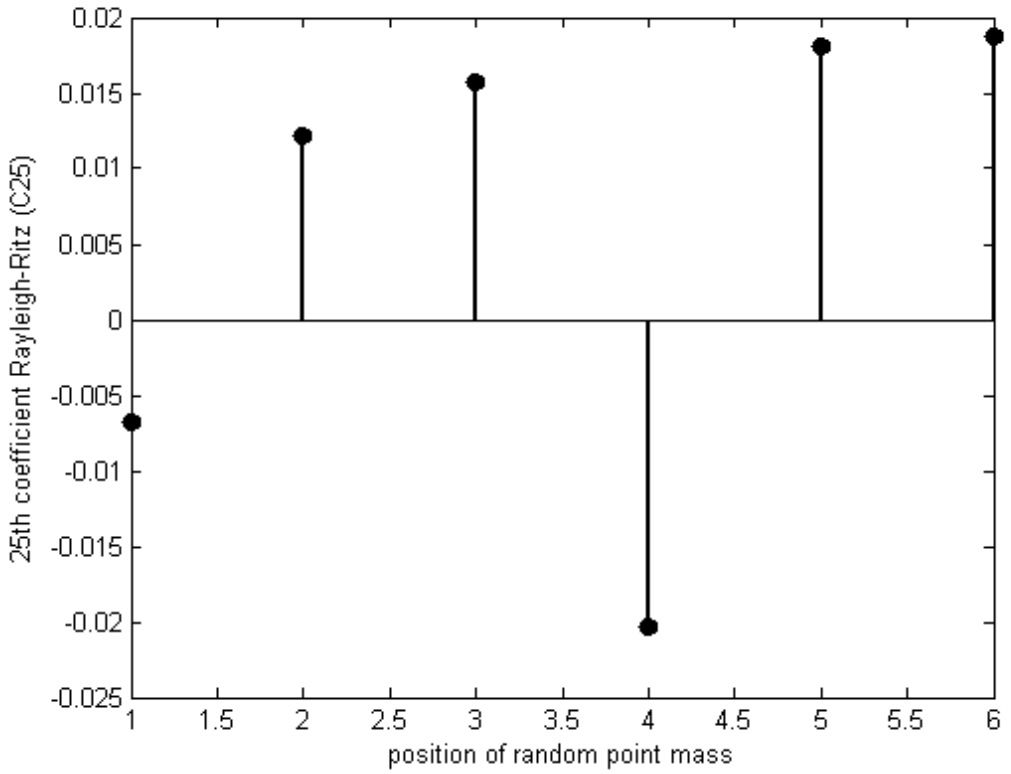

Figure 4.13 The generalised Rayleigh-Ritz coordinates (C25) vary with 6 random positions of the point mass along the beam for the first mode.

4.2 Maximum likelihood based uncertainty identification using estimation mode shape information obtained by the Rayleigh-Ritz method

The eigenvectors that represent the weights of the deflection functions obtained by using the Rayleigh-Ritz method can be considered as response data (equation 2.4) in the estimation method with the perturbation approach. The procedure for maximizing the likelihood function are first, generate following a normal distribution (equation 2.7), a set of random positions of the attached mass along the beam length in the x and y direction. Second, obtain the eigenvectors of the all-sides-clamped plate with an attached mass (at those random positions generated in the first procedure) by using the Rayleigh-Ritz method with 25 terms. In Chapter 2, page 31, it has been discussed that the number of response variables should not exceed the number of uncertain parameters. The mode shape approximation in equation (2.32) with only two uncertain parameters, then only a pair of the coefficients from C_1, C_2, C_3,…,C_n

can be used in the method to generate statistical estimate at any one time. Third, calculate the Jacobian (J0) around x^0, which is chosen to be in the vicinity of the mean of x and y, but as previously mentioned in Chapter 2, small intervals of dx and dy should be used. The values of dx and dy can vary but one needs to be aware that when they become too small, the derivatives can become unstable. Fourth, maximize the likelihood function to obtain the standard deviation on x direction by using equation 2.14 by calculating the mean (μ_y) and sigy (σ_y) from equation 2.13 and equation 2.14.

Position	x (m)	y (m)
1	0.045	0.042
2	0.130	0.129
3	0.194	0.030
4	0.037	0.181
5	0.146	0.196
6	0.076	0.126

Table 4.6 Random positions with chosen mean and standard deviation are 0.10 and 0.15 (for the mean in x and y direction) and 0.05 (for the standard deviation in the x and y direction).

Table 4.7 shows the results of applying the uncertainty identification method to measured data based on six random positions. Here the standard deviation of the mass position is relatively high as shown in the caption of table 4.7.

Table 4.8 shows results of applying the uncertainty identification method similar to those shown in table 4.7 but now with a reduced standard deviation.

Table 4.9 shows for mode 1 only, for the low standard deviation case, shows 6 sets of realisation each with 6 random positions of the point mass (in both directions). Column 5 of table 4.9 corresponds to mode 1 in table 4.8. Table 4.10 shows a similar set of for results as table 4.9 but for mode 3 (for mode 2 all cases were regular). Table 4.11 and 4.12 show results similar to table 4.9 and 4.10 but now using 10 sets of results for 10 random positions of the point mass.

Figure 4.6 shows the likelihood function as an example of good estimation corresponding to the Rayleigh Ritz coefficient combination C7 and C8 in table 4.9.

Set of coefficients	Mode 1	Mode 2	Mode 3
C1&C2	0.0920	excluded	0.0220
C3&C4	excluded	excluded	0.0380
C5&C6	excluded	excluded	excluded
C7&C8	excluded	excluded	excluded
C9&C10	0.0710	excluded	excluded
C11&C12	0.0420	excluded	excluded
C13&C14	excluded	excluded	excluded
C15&C16	excluded	excluded	excluded
C17&C18	excluded	excluded	excluded
C19&C20	excluded	excluded	excluded
C21&C22	0.0580	excluded	excluded
C23&C24	excluded	excluded	excluded
Average	0.0657	N/A	0.0030

Table 4.7 Standard deviation estimation of an uncertain position of a point mass at x direction on an all-sides clamped rectangular plate using a 25-term of the Rayleigh-Ritz coefficients from the first-three modes calculated using MLE with perturbation approach with a set point mass position in table 4.6 (random sample each set = 6, μ_x = 0.1 m, μ_y = 0.15 m, σ_y = 0.05 m, and target σ_x = 0.05 m).

Set of coefficients	Mode 1	Mode 2	Mode 3
C1&C2	0.044	excluded	0.0200
C3&C4	excluded	excluded	0.0220
C5&C6	excluded	excluded	excluded
C7&C8	0.0280	excluded	0.0740
C9&C10	0.0310	excluded	excluded
C11&C12	0.0410	excluded	excluded
C13&C14	0.0350	excluded	excluded
C15&C16	excluded	excluded	excluded
C17&C18	excluded	excluded	excluded
C19&C20	excluded	excluded	excluded
C21&C22	0.0480	excluded	excluded
C23&C24	0.0290	excluded	excluded
Average	0.0365	N/A	0.0386

Table 4.8 Standard deviation estimates for the uncertain position of a point mass in the x direction on an all-sides-clamped rectangular plate (using coefficients from the Rayleigh-Ritz method with 5 terms) obtained by using MLE and the perturbation approach using one of the set point mass positions (random sample each set = 6, μ_x = 0.1 m, μ_y = 0.15 m, σ_y = 0.03 m, and target σ_x = 0.03 m).

Rayleigh-Ritz coefficients combination	1st set of 6 random positions σ_x (m)	2nd set of 6 random positions σ_x (m)	3rd set of 6 random positions σ_x (m)	4th set of 6 random positions σ_x (m)	5th set of 6 random positions σ_x (m)	6th set of 6 random positions σ_x (m)	Total Average $\widehat{\sigma}_x$ (m) =
C1&C2	0.0740	0.0460	0.0490	0.0150	0.0440	0.0880	
C3&C4	excluded	excluded	excluded	excluded	excluded	0.0928	
C5&C6	excluded						
C7&C8	0.0210	0.0230	0.0340	0.0170	0.0280	0.0302	
C9&C10	0.0230	0.0200	0.0190	0.0300	0.0310	0.0218	
C11&C12	0.0340	0.0170	0.0370	0.0280	0.0410	0.0308	
C13&C14	0.0200	0.0100	0.0230	0.0090	0.0350	0.0218	
C15&C16	excluded						
C17&C18	excluded	excluded	excluded	0.0860	excluded	0.0977	
C19&C20	excluded						
C21&C22	0.0140	0.0250	0.0570	0.0240	0.0480	0.0302	
C23&C24	0.0340	0.0280	0.0260	0.0240	0.0290	0.0267	
Average =	0.0314	0.0241	0.0350	0.0290	0.0365	0.0488	0.0341

Table 4.9 Standard deviation estimates of the uncertain position of a point mass (x direction) for an all-sides clamped rectangular plate using a 25-term of Rayleigh-Ritz coefficients for the first mode calculated using MLE with the Perturbation approach (random sample each set = 6, μ_x = 0.1 m, μ_y = 0.15 m, σ_y = 0.03 m, and target σ_x = 0.03 m).

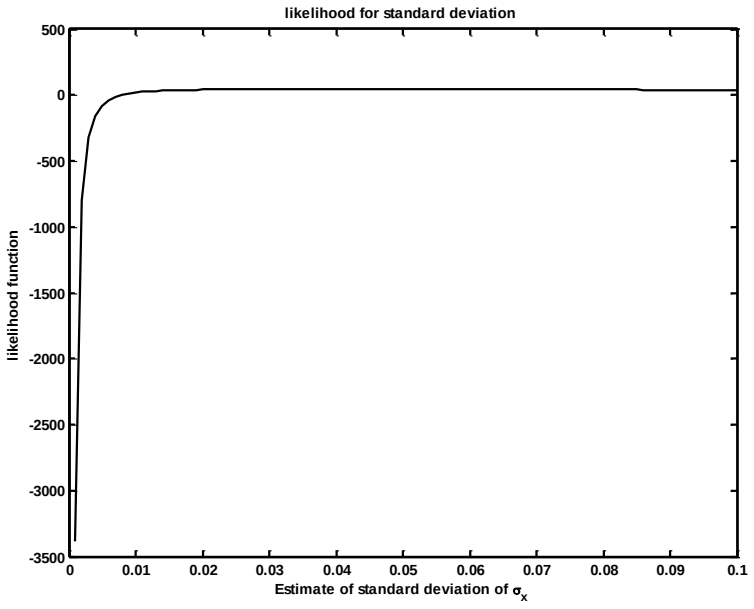

Figure 4.14 Log-likelihood function for standard deviation estimation in one dimensional for the point mass position attached to an all-sides-clamped rectangular plate obtained via the Perturbation method using combination of C7 & C8 from the first mode shape (which is achieved from Rayleigh-Ritz method) and also the 6th set of 6 random positions of the point mass.

Rayleigh-Ritz coefficients combination	1st set of 6 random positions σ_x (m)	2nd set of 6 random positions σ_x (m)	3rd set of 6 random positions σ_x (m)	4th set of 6 random positions σ_x (m)	5th set of 6 random positions σ_x (m)	6th set of 6 random positions σ_x (m)	Total Average $\hat{\sigma}_x$ (m) =
C1&C2	0.0240	0.0260	0.0250	0.0140	0.0150	0.0160	
C3&C4	0.0200	0.0250	0.0320	0.0250	0.0210	0.0120	
C5&C6	excluded						
C7&C8	0.0090	0.0350	0.0050	0.0350	0.0070	0.0060	
C9&C10	0.0310	0.0180	0.0250	0.0260	0.0250	0.0040	
C11&C12	excluded	0.0390	0.0810	0.0480	0.0950	excluded	
C13&C14	0.0310	0.0310	0.0110	0.0310	0.0190	0.0560	
C15&C16	excluded						
C17&C18	0.0620	0.0510	0.0590	0.0220	0.0800	0.0400	
C19&C20	excluded						
C21&C22	0.0910	0.0830	0.0840	0.0180	0.0410	0.0660	
C23&C24	excluded	excluded	excluded	excluded	0.0660	0.0380	
Average =	0.0338	0.0336	0.0402	0.0273	0.0410	0.0297	0.0342

Table 4.10 Standard deviation estimation of an uncertain position of a point mass (x direction) on an all-sides-clamped rectangular plate using a 25-term of Rayleigh Ritz coefficients from the third mode calculated using MLE with Perturbation approach (random sample each set = 6, μ_x = 0.1 m, μ_y = 0.15 m, σ_y = 0.03 m, and target σ_x = 0.03 m).

Rayleigh-Ritz coefficients combination	1st set of 10 random positions σ_x (m)	2nd set of 10 random positions σ_x (m)	3rd set of 10 random positions σ_x (m)	4th set of 10 random positions σ_x (m)	5th set of 10 random positions σ_x (m)	6th set of 10 random positions σ_x (m)	7th set of 10 random positions σ_x (m)	8th set of 10 random positions σ_x (m)	9th set of 10 random positions σ_x (m)	10th set of 10 random positions σ_x (m)	Total Average $\hat{\sigma}_x$ (m) =
C1&C2	excluded	0.0510	0.0480	0.0850	0.0890	0.0490	0.0610	0.0510	0.1000	0.0410	
C3&C4	excluded										
C5&C6	excluded										
C7&C8	0.0290	0.0370	0.0320	0.0320	0.0470	0.0620	0.0240	0.0250	0.0230	0.0270	
C9&C10	0.0270	0.0320	0.0240	0.0260	0.0280	0.0360	0.0350	0.0230	0.0250	0.0140	
C11&C12	0.0290	0.0330	0.0360	0.0360	0.0300	0.0230	0.0300	0.0260	0.0310	0.0230	
C13&C14	0.0340	0.0170	0.0120	0.0180	0.0440	0.0150	0.0280	0.0200	0.0160	0.0240	
C15&C16	excluded										
C17&C18	excluded	0.0750	0.0860	excluded	excluded	excluded	excluded	excluded	excluded	excluded	
C19&C20	excluded										
C21&C22	0.0270	0.0390	0.0160	0.0300	0.0240	0.0150	0.0230	0.0300	0.0360	0.0250	
C23&C24	0.0770	0.0190	0.0140	0.0210	0.0310	0.0290	0.0260	0.0330	0.0220	0.0160	
Average =	0.0503	0.0468	0.0548	0.0593	0.0529	0.0527	0.0508	0.0553	0.047	0.0503	0.0331

Table 4.11 Standard deviation estimation of an uncertain position of a point mass at (x direction) on an all-sides-clamped rectangular plate using 25-term of Rayleigh-Ritz coefficients from first mode, calculated using MLE with the Perturbation approach (random sample each set = 10, μ_x = 0.1 m, μ_y = 0.15 m, σ_y = 0.03 m, and target σ_x = 0.03 m).

Rayleigh-Ritz coefficients combination	1st set of 10 random positions σ_x (m)	2nd set of 10 random positions σ_x (m)	3rd set of 10 random positions σ_x (m)	4th set of 10 random positions σ_x (m)	5th set of 10 random positions σ_x (m)	6th set of 10 random positions σ_x (m)	7th set of 10 random positions σ_x (m)	8th set of 10 random positions σ_x (m)	9th set of 10 random positions σ_x (m)	10th set of 10 random positions σ_x (m)	Total Average $\hat{\sigma}_x$ (m) =
C1&C2	0.0190	0.0230	0.0220	0.0110	0.0160	0.0150	0.0130	0.0120	0.0150	0.0160	
C3&C4	0.0220	0.0210	0.0300	0.0310	0.0230	0.0240	0.0230	0.0240	0.0240	0.0240	
C5&C6	excluded										
C7&C8	0.0280	0.0430	0.0310	0.0210	0.0210	0.0200	0.0270	0.0210	0.0270	0.0280	
C9&C10	0.0280	0.0200	0.0140	0.0200	0.0150	0.0190	0.0250	0.0250	0.0060	0.0150	
C11&C12	0.0410	0.0750	0.0860	0.0590	excluded	0.0730	0.0850	excluded	excluded	0.0830	
C13&C14	0.0210	0.0350	0.0220	0.0470	0.0180	0.0230	0.0100	0.0210	0.0700	0.0380	
C15&C16	excluded										
C17&C18	0.0660	0.0700	0.0240	0.0490	0.0610	0.0630	0.0490	0.0490	0.0440	excluded	
C19&C20	excluded										
C21&C22	0.0730	0.0220	0.0230	0.0190	0.0880	0.0520	0.0200	0.0190	0.0680	0.0490	
C23&C24	excluded	excluded	0.0520	excluded	excluded	excluded	excluded	excluded	excluded	excluded	
Average =	0.0385	0.0386	0.0337	0.0367	0.0345	0.0361	0.0315	0.0244	0.0362	0.0361	0.0346

Table 4.12 Standard deviation estimation of an uncertain position of a point mass at x direction on all-sides clamped rectangular plate using a 25-term of Rayleigh-Ritz coefficients from third mode calculated using MLE with perturbation approach (random sample each set = 10, μ_x = 0.1 m, μ_y = 0.15 m, σ_y = 0.03 m, and target σ_x = 0.03 m).

Discussion of Results

The results shown in table 4.7, with a target standard deviation 0.05 do not produce good estimates by using the first, second or third mode. Linearity is important for obtaining a good estimate. By reducing the standard deviation however to 0.03, the results are shown to be good as presented in tables 4.9 – 4.10 (for mode 1) with sets of six random positions for 6 realisations and tables 4.11 – 4.12 (for mode 3) with sets of ten random positions for 10 realisations.

In some cases like the combinations of C5 & C6 and C15 & C16, the maximum likelihood estimates are not being found. These are outlier estimates due to singular behaviour of the magnitude of determinant for the Jacobian. The estimate σ_x using the Rayleigh-Ritz coefficient combinations of C7 and C8 (see log-likelihood function in figure 4.14) confirm that uncertainty identification using mode shape information does indeed work. The estimation of the standard deviation of point mass positions in the x direction (σ_x) obtained by using this combination is 0.0302 m whereas the target is 0.0300 m.

It is evident that the second mode of the all-sides-clamped rectangular plate cannot be used to estimate the standard deviation using the maximum likelihood estimation via Perturbation approach because the magnitude of the determinant of each Jacobian (J0) indicates singular behaviour. The reason why this is the case is not yet clear so further investigation is required.

Maximum likelihood estimates however are not being successfully found by using the combination of C15 & C16 from the third mode for the all-sides-clamped rectangular plate. The magnitude of the determinant of the Jacobian is singular.

Conclusions of Chapter 4

The average of the overall standard deviation was obtained by using many different sets of position of the point mass. The use of the first mode is better than the third mode when using smaller number of samples. The average estimate for σ_x using Rayleigh-Ritz coefficients obtained from the first and third mode shape are 0.0341 m and 0.0342 m (table 4.9 and 4.10) where the target is 0.0300 m. And also it proved that the use of the third mode is better than the first mode when increasing number of samples. The average estimate for σ_x using Rayleigh-Ritz coefficients obtained from the first and third mode shape are 0.0331 m and 0.0346 m (table 4.11 and 4.12) where the target is 0.0300 m.

The advantages of using mode shapes instead of frequency are the variability is more linear and contain more information that can be used to calculate the likelihood estimation. The mode shape variability can be seen on figure 4.9 – 4.13.

CHAPTER 5

HOLOGRAPHIC MEASUREMENT OF PLATE FREQUENCIES AND MODE SHAPES USING VIBROMAP 1000

In order to verify how effective free vibration-based uncertainty identification is, validation using experimental measurement is needed. The predictions (in Chapter 4) used the assumption of free vibration (i.e. with no damping), while measurement of real plate structures must involve forced-damped vibration. In this chapter experimental measurement represents an initial stage in the estimation of the standard deviation of the point mass positions for an all-side-clamped rectangular plate. The first step is obtaining the mode shapes of an all-sides-clamped rectangular plate with uncertain positions of the point mass, and then extracting the weights or coefficients of the base functions that satisfy boundary conditions. The next step is to maximize the log-likelihood function via the perturbation method with a set of coefficients obtained from an approximate mode shape fitted to measured data. The result will be presented in Chapter 6, namely experimental verification of efficient uncertainty estimation method on plate structures. Here the purpose of this chapter is to describe the experimental rig and the measurement facilities used to collect the data needed.

The Experimental Facilities

The experimental facilities needed to generate data for an uncertain plate structure are now described. First the laser-based frequency and mode shape measurement system VibroMap 1000 is described. Then the experimental rectangular plate rig and the arrangement for attaching point masses in random positions are discussed in detail. A description is also given of the method of excitation and data capture. The chapter is completed first by showing measured mode shapes, without point masses attached, compared with mode shapes obtained with the FEM, Virtual Work, and Rayleigh Ritz method. Then finally VibroMap measurements are shown for the plate with a point mass attached in a random position.

5.1 Optonor VibroMap 1000 – An ESPI System for mode shape measurement.

The main instrument for obtaining the mode shapes of an all-sides-clamped plate structure is VibroMap 1000 from Optonor (see figure 5.1). "*The VibroMap 1000 is equipment based on the technique of TV-holography (or ESPI - Electronic Speckle Pattern Interferometry)"* [www.optonor.com]. TV-holography is a laser-based interferometry technique that is used for noncontact measurements of surface vibrations and static deflections of specimen testing. The VibroMap 1000 system not only can give accurate measurement of an object where the size may vary from less than a centimeter up to several metres and, with unique computer software, it can also give display options either in 2D or 3D. It can detect the amplitude of deflection of the surface down to a nanometer.

Figure 5.1 The holographic sensor (HS) instrument consists of 1 or more illumination lenses, 1 zoom objective, 1 close-up lens (+2 -49mm), 1 illumination mirror, and 1 or more neutral density filters (for optional use).

Specification for VibroMap 1000 standard 5 mW system

Size of optical head:	525x230x100 mm (LxWxH)
Weight of optical head:	7 kg
Imaging system:	zooming lens 12.5 - 75 mm (standard)
Frame grabber:	matrix
Operating system:	Windows XP or others
Laser class:	III b
Laser:	5/7 mW HeNe standard. Up to 200 mW or more non-standard.
Minimum vibration frequency:	< 30 Hz
Maximum vibration frequency:	unlimited for qualitative analysis 50 kHz (or higher) for quantitative analysis
Minimum object size:	< 1 cm
Maximum object size:	appr. 2x2 meters (retroreflective tape or high power laser required).
Object surface:	Surface preparation is normally not required. Specular surfaces should be covered with powder (removable). Very large surfaces should be covered with retroreflective paint or tape to get enough light reflected from the surface when standard laser is used.
Environments:	Normal laboratory environments, no vibration isolation required. No rotating machinery or noise source should be allowed nearby testing site.

The VibroMap 1000 is an excellent piece of equipment for designing mechanical structures either without vibrations and resonances, or with controlled vibration and resonances. It assists in avoiding noise and fatigue fracture by evaluating and controlling the results from model predictions obtained by using the Finite Element method.

The Experimental Rig for an all-sides-clamped rectangular plate.

The geometry and material properties of the measurement specimen plate have been described in Chapter 4. Figure 5.2 shows a photograph of the rig.

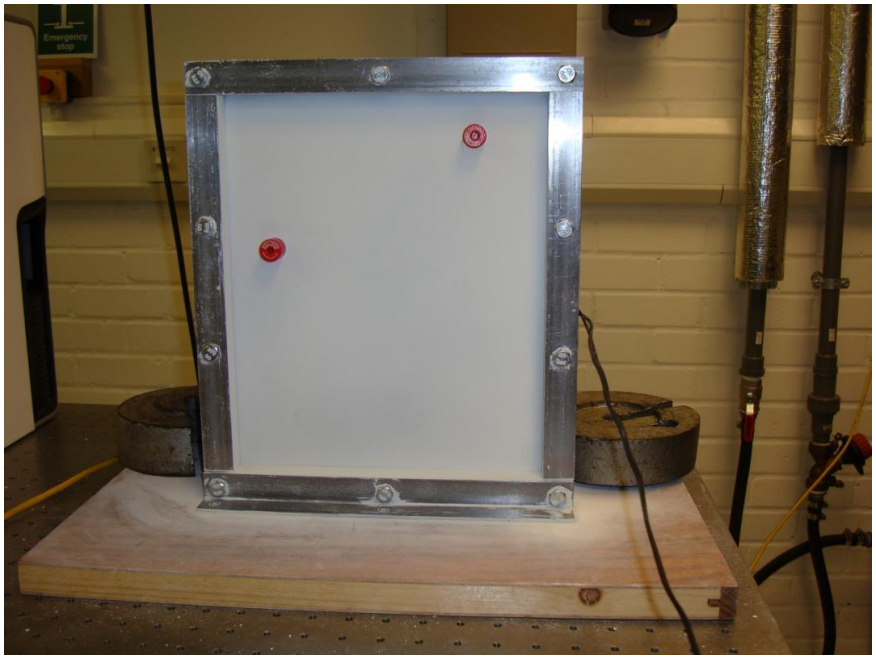

Figure 5.2 The all-sides-clamped rectangular steel plate shown covered with powder from spray developer.

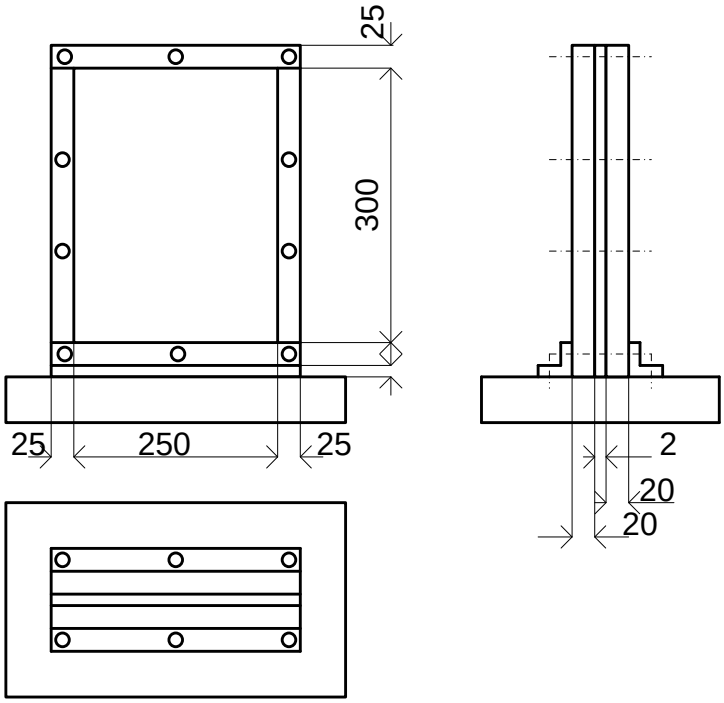

Figure 5.3 A schematic view of the all-sides-clamped rectangular plate used in experiment measurements with Vibromap 1000 (unit mm).

The rig is robust by not allowing deformation during experiment measurements when applied the excitation to the plate structure.

The Exciter (source of excitation)

The source of excitation that was used to excite the plate structure is a loud speaker (see figure 5.4). The load speaker does not require surface contact with the plate surface and easily allows frequency variation. A piezo transducer had been implemented on a plate structure (i.e. an aluminium cantilever rectangular plate) but was subsequently found to be not strong enough to excite the steel all-sides clamped rectangular plate.

Figure 5.4 Loud speaker with a built-in amplifier as the source of excitation

The Signal generator

A Signal generator was used and controlled and adjusted over the frequency range to provide the excitation of the plate structure. The VibroMap 1000 came with a controller and two signal generators, plus a Digital Analog Converter (DAC) and an analog video filter (shown at figure 5.5)

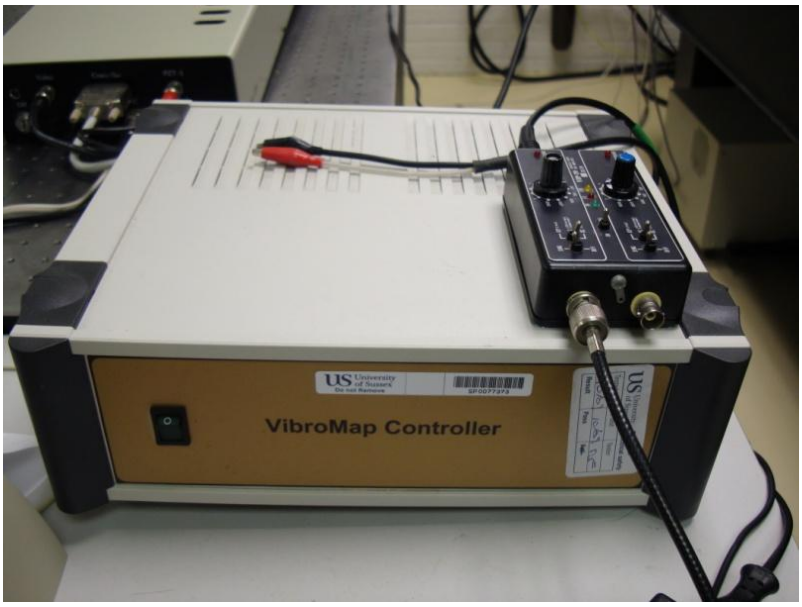

Figure 5.5 VibroMap controller (a component which is part of the Optonor VibroMap 1000 holographic system).

The PC

The Computer instruments include a screen (monitor), keyboard, mouse, matrix frame grabber, and computer software for vibration analysis (VibraLab).

The point mass

The point mass that was used as a source of uncertainty on the plate structure was a simple magnetic mass. This gives the flexibility to move the point mass from one location to another without damaging the surface. The permanent magnet field strength is high enough to avoid the risk of mass movement during vibration.

Additional equipment

The following additional equipment was needed to successfully run the experiment:

- A Flaw spray developer 3

- Laser goggles used to protect eyes from coming into contact with the laser beam (Class 3B)
- A dust mask used when coating the surface of the plate structure with a spray developer

5.2 The Measurement procedure for the all-sides-clamped rectangular plate structure using VibroMap 1000

The experimental set-up of the all-sides-clamped rectangular plate structure using VibroMap 1000 is shown in figure 5.6, and figure 5.7.

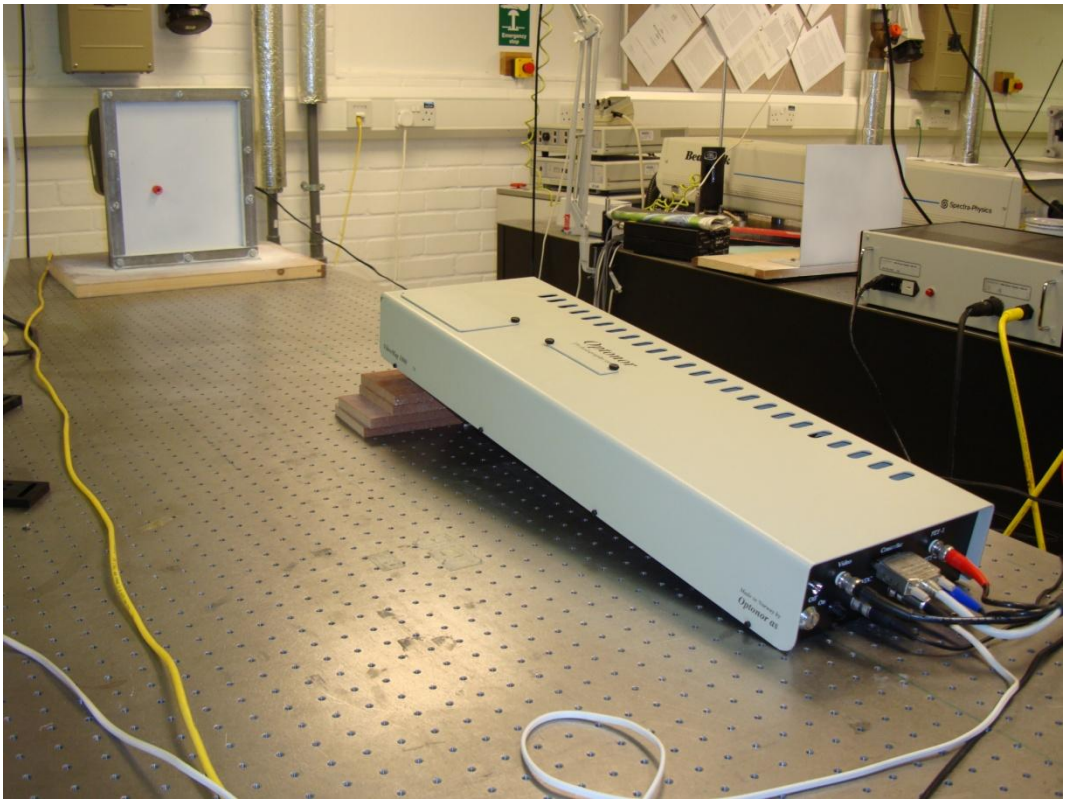

Figure 5.6 Experiment setup using VibroMap 1000 for all-sides steel rectangular plate (25 cm x 30cm) with 1.9 mm thickness.

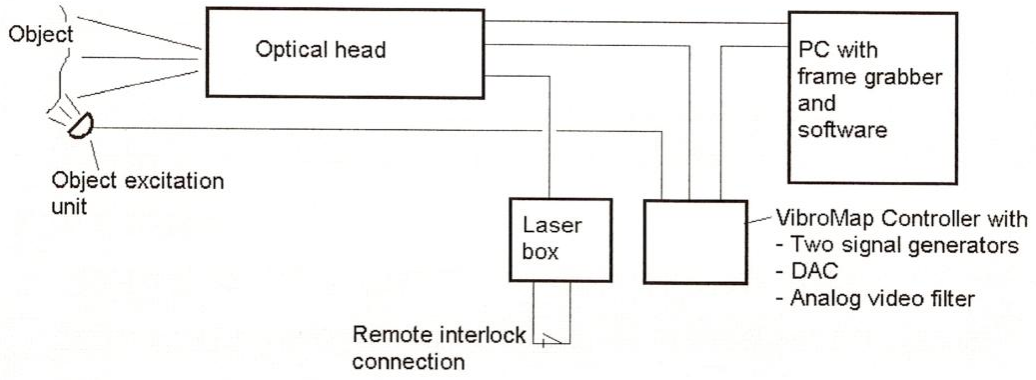

Figure 5.7 VibroMap measurement system schematic configurations [figure taken from the VibroMap manual guide]

The plate was positioned vertically and clamped to rig that connected to a robust wooden base. This configuration was chosen because of the simplicity it provided which also allowed the clamped plate to be moved easily.

Measurement procedures

These are the steps needed to take measurements with Vibromap 1000:

- Turn on the signal generator and the loud speaker. The combination was used to excite the plate.
- Turn on the computer.
- Switch key position to “on” on the holographic sensor (HS).
- Open the program VibraLab in the Computer.
- Click “view” and start the camera.
- Select vibration mode.
- Pull out a little bit lever arm.
- Adjust the reference until less saturated.
- Adjust the mirror to make sure all of the laser scan is in the centre of the plate (covering the plate surface)
    - If the image becomes brighter (i.e. when the laser box is far) it is coherent. If laser box is put closer, and the image is getting darker, it is important to adjust the reference.

  - Set the lens (+2) at a distance between the laser box to object 40 cm, but if the distance is longer than 42 cm, take off lens +2.

- Set intensity adjustment.
- When doing measurement, there are 2 basic real time image settings: with phase shifting (direct and deformation), and without phase shifting (vibration). In vibration mode, the quality of the image will decrease.
- Select measurement method, such as “real time”, “quantitative,” “qualitative II,” or “HQ fringe.” Then run all the procedures for measuring vibration (based on the Vibromap 1000 short course handbook).
- Mode shapes that obtained by using Vibromap are then pre-processing (such as with the use of Matlab software).

Measurement Results using VibroMap 1000

The mode shapes obtained by using the VibroMap measurement (see figure 5.8) needed to be pre-processed (into a Matlab file) for manipulation purposes without the need to have the VibraLab software installed on the computer. Examples of mode shapes (figure 5.9) are presented (by Matlab) so the data can be numerically processed for further work. The size of the raw data array for a mode shape (480 x 640) was quite large but to be able to see the depth of the deflected surface, the array size needed to be interpolated to a smaller array size, for example 100 x 100 or any desired array size (see figure 5.10, 5.11, 5.12, and 5.13 for individual plots of each mode).

On the VibroMap 100 specification section on Chapter 5 page 92, during the measurement using the Vibromap 1000 although the room does not require vibration isolation, the room should not have rotating machinery or noise that can affect the measurement. The potential sources of noise that affected the measured data are rotating machinery (fans, blowers, compressors, etc) inside the building, and the airflow from the heating and cooling system inside the room.

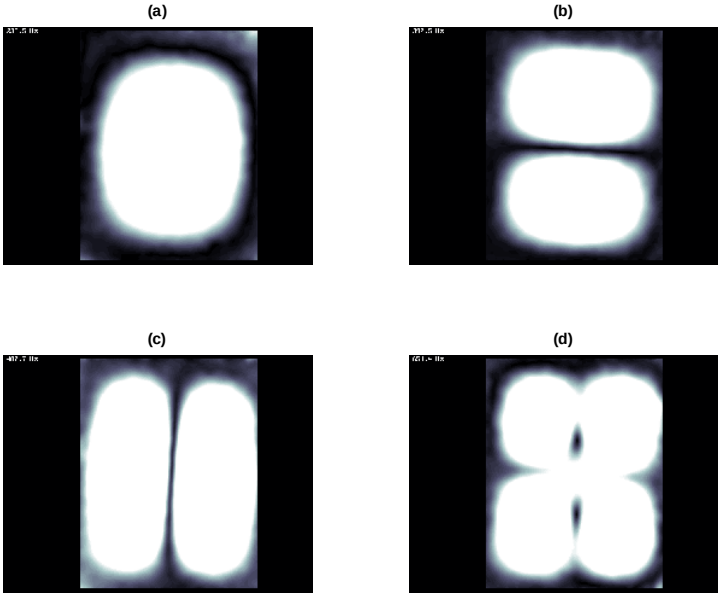

Figure 5.8 The first-four mode shape images of an all-sides-clamped rectangular plate obtained by using the Optonor Vibromap 1000. (a): first mode; (b): second mode; (c): third mode; and (d): fourth mode.

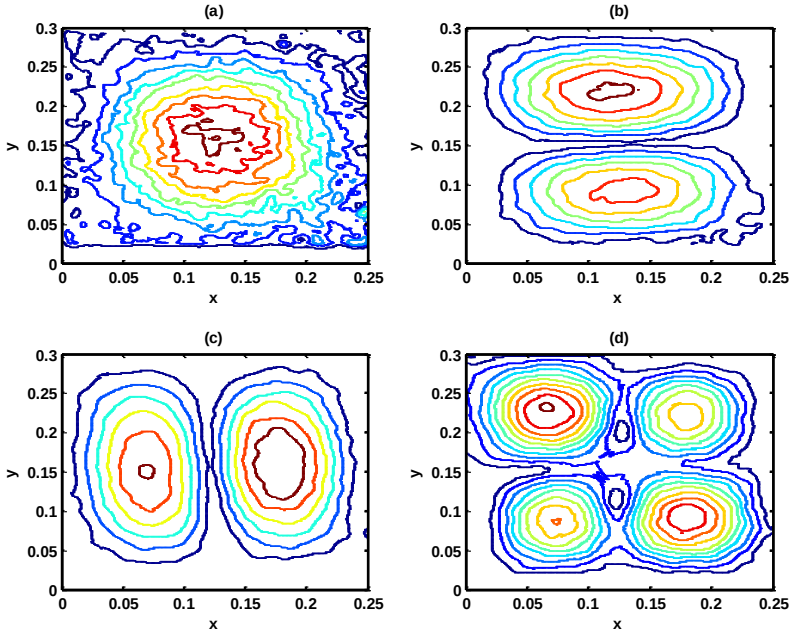

Figure 5.9 The first-four mode shape images of an all-sides-clamped rectangular plate obtained by using the Optonor Vibromap 1000 (presented in Matlab). (a): first mode; (b): second mode; (c): third mode; and (d): fourth mode.

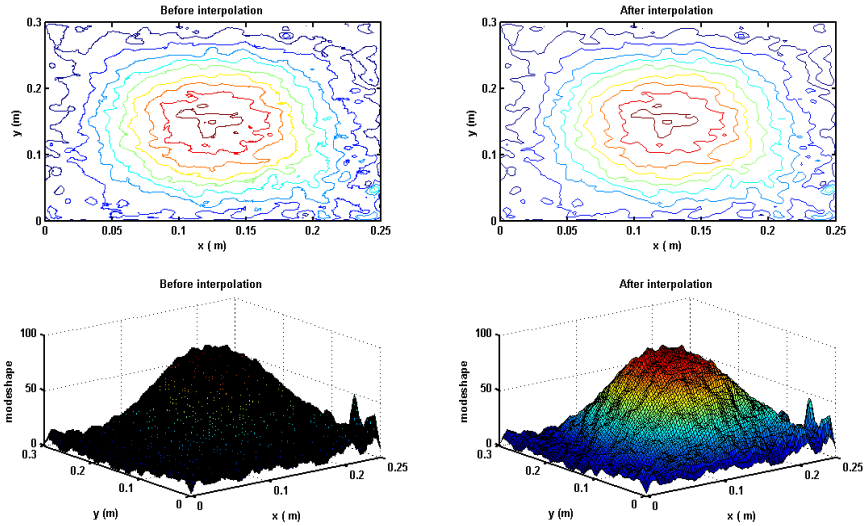

Figure 5.10 Contour and surface plots of the first mode of an all-sides-clamped rectangular plate measured by using the Optonor VibroMap 1000 (presented in Matlab).

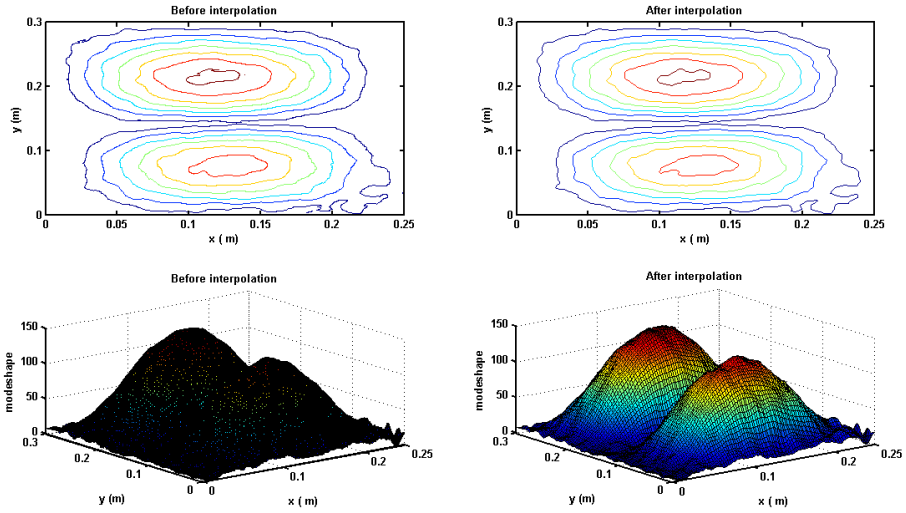

Figure 5.11 Contour and surface plots of the second mode of an all-sides-clamped rectangular plate measured by using the Optonor VibroMap 1000 (presented in Matlab).

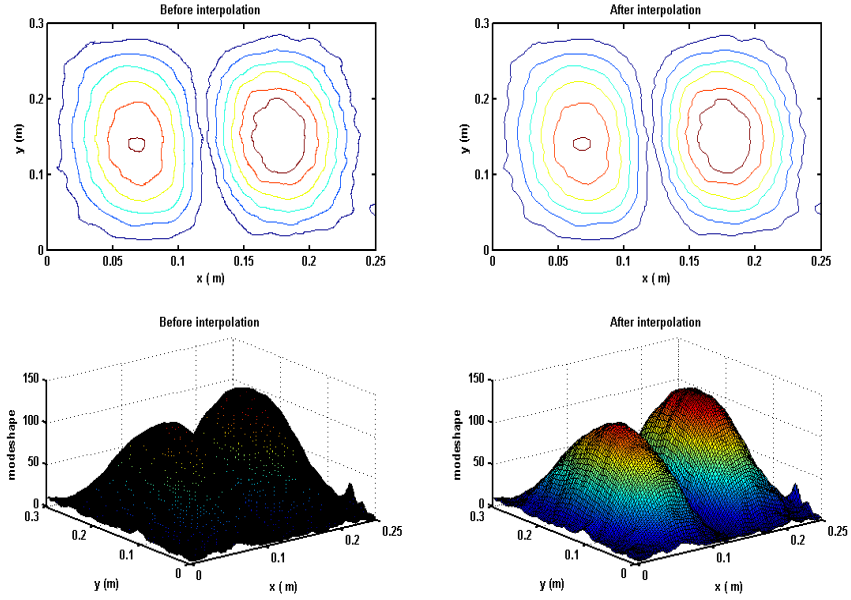

Figure 5.12 Contour and surface plots of the third mode of an all-sides-clamped rectangular plate measured by using the Optonor VibroMap 1000 (presented in Matlab).

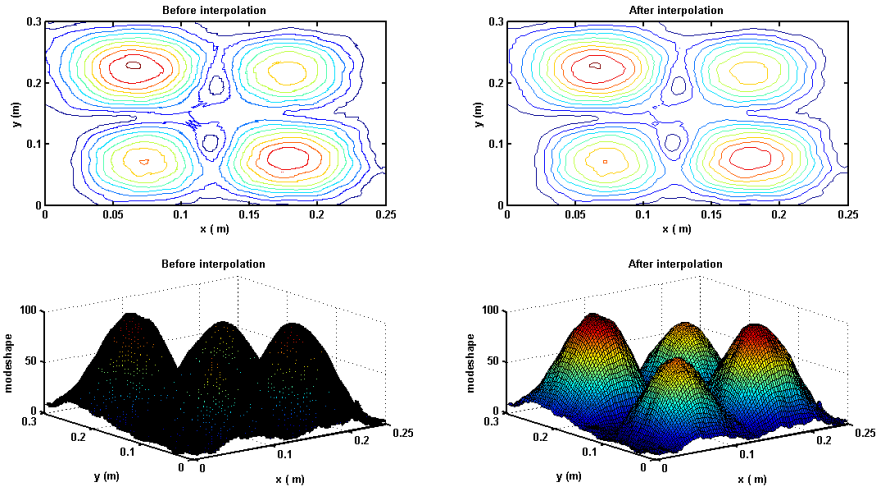

Figure 5.13 Contour and surface plots of the fourth mode of an all-sides-clamped rectangular plate measured by using the Optonor VibroMap 1000 (presented in Matlab).

The frequencies of the all-sides-clamped rectangular plate obtained from other methods (have been mentioned in Chapter 4) are compared here with measurements taken from the Optonor VibroMap 1000.

Frequency	Finite Element Method (Hz)	Rayleigh-Ritz Method (Hz)	Virtual Work Method (Hz)	VibroMap Measurement (Hz)
First	233.64	233.30	233.33	233.50
Second	442.61	424.43	422.48	390.50
Third	526.82	528.13	525.62	487.70
Fourth	700.39	707.41	700.54	651.40

Table 5.1 Comparison of the first-four frequencies of an all-sides-clamped rectangular plate between the Finite Element Method (FEM), the Rayleigh-Ritz method, the Virtual work method, and the VibroMap measurement.

The percentage difference is calculated by the equation:

$$\text{PD} = \left(\frac{\text{abs(other method - VibroMap measurement)}}{\text{VibroMap measurement}}\right) \times 100\% \qquad (5.1)$$

The results of percentage different between VibroMap measurement and other prediction methods are presented on table 5.2.

Frequency	Percentage difference (PD) 1 (%)	Percentage difference (PD) 2 (%)	Percentage difference (PD) 3 (%)
First	0.0599	0.0857	0.0728
Second	12.5098	8.3271	7.8674
Third	7.7120	7.9600	7.4843
Fourth	7.2482	8.2440	7.2696

Table 5.2 Percentage difference (PD) for frequencies between the Optonor VibroMap 1000 measurement and other methods.

Table 5.2 shows the errors in the mode frequency between vibromap and various prediction methods. PD 1 is percentage difference between the FEM and VibroMap measurement, PD 2 is percentage difference between the Rayleigh-Ritz method and VibroMap measurement, and PD 3 is percentage difference between the Virtual work method and VibroMap measurement.

Not only has the measured frequency information of an all-sides-clamped rectangular plate without an attached mass been compared with other methods but also the mode shape information using the Root Mean Square (RMS) error. The first step before compare the mode shapes obtained from theoretical and experimental is applied normalisation to the mode shape data. Previously described in Chapter 2 page 30, normalisation is essentially a scaling of a mode shape either by insisting that the generalised is unity or by insisting that the largest component is set to some value, such as unity. In this case, the normalisation that applied to the mode shape data obtained using theory and experiment are scaling the largest component to unity. Each displacement value in a particular mode shape is scaled so that maximum displacement is 1 by dividing each value in the mode shape (eigenvector) by the maximum value in the mode shape. To measure the mode shape error between Rayleigh-Ritz method and other methods is by using the Root Mean Square (RMS) error. The RMS error is a statistical measure to quantify the varying difference between the predicted values and the observed true values.

The percentage error between the mode shape from other methods and the measured mode shape from Vibromap is obtained from:

$$\text{Mean difference}=\text{mean}\left[\frac{\text{difference}}{\max(\max(\text{measured mode shape}))}\right] \tag{5.2}$$

and

$$RMS_{error} = \sqrt[2]{(Mean\ difference)^2} \times 100\ \% \tag{5.3}$$

Mode shapes	PE 1 (%)	PE 2 (%)	PE 3 (%)
First mode	6.5648	6.5243	6.4229
Second mode	48.1568	52.7359	52.3996
Third mode	53.6759	52.8673	52.0700
Fourth mode	46.1109	54.8118	55.7534

Table 5.3 Percentage error (PE) for mode shapes between the Optonor VibroMap 1000 measurement and other methods.

Table 5.3 shows the RMS mode shape error where = PE 1 is the percentage error between the Rayleigh-Ritz method and the VibroMap measurement, PE 2 is the percentage error between the Finite Element method and the VibroMap measurement, and PE 3 is the percentage error between the Virtual work method and the VibroMap measurement.

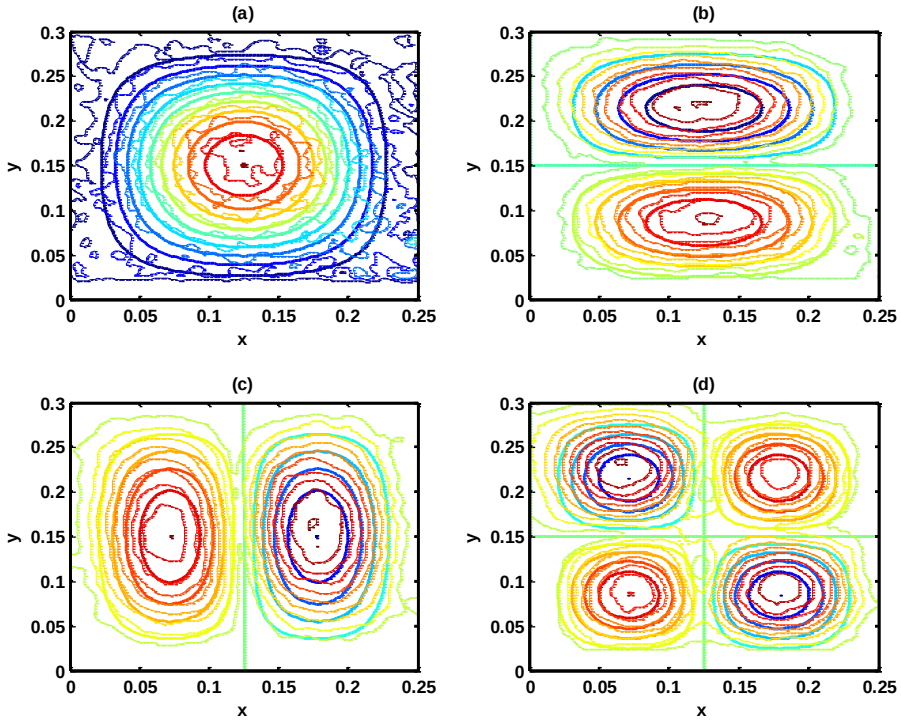

Figure 5.14 Contour plots of the first-four mode shapes from an all-sides-clamped rectangular plate without an attached mass where (-) is from the Rayleigh-Ritz method and (.) is from VibroMap measurement. (a): first mode; (b): second mode; (c): third mode; and (d): fourth mode.

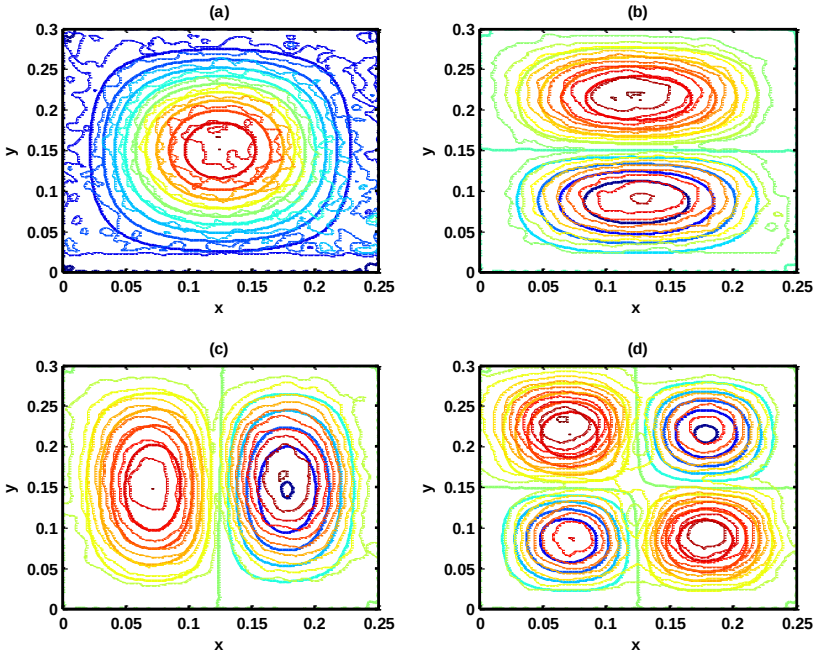

Figure 5.15 Contour plots of the first-four mode shapes from all-sides-clamped rectangular plate without an attached mass where (-) is from the FEM method and (.) is from VibroMap measurement. (a): first mode; (b): second mode; (c): third mode; and (d): fourth mode.

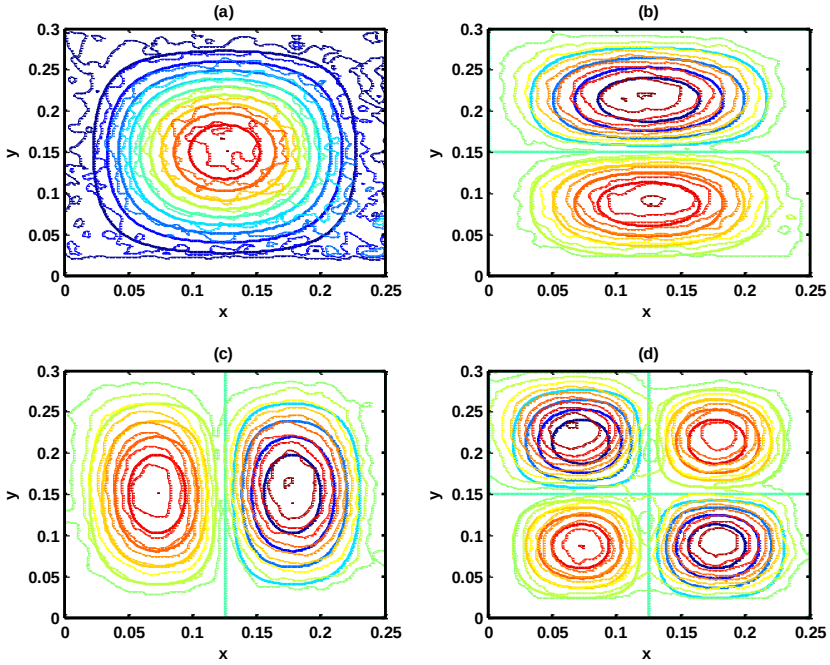

Figure 5.16 Contour plots of the first-four mode shapes from an all-sides-clamped rectangular plate without an attached mass where (-) is from the Virtual method and (.) is from VibroMap measurement. (a): first mode; (b): second mode; (c): third mode; and (d): fourth mode.

5.3 Mode shapes of all-sides clamped rectangular plate with an attached mass

Placing a point mass in a random position is one of approaches for introducing uncertainty into the plate structures (previously explained in Chapter 4). Measuring the mode shape of an all-sides-clamped rectangular plate with an attached mass follows exactly the same procedure as for the case without an attached mass. The random sections of a point mass are generated by Monte Carlo simulation and used position for placing a point mass on the plate. Table 5.4 shows the random sections of the point mass for example in 6 positions.

Position	x (m)	y (m)
1	0.045	0.042
2	0.130	0.129
3	0.194	0.030
4	0.037	0.181
5	0.146	0.196
6	0.076	0.126

Table 5.4 Random positions of a point mass on the all-sides-clamped rectangular plate.

For these 6 positions it is useful to shortly see the measured mode shapes and the corresponding reduced array (presented by Matlab).

Frequency	Using Rayleigh-Ritz (Hz)	VibroMap (Hz)
First Frequency	233.22	241.90
Second Frequency	423.60	386.90
Third Frequency	527.05	481.60
Fourth Frequency	700.62	618.60

Table 5.5 The first-four frequencies of all-sides clamped rectangular plate with an attached point mass (x=0.045 m and y=0.042 m) using the Rayleigh-Ritz method and the VibroMap measurement.

Figure 5.17 shows the measured mode shapes for the first 4 modes and 5.18 shows the reduced array contour plot (for the first mass position in Table 5.4). Figure 5.19 – 5.27 show the corresponding results for the other five positions.

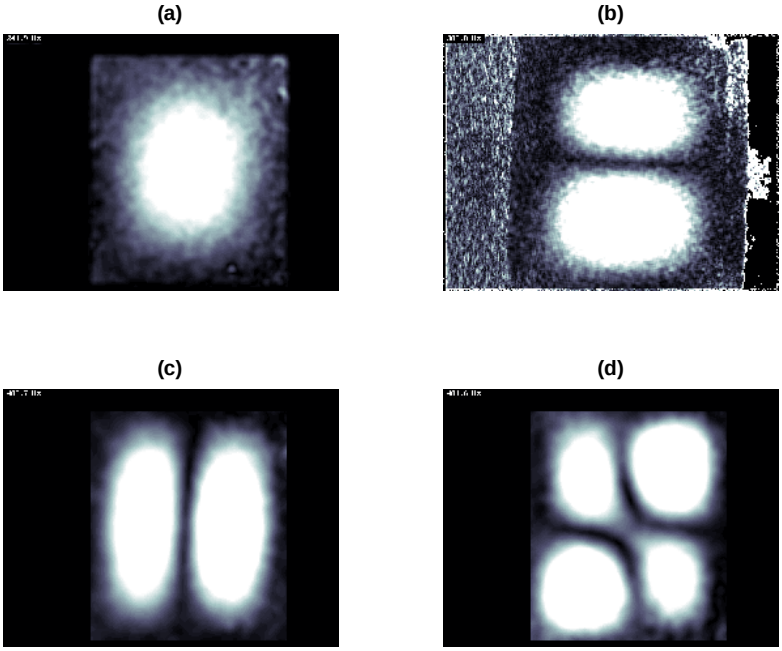

Figure 5.17 The first-four mode shape images of the all-sides-clamped rectangular plate with an attached mass at the first location 0.045 m (x direction) and 0.042 m (y direction) obtained by using the Optonor Vibromap 1000. (a): first mode; (b): second mode; (c): third mode; and (d): fourth mode.

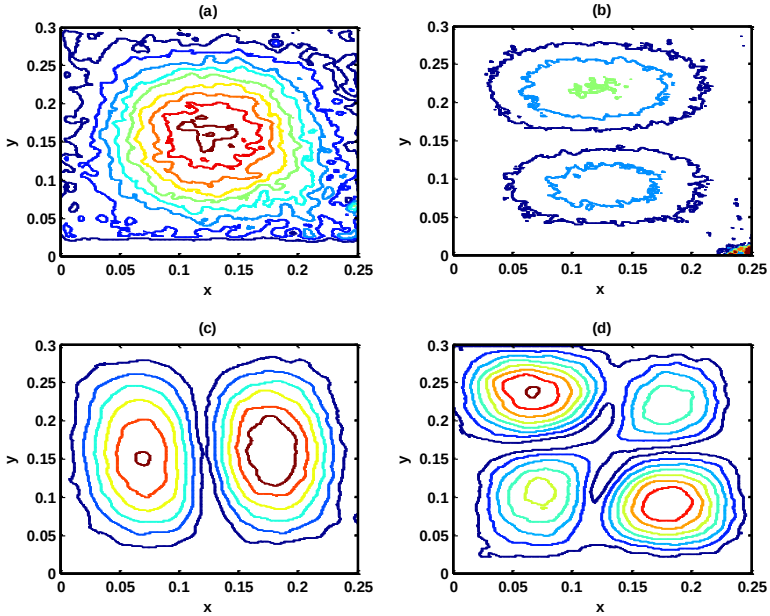

Figure 5.18 Contour of the first four mode shapes of the all-sides-clamped rectangular plate with an attached mass at location 0.045 m x direction and 0.042 m y direction, measured by using the Optonor VibroMap 1000 (presented in Matlab). (a): first mode; (b): second mode; (c): third mode; and (d): fourth mode.

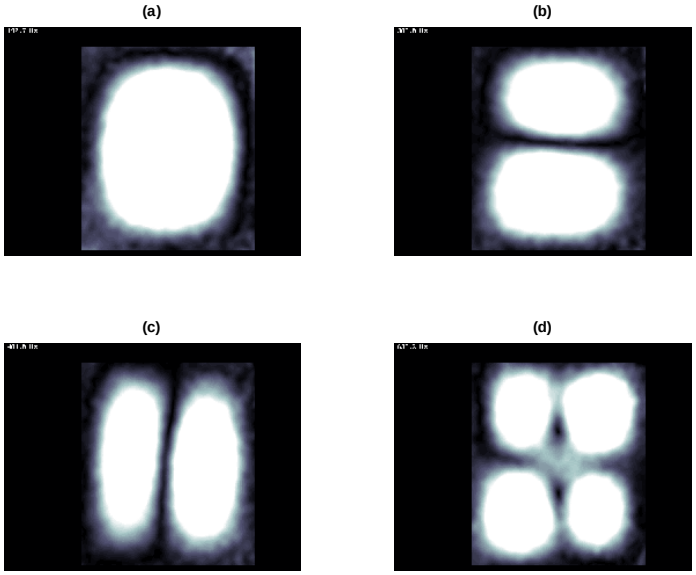

Figure 5.19 The first-four mode shape images of the all-sides-clamped rectangular plate obtained by using the Optonor Vibromap 1000 at second position 0.130 m x direction and 0.129 m y direction. (a): first mode; (b): second mode; (c): third mode; and (d): fourth mode.

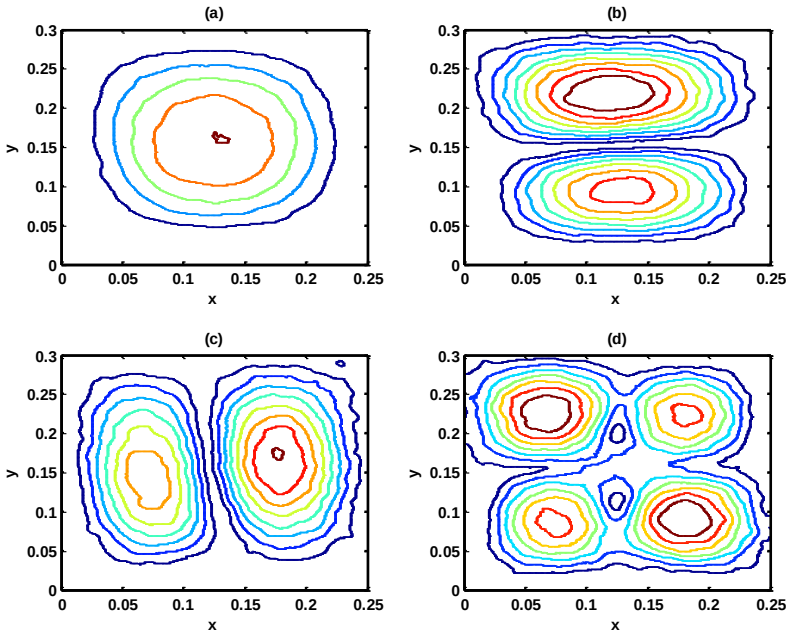

Figure 5.20 Contour of the first four mode shapes of the all-sides-clamped rectangular plate with an attached mass at location 0.130 m x direction and 0.129 m y direction, measured by using the Optonor VibroMap 1000 (presented in Matlab). (a): first mode; (b): second mode; (c): third mode; and (d): fourth mode.

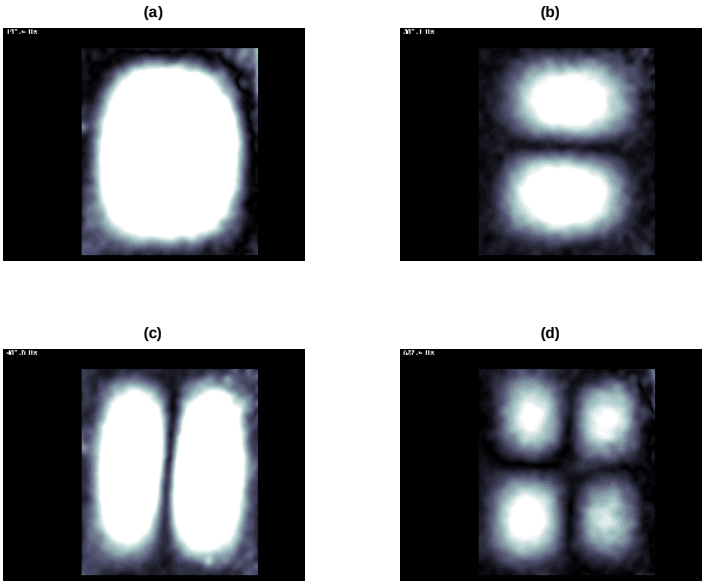

Figure 5.21 The first-four mode shape images of the all-sides-clamped rectangular plate obtained by using the Optonor Vibromap 1000 at third position 0.194 m x direction and 0.030 m y direction. (a): first mode; (b): second mode; (c): third mode; and (d): fourth mode.

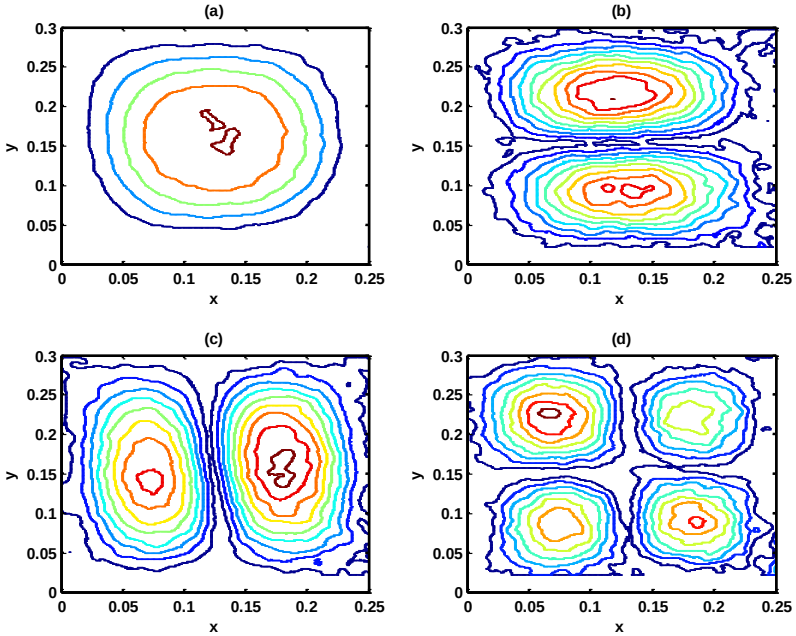

Figure 5.22 Contour of first four mode shapes of all-sides clamped rectangular plate with an attached mass at location 0.194 m x direction and 0.030 m y direction, measured by using the Optonor VibroMap 1000 and presented in Matlab figure. (a): first mode; (b): second mode; (c): third mode; and (d): fourth mode.

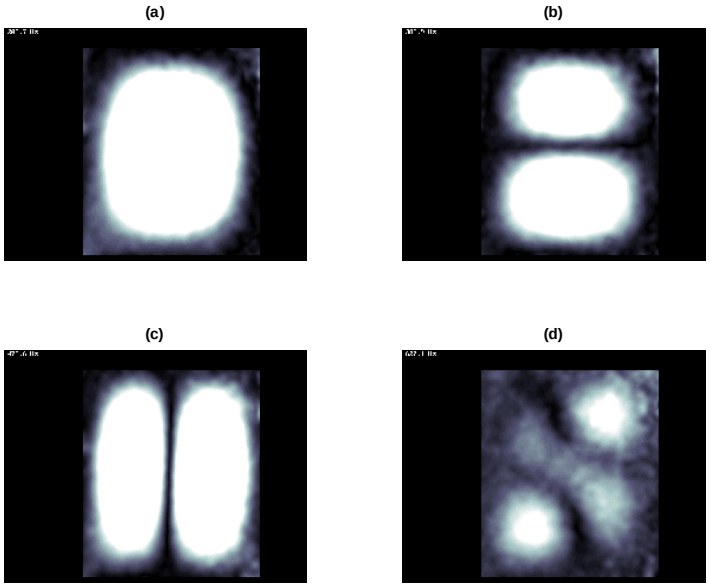

Figure 5.23 The first-four mode shape images of the all-sides-clamped rectangular plate obtained by using the Optonor Vibromap 1000 at fourth position 0.037 m x direction and 0.181 m y direction. (a): first mode; (b): second mode; (c): third mode; and (d): fourth mode.

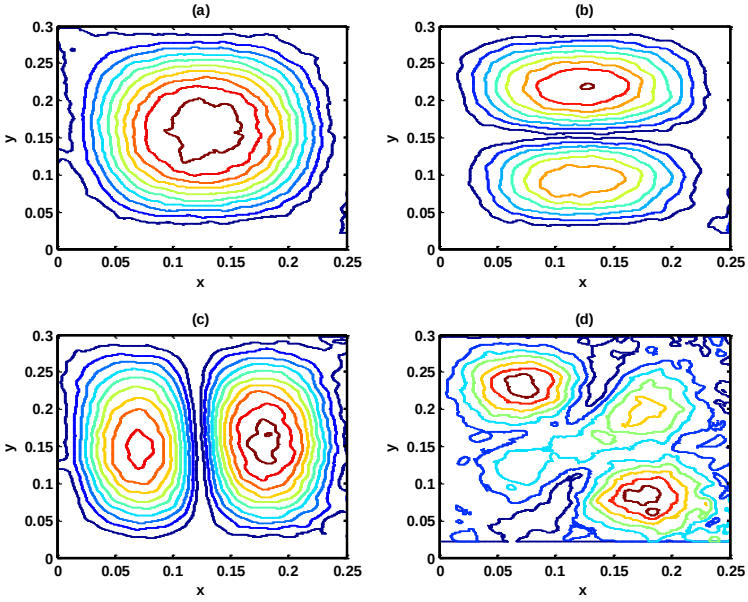

Figure 5.24 Contour of the first four mode shapes of the all-sides-clamped rectangular plate with an attached mass at location 0.037 m x direction and 0.181 m y direction, measured by using the Optonor VibroMap 1000 (presented in Matlab). (a): first mode; (b): second mode; (c): third mode; and (d): fourth mode.

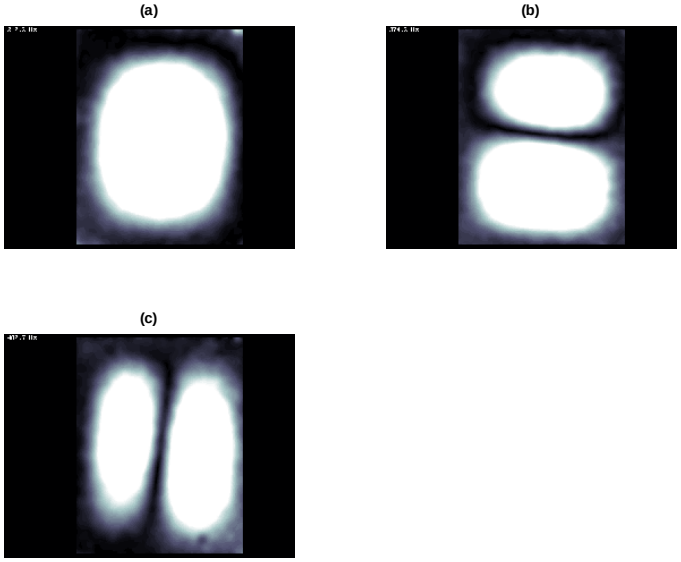

Figure 5.22 The first-three mode shape images of the all-sides-clamped rectangular plate obtained by using the Optonor Vibromap 1000 at fifth position 0.146 m x direction and 0.196 m y direction. (a): first mode; (b): second mode; and (c): third mode. The fourth mode cannot be found for this case.

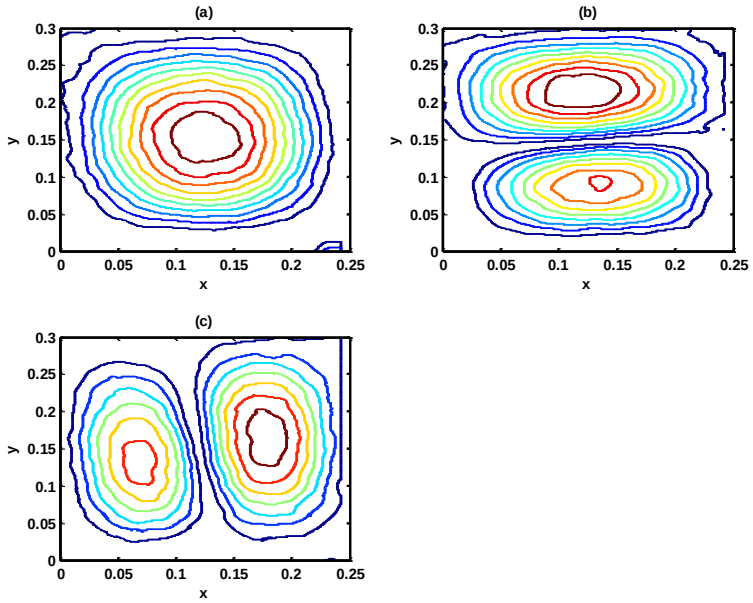

Figure 5.25 Contour of the first three mode shapes of the all-sides-clamped rectangular plate with an attached mass at location 0.146 m x direction and 0.196 m y direction, measured by using the Optonor VibroMap 1000 (presented in Matlab). (a): first mode; (b): second mode; (c): third mode; and (d): fourth mode: The fourth mode could not be found from this case.

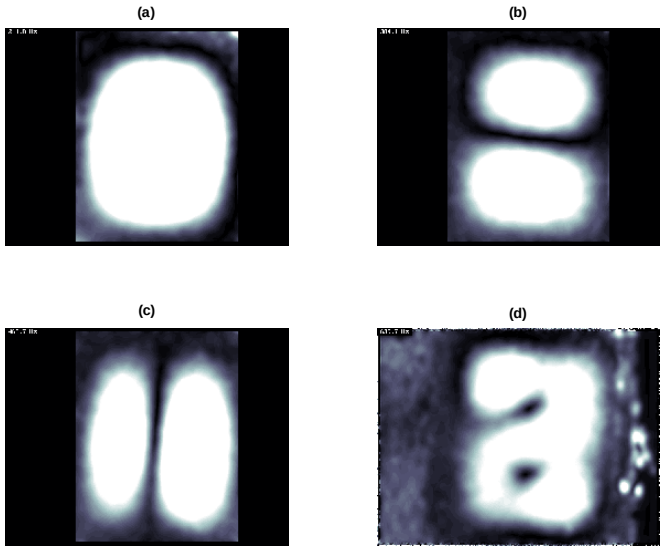

Figure 5.26 The first-four mode shape images of the all-sides-clamped rectangular plate obtained by using the Optonor Vibromap 1000 at sixth position 0.076 m x direction and 0.126 m y direction. (a): first mode; (b): second mode; (c): third mode; and (d): fourth position. The fourth mode did not captured clear enough.

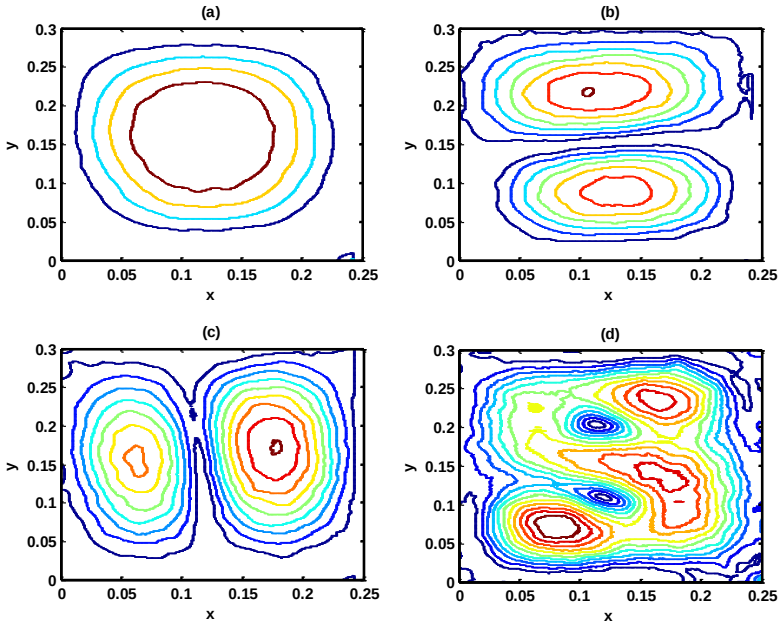

Figure 5.27 Contour of the first four mode shapes of the all-sides-clamped rectangular plate with an attached mass at location 0.076 m x direction and 0.126 m y direction, measured by using the Optonor VibroMap 1000 (presented in Matlab). (a): first mode; (b): second mode; (c): third mode; and (d): fourth mode.

Conclusions of Chapter 5

The VibroMap measured mode shapes with the mass point random positions varying in the x and y direction can now be used for estimating the log-likelihood for example to obtain the standard deviation of the mass position instead of using predicted mode shapes (as in Chapter 5).

A laser-based measurement system has been discussed along with an experimental plate rig to enable the effect of positioning a point mass randomly to be quantified. The system enables both plate frequencies and mode shapes to be measured.

In summarising the achievements using laser-based VibroMap 1000 to identify mode shapes it has been possible to use VibroMap in quantitative mode to measure displacement amplitudes very accurately. The measured mode frequencies and mode shapes can be used to verify approximate free-vibration predictions of frequencies and mode shapes. Appropriate tuning of the noise reduction capabilities made it possible to minimise measurement noise (although not entirely).

VibroMap is very sensitive to external sources of background noise, such as ventilation fans in buildings. Completely isolating the influence of this background noise can be a major problem. Also owing the high level of sensitivity VibroMap is sensitive to changes in temperature, which can be a source of error. VibroMap is used to measure forced-vibration mode shapes, and therefore any comparison with free-vibration predictions will be in error owing the presence of damping in the measurement. Because VibroMap relies on observation with the naked eye, it can be difficult to identify higher modes.

CHAPTER 6

EXPERIMENTAL VERIFICATION OF AN EFFICIENT UNCERTAINTY IDENTIFICATION METHOD ON PLATE STRUCTURES

Experimental verification and validation is needed to see how efficient the uncertainty estimation method is on the plate structure discussed in Chapter 4. The mode shapes obtained by using VibroMap (presented in Chapter 5) will now be used as the response information for estimating the standard deviation of the point mass positions for the all-sides-clamped rectangular plate.

6.1 Approximating the mode shapes from VibroMap measured data.

The mode shape approximation function, equation (4.10), is used to derive the weights of the base functions (by multiplying left and right terms with chosen base functions and double integrating the base functions). Equation (4.10) then becomes:

$$W(x,y)X_p(x)Y_q(y)=\sum_{m=1}^{M}\sum_{n=1}^{N}C_{mn}X_m(x)Y_n(y)X_p(x)Y_q(y) \tag{6.1}$$

The double integration of equation (6.1) can be written:

$$\int_0^a\int_0^b W(x,y)X_p(x)Y_q(y)\,dx\,dy=\sum_{m=1}^{M}\sum_{n=1}^{N}C_{mn}\int_0^a\int_0^b X_m(x)Y_n(y)X_p(x)Y_q(y)\,dx\,dy \tag{6.2}$$

In matrix form, equation (6.2) becomes:

$$[I_{pq}]=[I_{mnpq}][C_{mn}] \tag{6.3}$$

The coefficients C_{mn} in equation (6.1) are obtained by solving the matrix equation (6.3) to determine as many terms as needed to get the weights of the base functions where:

$$[I_{pq}] = \int_0^a \int_0^b W_{(x,y)} X_p(x) Y_q(y)\, dx\, dy \tag{6.4}$$

and

$$[I_{mnpq}] = \int_0^a \int_0^b X_m(x) Y_n(y) X_p(x) Y_q(y)\, dx\, dy \tag{6.5}$$

Maple (mathematical software) has been used to calculate the individual terms I_{mnpq} (eq. 6.4), for example I_{1111}, I_{2111}, I_{3111}, and so on.
As an example for m = n = p = q = 1, I_{1111} from Maple is:

$$I_{1111} = \int_0^a \int_0^b X_m(x) Y_n(y) X_p(x) Y_q(y)\, dx\, dy \tag{6.6}$$

On substitution of X_m (x), Y_n (y), X_p (x) and Y_q (y) using the base function in table 4.1 for a beam of clamped-clamped type, equation (6.6) becomes:

$$I_{1111} = \int_0^a \int_0^b \sin\left(\frac{\pi x}{a}\right) \sin\left(\frac{m\pi x}{a}\right) \sin\left(\frac{\pi y}{b}\right) \sin\left(\frac{n\pi y}{b}\right) \sin\left(\frac{\pi x}{a}\right) \sin\left(\frac{p\pi x}{a}\right) \sin\left(\frac{\pi y}{b}\right) \sin\left(\frac{q\pi y}{b}\right) dxdy \tag{6.7}$$

For example putting the values m = n = p = q =1, equation (6.7) becomes:

$$I_{1111} = \int_0^a \int_0^b \sin\left(\frac{\pi x}{a}\right) \sin\left(\frac{1\pi x}{a}\right) \sin\left(\frac{\pi y}{b}\right) \sin\left(\frac{1\pi y}{b}\right) \sin\left(\frac{\pi x}{a}\right) \sin\left(\frac{1\pi x}{a}\right) \sin\left(\frac{\pi y}{b}\right) \sin\left(\frac{1\pi y}{b}\right) dxdy \tag{6.8}$$

which reduces to:

$$I_{1111} = \frac{9}{64} a \times b \tag{6.9}$$

Other index combinations of m, n, p and q that vary with the number of terms (M and N), can easily be constructed with Maple, for example putting the result into a matrix equation gives for the following five cases: for M = N = 1 represented by equations (6.10) and (6.11); for M = N = 2 represented by equations (6.12) and (6.13); for M = N = 3 represented by equations (6.14) and (6.15); for M = N = 4 represented by equations (6.16) and (6.17); and for M = N = 5 represented by equations (6.18) and (6.19).

- For M = N = 1

$$[I_{11}] = [I_{1111}][C_{11}] \tag{6.10}$$

or

$$[I_{11}] = \left[\frac{9}{64}ab\right][C_{11}] \tag{6.11}$$

- For M = N = 2

$$\begin{bmatrix} I_{11} \\ I_{21} \\ I_{12} \\ I_{22} \end{bmatrix} = \begin{bmatrix} I_{1111} & I_{2111} & I_{1211} & I_{2211} \\ I_{1121} & I_{2121} & I_{1221} & I_{2221} \\ I_{1112} & I_{2112} & I_{1212} & I_{2212} \\ I_{1122} & I_{2122} & I_{1222} & I_{2222} \end{bmatrix} \begin{bmatrix} C_{11} \\ C_{21} \\ C_{12} \\ C_{22} \end{bmatrix} \tag{6.12}$$

or

$$\begin{bmatrix} I_{11} \\ I_{21} \\ I_{12} \\ I_{22} \end{bmatrix} = \begin{bmatrix} \frac{9}{64}ab & 0 & 0 & 0 \\ 0 & \frac{3}{32}ab & 0 & 0 \\ 0 & 0 & \frac{3}{32}ab & 0 \\ 0 & 0 & 0 & \frac{1}{16}ab \end{bmatrix} \begin{bmatrix} C_{11} \\ C_{21} \\ C_{12} \\ C_{22} \end{bmatrix} \tag{6.13}$$

- For M = N = 3

$$\begin{bmatrix} I_{11} \\ I_{21} \\ I_{31} \\ I_{12} \\ I_{22} \\ I_{32} \\ I_{13} \\ I_{23} \\ I_{33} \end{bmatrix} = \begin{bmatrix} I_{1111} & I_{2111} & I_{3111} & I_{1211} & I_{2211} & I_{3211} & I_{1311} & I_{2311} & I_{3311} \\ I_{1121} & I_{2121} & I_{3121} & I_{1221} & I_{2221} & I_{3221} & I_{1321} & I_{2321} & I_{3321} \\ I_{1131} & I_{2131} & I_{3131} & I_{1231} & I_{2231} & I_{3231} & I_{1331} & I_{2331} & I_{3331} \\ I_{1112} & I_{2112} & I_{3112} & I_{1212} & I_{2212} & I_{3212} & I_{1312} & I_{2312} & I_{3312} \\ I_{1122} & I_{2122} & I_{3122} & I_{1222} & I_{2222} & I_{3222} & I_{1322} & I_{2322} & I_{3322} \\ I_{1132} & I_{2132} & I_{3132} & I_{1232} & I_{2232} & I_{3232} & I_{1332} & I_{2332} & I_{3332} \\ I_{1113} & I_{2113} & I_{3113} & I_{1213} & I_{2213} & I_{3213} & I_{1313} & I_{2313} & I_{3313} \\ I_{1123} & I_{2123} & I_{3123} & I_{1223} & I_{2223} & I_{3223} & I_{1323} & I_{2323} & I_{3323} \\ I_{1133} & I_{2133} & I_{3133} & I_{1233} & I_{2233} & I_{3233} & I_{1333} & I_{2333} & I_{3333} \end{bmatrix} \begin{bmatrix} C_{11} \\ C_{21} \\ C_{31} \\ C_{12} \\ C_{22} \\ C_{32} \\ C_{13} \\ C_{23} \\ C_{33} \end{bmatrix} \tag{6.14}$$

or

$$\begin{bmatrix} I_{11} \\ I_{21} \\ I_{31} \\ I_{12} \\ I_{22} \\ I_{32} \\ I_{13} \\ I_{23} \\ I_{33} \end{bmatrix} = \begin{bmatrix} \frac{9}{64}ab & 0 & -\frac{3}{64}ab & 0 & 0 & 0 & -\frac{3}{64}ab & 0 & \frac{1}{64}ab \\ 0 & \frac{3}{32}ab & 0 & 0 & 0 & 0 & 0 & -\frac{1}{32}ab & 0 \\ -\frac{3}{64} & 0 & \frac{3}{32}ab & 0 & 0 & 0 & \frac{1}{64}ab & 0 & -\frac{1}{32}ab \\ 0 & 0 & 0 & \frac{3}{32}ab & 0 & -\frac{1}{32}ab & 0 & 0 & 0 \\ 0 & 0 & 0 & 0 & \frac{1}{16}ab & 0 & 0 & 0 & 0 \\ 0 & 0 & 0 & -\frac{1}{32}ab & 0 & \frac{1}{16}ab & 0 & 0 & 0 \\ -\frac{3}{64}ab & 0 & \frac{1}{64}ab & 0 & 0 & 0 & \frac{3}{32}ab & 0 & -\frac{1}{32}ab \\ 0 & -\frac{1}{32}ab & 0 & 0 & 0 & 0 & 0 & \frac{1}{16}ab & 0 \\ \frac{1}{64}ab & 0 & -\frac{1}{32}ab & 0 & 0 & 0 & -\frac{1}{32}ab & 0 & \frac{1}{16}ab \end{bmatrix} \begin{bmatrix} C_{11} \\ C_{21} \\ C_{31} \\ C_{12} \\ C_{22} \\ C_{32} \\ C_{13} \\ C_{23} \\ C_{33} \end{bmatrix} \tag{6.15}$$

- For M = N = 4, the matrices are shown on equations (6.16) and (6.17).
- For M = N = 5, the matrices are shown on equations (6.18) and (6.19).

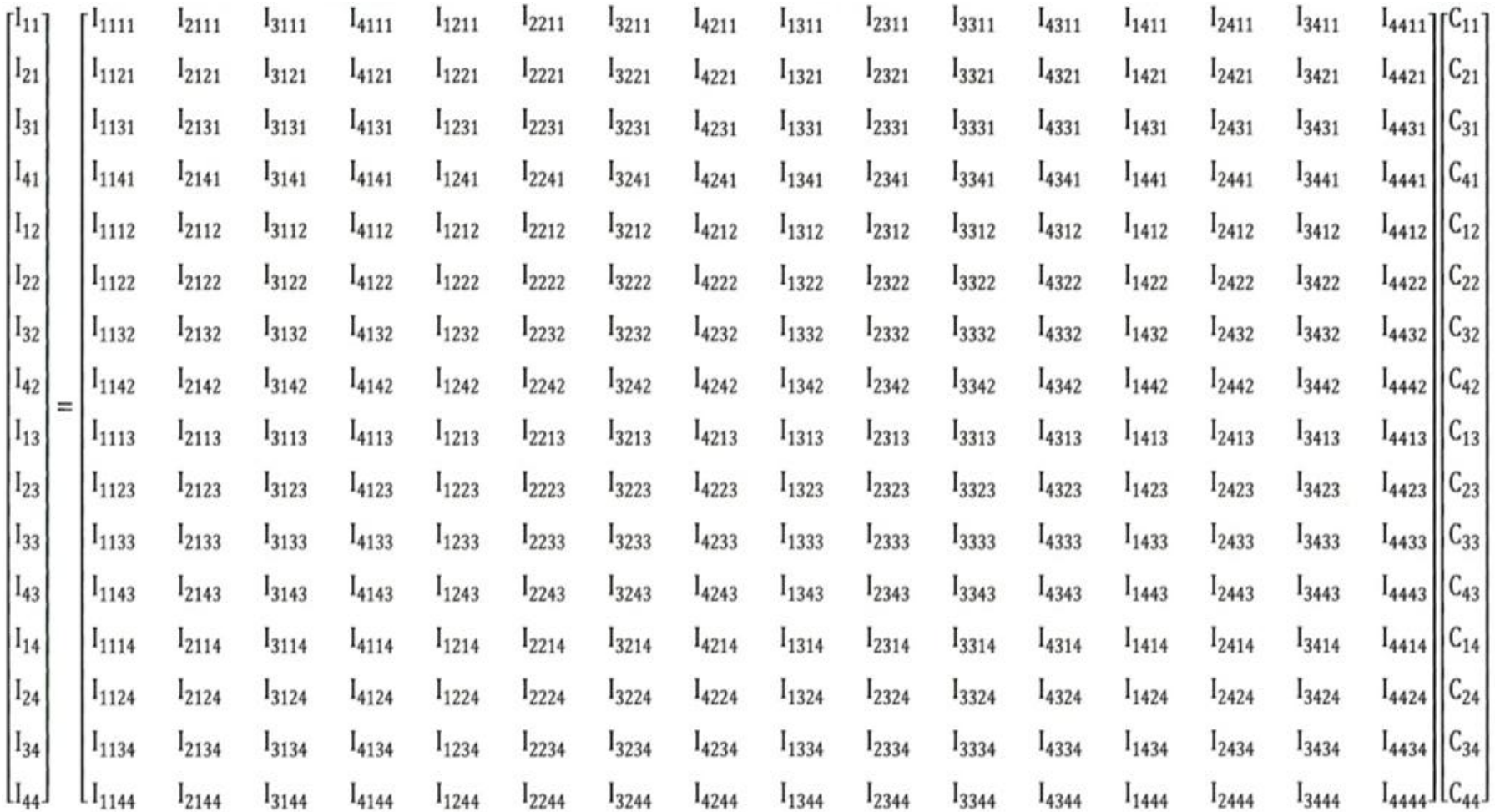

$$\begin{bmatrix} I_{11} \\ I_{21} \\ I_{31} \\ I_{41} \\ I_{12} \\ I_{22} \\ I_{32} \\ I_{42} \\ I_{13} \\ I_{23} \\ I_{33} \\ I_{43} \\ I_{14} \\ I_{24} \\ I_{34} \\ I_{44} \end{bmatrix} = \begin{bmatrix} I_{1111} & I_{2111} & I_{3111} & I_{4111} & I_{1211} & I_{2211} & I_{3211} & I_{4211} & I_{1311} & I_{2311} & I_{3311} & I_{4311} & I_{1411} & I_{2411} & I_{3411} & I_{4411} \\ I_{1121} & I_{2121} & I_{3121} & I_{4121} & I_{1221} & I_{2221} & I_{3221} & I_{4221} & I_{1321} & I_{2321} & I_{3321} & I_{4321} & I_{1421} & I_{2421} & I_{3421} & I_{4421} \\ I_{1131} & I_{2131} & I_{3131} & I_{4131} & I_{1231} & I_{2231} & I_{3231} & I_{4231} & I_{1331} & I_{2331} & I_{3331} & I_{4331} & I_{1431} & I_{2431} & I_{3431} & I_{4431} \\ I_{1141} & I_{2141} & I_{3141} & I_{4141} & I_{1241} & I_{2241} & I_{3241} & I_{4241} & I_{1341} & I_{2341} & I_{3341} & I_{4341} & I_{1441} & I_{2441} & I_{3441} & I_{4441} \\ I_{1112} & I_{2112} & I_{3112} & I_{4112} & I_{1212} & I_{2212} & I_{3212} & I_{4212} & I_{1312} & I_{2312} & I_{3312} & I_{4312} & I_{1412} & I_{2412} & I_{3412} & I_{4412} \\ I_{1122} & I_{2122} & I_{3122} & I_{4122} & I_{1222} & I_{2222} & I_{3222} & I_{4222} & I_{1322} & I_{2322} & I_{3322} & I_{4322} & I_{1422} & I_{2422} & I_{3422} & I_{4422} \\ I_{1132} & I_{2132} & I_{3132} & I_{4132} & I_{1232} & I_{2232} & I_{3232} & I_{4232} & I_{1332} & I_{2332} & I_{3332} & I_{4332} & I_{1432} & I_{2432} & I_{3432} & I_{4432} \\ I_{1142} & I_{2142} & I_{3142} & I_{4142} & I_{1242} & I_{2242} & I_{3242} & I_{4242} & I_{1342} & I_{2342} & I_{3342} & I_{4342} & I_{1442} & I_{2442} & I_{3442} & I_{4442} \\ I_{1113} & I_{2113} & I_{3113} & I_{4113} & I_{1213} & I_{2213} & I_{3213} & I_{4213} & I_{1313} & I_{2313} & I_{3313} & I_{4313} & I_{1413} & I_{2413} & I_{3413} & I_{4413} \\ I_{1123} & I_{2123} & I_{3123} & I_{4123} & I_{1223} & I_{2223} & I_{3223} & I_{4223} & I_{1323} & I_{2323} & I_{3323} & I_{4323} & I_{1423} & I_{2423} & I_{3423} & I_{4423} \\ I_{1133} & I_{2133} & I_{3133} & I_{4133} & I_{1233} & I_{2233} & I_{3233} & I_{4233} & I_{1333} & I_{2333} & I_{3333} & I_{4333} & I_{1433} & I_{2433} & I_{3433} & I_{4433} \\ I_{1143} & I_{2143} & I_{3143} & I_{4143} & I_{1243} & I_{2243} & I_{3243} & I_{4243} & I_{1343} & I_{2343} & I_{3343} & I_{4343} & I_{1443} & I_{2443} & I_{3443} & I_{4443} \\ I_{1114} & I_{2114} & I_{3114} & I_{4114} & I_{1214} & I_{2214} & I_{3214} & I_{4214} & I_{1314} & I_{2314} & I_{3314} & I_{4314} & I_{1414} & I_{2414} & I_{3414} & I_{4414} \\ I_{1124} & I_{2124} & I_{3124} & I_{4124} & I_{1224} & I_{2224} & I_{3224} & I_{4224} & I_{1324} & I_{2324} & I_{3324} & I_{4324} & I_{1424} & I_{2424} & I_{3424} & I_{4424} \\ I_{1134} & I_{2134} & I_{3134} & I_{4134} & I_{1234} & I_{2234} & I_{3234} & I_{4234} & I_{1334} & I_{2334} & I_{3334} & I_{4334} & I_{1434} & I_{2434} & I_{3434} & I_{4434} \\ I_{1144} & I_{2144} & I_{3144} & I_{4144} & I_{1244} & I_{2244} & I_{3244} & I_{4244} & I_{1344} & I_{2344} & I_{3344} & I_{4344} & I_{1444} & I_{2444} & I_{3444} & I_{4444} \end{bmatrix} \begin{bmatrix} C_{11} \\ C_{21} \\ C_{31} \\ C_{41} \\ C_{12} \\ C_{22} \\ C_{32} \\ C_{42} \\ C_{13} \\ C_{23} \\ C_{33} \\ C_{43} \\ C_{14} \\ C_{24} \\ C_{34} \\ C_{44} \end{bmatrix}$$

(6.16)

$$\begin{bmatrix} I_{11} \\ I_{21} \\ I_{31} \\ I_{41} \\ I_{12} \\ I_{22} \\ I_{32} \\ I_{42} \\ I_{13} \\ I_{23} \\ I_{33} \\ I_{43} \\ I_{14} \\ I_{24} \\ I_{34} \\ I_{44} \end{bmatrix} = \begin{bmatrix} \frac{9}{64}ab & 0 & -\frac{3}{64}ab & 0 & 0 & 0 & 0 & 0 & -\frac{3}{64}ab & 0 & \frac{1}{64}ab & 0 & 0 & 0 & 0 & 0 \\ 0 & \frac{3}{32}ab & 0 & -\frac{3}{64}ab & 0 & 0 & 0 & 0 & 0 & -\frac{1}{32}ab & 0 & \frac{1}{64}ab & 0 & 0 & 0 & 0 \\ -\frac{3}{64}ab & 0 & \frac{3}{32}ab & 0 & 0 & 0 & 0 & 0 & \frac{1}{64}ab & 0 & -\frac{1}{32}ab & 0 & 0 & 0 & 0 & 0 \\ 0 & -\frac{3}{64}ab & 0 & \frac{3}{32}ab & 0 & 0 & 0 & 0 & 0 & \frac{1}{64}ab & 0 & -\frac{1}{32}ab & 0 & 0 & 0 & 0 \\ 0 & 0 & 0 & 0 & \frac{3}{32}ab & 0 & -\frac{1}{32}ab & 0 & 0 & 0 & 0 & 0 & -\frac{3}{64}ab & 0 & \frac{1}{64}ab & 0 \\ 0 & 0 & 0 & 0 & 0 & \frac{1}{16}ab & 0 & -\frac{1}{32}ab & 0 & 0 & 0 & 0 & 0 & -\frac{1}{32}ab & 0 & \frac{1}{64}ab \\ 0 & 0 & 0 & 0 & -\frac{1}{32}ab & 0 & \frac{1}{16}ab & 0 & 0 & 0 & 0 & 0 & \frac{1}{64}ab & 0 & -\frac{1}{32}ab & 0 \\ 0 & 0 & 0 & 0 & 0 & -\frac{1}{32}ab & 0 & \frac{1}{16}ab & 0 & 0 & 0 & 0 & 0 & \frac{1}{64}ab & 0 & -\frac{1}{32}ab \\ -\frac{3}{64}ab & 0 & \frac{1}{64}ab & 0 & 0 & 0 & 0 & 0 & \frac{3}{32}ab & 0 & -\frac{1}{32}ab & 0 & 0 & 0 & 0 & 0 \\ 0 & -\frac{1}{32}ab & 0 & \frac{1}{64}ab & 0 & 0 & 0 & 0 & 0 & \frac{1}{16}ab & 0 & -\frac{1}{32}ab & 0 & 0 & 0 & 0 \\ \frac{1}{64}ab & 0 & -\frac{1}{32}ab & 0 & 0 & 0 & 0 & 0 & -\frac{1}{32}ab & 0 & \frac{1}{16}ab & 0 & 0 & 0 & 0 & 0 \\ 0 & \frac{1}{64}ab & 0 & -\frac{1}{32}ab & 0 & 0 & 0 & 0 & 0 & -\frac{1}{32}ab & 0 & \frac{1}{16}ab & 0 & 0 & 0 & 0 \\ 0 & 0 & 0 & 0 & -\frac{3}{64}ab & 0 & \frac{1}{64}ab & 0 & 0 & 0 & 0 & 0 & \frac{3}{32}ab & 0 & -\frac{1}{32}ab & 0 \\ 0 & 0 & 0 & 0 & 0 & -\frac{1}{32}ab & 0 & \frac{1}{64}ab & 0 & 0 & 0 & 0 & 0 & \frac{1}{16}ab & 0 & -\frac{1}{32}ab \\ 0 & 0 & 0 & 0 & \frac{1}{64}ab & 0 & -\frac{1}{32}ab & 0 & 0 & 0 & 0 & 0 & -\frac{1}{32}ab & 0 & \frac{1}{16}ab & 0 \\ 0 & 0 & 0 & 0 & 0 & \frac{1}{64}ab & 0 & -\frac{1}{32}ab & 0 & 0 & 0 & 0 & 0 & -\frac{1}{32}ab & 0 & \frac{1}{16}ab \end{bmatrix} \begin{bmatrix} C_{11} \\ C_{21} \\ C_{31} \\ C_{41} \\ C_{12} \\ C_{22} \\ C_{32} \\ C_{42} \\ C_{13} \\ C_{23} \\ C_{33} \\ C_{43} \\ C_{14} \\ C_{24} \\ C_{34} \\ C_{44} \end{bmatrix}$$

(6.17)

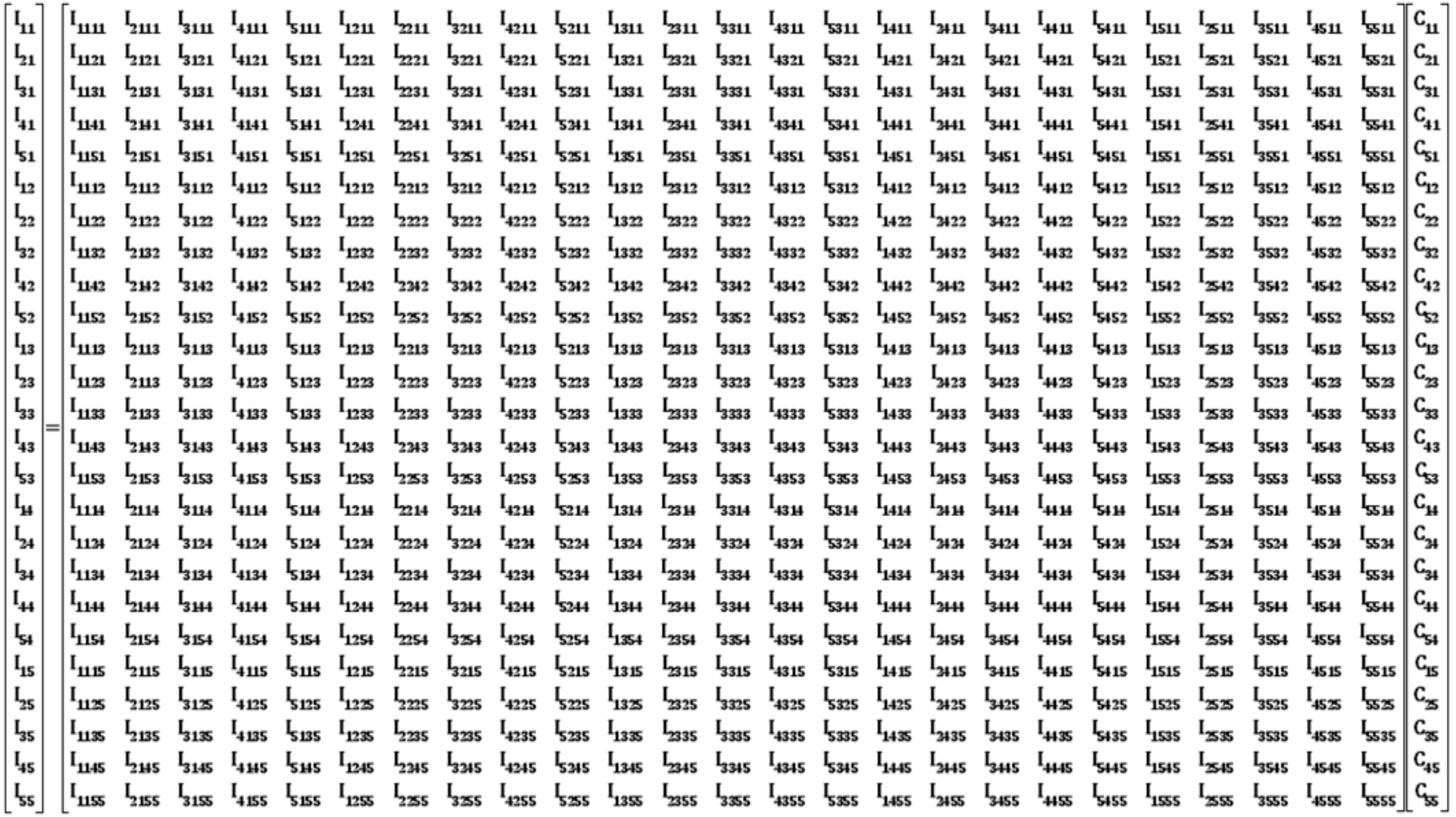

(6.18)

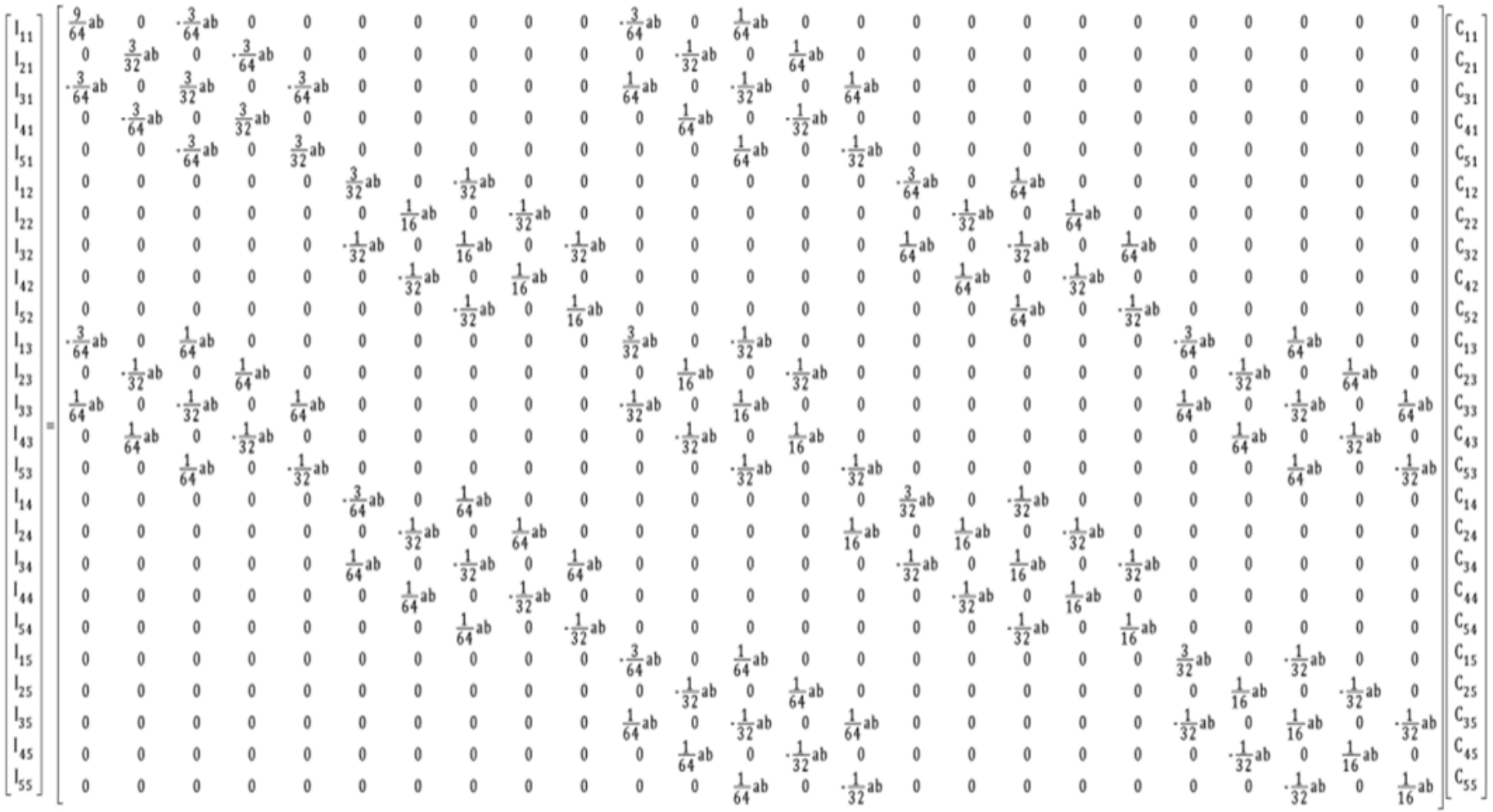

(6.19)

The number of terms used in these symbolic computations are up to 25 terms (M = N = 5). Since W(x,y) is obtained from VibroMap measured data, the term I_{pq} cannot be obtained using Maple because numerical values are needed. I_{pq} is therefore calculated numerically by using Matlab (with the trapz function).

These are the following procedures to fit an approximate mode shape to measured data previously taken via the VibroMap procedure (Chapter 5):

i) Normalise the measured mode shape by dividing by its maximum value and calculating I_{pq} for each set of indices.

ii) Obtain the coefficients (C_{mn}) by solving eq. 6.3 using 1-term, 4-terms, 16-terms and 25-terms.

iii) Use the weights or coefficients (C_{mn}) in the series of base functions in equation (6.1) depending on how many terms have been used.

iv) Compare the approximate (fitted) mode shapes from procedure (iii) with the new measured mode shapes obtained by VibroMap, and the generated mode shapes by Rayleigh-Ritz method, calculating the percentage error (PE) between these methods.

Approximating the mode shape of the all-sides-clamped rectangular plate needs to be verified first by taking the case of the all-sides-clamped rectangular plate without an attached mass.

The measured mode shape of the all-sides-clamped rectangular plate without an attached mass (as previously shown on figure 5.14) is normalised and the weights are extracted using the above procedure. The coefficient vectors are actually eigenvectors (when obtained via the Rayleigh-Ritz method). To make a comparison it is necessary to normalise the magnitude of these vectors to be of magnitude 1 (which Matlab automatically does). The coefficients from these measured mode shapes (both the pre-normalised and the normalised to magnitude 1) are respectively presented in table 6.1 and 6.2 for the first mode, table 6.2 and 6.4 for the second mode, table 6.5 and 6.6 for the third mode, and table 6.7 and 6.8 for the fourth mode.

Coefficient	1 term	4 terms	9 terms	16 terms	25 terms
C1	1.1117	1.1117	1.1897	1.2338	1.2761
C2	N/A	-0.0471	-0.0319	-0.0247	-0.0120
C3		N/A	0.1561	0.1782	0.2481
C4			N/A	0.0144	0.0180
C5				N/A	0.0932
C6		-0.0359	-0.0404	-0.0621	-0.0627
C7		-0.0331	-0.0331	-0.0545	-0.0545
C8		N/A	-0.0136	-0.0243	-0.0261
C9			N/A	-0.0036	-0.0036
C10				N/A	-0.0031
C11			0.0778	0.2101	0.2986
C12			0.0455	0.0534	0.0916
C13			0.0000	0.0662	0.1609
C14			N/A	0.0159	0.0265
C15				N/A	0.0882
C16				-0.0433	-0.0426
C17				-0.0447	-0.0447
C18				-0.0212	-0.0192
C19				-0.0110	-0.0110
C20				N/A	0.0034
C21					0.1276
C22					0.0637
C23					0.0983
C24					0.0178
C25					0.0475

Table 6.1 The coefficients (C_{mn}) of the approximate first mode shape derived from the measured data. C1=C_{11}, C2=C_{21}, C3=C_{31}, C4=C_{41}, C5=C_{51}, C6=C_{12}, C7=C_{22}, C8=C_{32}, C9=C_{42}, C10=C_{52}, C11=C_{13}, C12=C_{23}, C13=C_{33}, C14=C_{43}, C15=C_{53}, C16=C_{14}, C17=C_{24}, C18=C_{34}, C19=C_{44}, C20=C_{54}, C21=C_{15}, C22=C_{25}, C23=C_{35}, C24=C_{45}, and C25=C_{55} (pre-normalised).

Coefficient	1 term	4 terms	9 terms	16 terms	25 terms
C1	1.0000	0.9981	0.9874	0.9699	0.9318
C2	**N/A**	-0.0423	-0.0265	-0.0194	-0.0087
C3		**N/A**	0.1296	0.1401	0.1811
C4			**N/A**	0.0113	0.0131
C5				**N/A**	0.0681
C6		-0.0322	-0.0335	-0.0488	-0.0458
C7		-0.0297	-0.0275	-0.0428	-0.0398
C8		**N/A**	-0.0113	-0.0191	-0.0191
C9			**N/A**	-0.0029	-0.0027
C10				**N/A**	-0.0022
C11			0.0646	0.1652	0.2181
C12			0.0377	0.0420	0.0669
C13			0.0000	0.0520	0.1175
C14			**N/A**	0.0125	0.0194
C15				**N/A**	0.0644
C16				-0.0340	-0.0311
C17				-0.0351	-0.0326
C18				-0.0167	-0.0140
C19				-0.0087	-0.0081
C20				**N/A**	0.0025
C21					0.0932
C22					0.0465
C23					0.0718
C24					0.0130
C25					0.0347

Table 6.2 The normalised Coefficients (C_{mn}) of the approximate first mode shape derived from the measured data. C1=C_{11}, C2=C_{21}, C3=C_{31}, C4=C_{41}, C5=C_{51}, C6=C_{12}, C7=C_{22}, C8=C_{32}, C9=C_{42}, C10=C_{52}, C11=C_{13}, C12=C_{23}, C13=C_{33}, C14=C_{43}, C15=C_{53}, C16=C_{14}, C17=C_{24}, C18=C_{34}, C19=C_{44}, C20=C_{54}, C21=C_{15}, C22=C_{25}, C23=C_{35}, C24=C_{45}, and C25=C_{55}.

Coefficient	1 term	4 terms	9 terms	16 terms	25 terms
C1	0.9160	0.9160	1.1658	1.2461	1.2368
C2	N/A	-0.0878	-0.0940	-0.1832	-0.1855
C3		N/A	0.8333	0.8734	0.8239
C4			N/A	-0.1784	-0.1797
C5				N/A	-0.0953
C6		0.0224	0.0359	0.0371	0.0371
C7		-0.0917	-0.0917	-0.1181	-0.1181
C8		N/A	0.0405	0.0404	0.0405
C9			N/A	-0.0088	-0.0088
C10				N/A	0.0003
C11			-0.0840	0.1569	0.1884
C12			-0.0187	-0.0334	-0.0405
C13			0.0000	0.1205	0.1501
C14			N/A	-0.0295	-0.0335
C15				N/A	0.0113
C16				0.0024	0.0014
C17				-0.0544	-0.0544
C18				-0.0002	-0.0031
C19				-0.0209	-0.0209
C20				N/A	-0.0048
C21					0.0508
C22					-0.0118
C23					0.0444
C24					-0.0068
C25					0.0103

Table 6.3 The coefficients (C_{mn}) of the approximate second mode shape derived from the measured data. C1=C_{11}, C2=C_{21}, C3=C_{31}, C4=C_{41}, C5=C_{51}, C6=C_{12}, C7=C_{22}, C8=C_{32}, C9=C_{42}, C10=C_{52}, C11=C_{13}, C12=C_{23}, C13=C_{33}, C14=C_{43}, C15=C_{53}, C16=C_{14}, C17=C_{24}, C18=C_{34}, C19=C_{44}, C20=C_{54}, C21=C_{15}, C22=C_{25}, C23=C_{35}, C24=C_{45}, and C25=C_{55} (pre-normalised).

Coefficient	1 term	4 terms	9 terms	16 terms	25 terms
C1	1.0000	0.9981	0.9874	0.9699	0.8033
C2	N/A	-0.0423	-0.0265	-0.0194	-0.1205
C3		N/A	0.1296	0.1401	0.5351
C4			N/A	0.0113	-0.1167
C5				N/A	-0.0619
C6		-0.0322	-0.0335	-0.0488	0.0241
C7		-0.0297	-0.0275	-0.0428	-0.0767
C8		N/A	-0.0113	-0.0191	0.0263
C9			N/A	-0.0029	-0.0057
C10				N/A	0.0002
C11			0.0646	0.1652	0.1224
C12			0.0377	0.0420	-0.0263
C13			0.0000	0.0520	0.0975
C14			N/A	0.0125	-0.0218
C15				N/A	0.0073
C16				-0.0340	0.0009
C17				-0.0351	-0.0354
C18				-0.0167	-0.0020
C19				-0.0087	-0.0136
C20				N/A	-0.0031
C21					0.0330
C22					-0.0077
C23					0.0288
C24					-0.0044
C25					0.0067

Table 6.4 The normalised coefficients (C_{mn}) of the approximate second mode shape derived from the measured data. $C1=C_{11}$, $C2=C_{21}$, $C3=C_{31}$, $C4=C_{41}$, $C5=C_{51}$, $C6=C_{12}$, $C7=C_{22}$, $C8=C_{32}$, $C9=C_{42}$, $C10=C_{52}$, $C11=C_{13}$, $C12=C_{23}$, $C13=C_{33}$, $C14=C_{43}$, $C15=C_{53}$, $C16=C_{14}$, $C17=C_{24}$, $C18=C_{34}$, $C19=C_{44}$, $C20=C_{54}$, $C21=C_{15}$, $C22=C_{25}$, $C23=C_{35}$, $C24=C_{45}$, and $C25=C_{55}$.

Coefficient	1 term	4 terms	9 terms	16 terms	25 terms
C1	0.9068	0.9068	1.1745	1.2421	1.2414
C2	N/A	-0.0963	-0.1199	-0.1545	-0.1583
C3		N/A	0.1046	0.1384	0.1630
C4			N/A	-0.0691	-0.0695
C5				N/A	0.0442
C6		-0.0949	-0.0870	-0.0577	-0.0565
C7		0.0746	0.0746	0.0315	0.0315
C8		N/A	0.0236	0.0260	0.0294
C9			N/A	0.0020	0.0020
C10				N/A	0.0058
C11			0.6989	0.9013	0.8817
C12			-0.0707	-0.0983	-0.1097
C13			0.0000	0.1014	0.1219
C14			N/A	-0.0552	-0.0563
C15				N/A	0.0440
C16				0.0587	0.0603
C17				-0.0996	-0.0996
C18				0.0047	0.0093
C19				-0.0227	-0.0227
C20				N/A	0.0078
C21					-0.0443
C22					-0.0190
C23					-0.0003
C24					-0.0018
C25					0.0157

Table 6.5 The coefficients (C_{mn}) of the approximate third mode shape derived from measured data. C1=C_{11}, C2=C_{21}, C3=C_{31}, C4=C_{41}, C5=C_{51}, C6=C_{12}, C7=C_{22}, C8=C_{32}, C9=C_{42}, C10=C_{52}, C11=C_{13}, C12=C_{23}, C13=C_{33}, C14=C_{43}, C15=C_{53}, C16=C_{14}, C17=C_{24}, C18=C_{34}, C19=C_{44}, C20=C_{54}, C21=C_{15}, C22=C_{25}, C23=C_{35}, C24=C_{45}, and C25=C_{55} (pre-normalised).

Coefficient	1 term	4 terms	9 terms	16 terms	25 terms
C1	1.0000	0.9981	0.9874	0.9699	0.7962
C2	**N/A**	-0.0423	-0.0265	-0.0194	-0.1015
C3		**N/A**	0.1296	0.1401	0.1045
C4			**N/A**	0.0113	-0.0446
C5				**N/A**	0.0284
C6		-0.0322	-0.0335	-0.0488	-0.0362
C7		-0.0297	-0.0275	-0.0428	0.0202
C8		**N/A**	-0.0113	-0.0191	0.0189
C9			**N/A**	-0.0029	0.0013
C10				**N/A**	0.0037
C11			0.0646	0.1652	0.5655
C12			0.0377	0.0420	-0.0703
C13			0.0000	0.0520	0.0782
C14			**N/A**	0.0125	-0.0361
C15				**N/A**	0.0282
C16				-0.0340	0.0387
C17				-0.0351	-0.0639
C18				-0.0167	0.0060
C19				-0.0087	-0.0146
C20				**N/A**	0.0050
C21					-0.0284
C22					-0.0122
C23					-0.0002
C24					-0.0012
C25					0.0101

Table 6.6 The normalised coefficients (C_{mn}) of the approximate third mode shape derived from measured data. C1=C_{11}, C2=C_{21}, C3=C_{31}, C4=C_{41}, C5=C_{51}, C6=C_{12}, C7=C_{22}, C8=C_{32}, C9=C_{42}, C10=C_{52}, C11=C_{13}, C12=C_{23}, C13=C_{33}, C14=C_{43}, C15=C_{53}, C16=C_{14}, C17=C_{24}, C18=C_{34}, C19=C_{44}, C20=C_{54}, C21=C_{15}, C22=C_{25}, C23=C_{35}, C24=C_{45}, and C25=C_{55}.

Coefficient	1 term	4 terms	9 terms	16 terms	25 terms
C1	0.7426	0.7426	0.8132	1.2541	1.2548
C2	N/A	0.0179	0.0077	-0.0901	-0.0976
C3		N/A	0.6718	0.8922	0.9089
C4			N/A	-0.1956	-0.1938
C5				N/A	0.0334
C6		-0.0305	0.0014	0.0127	0.0243
C7		-0.2344	-0.2344	-0.3202	-0.3202
C8		N/A	0.0959	0.1135	0.1481
C9			N/A	-0.0492	-0.0492
C10				N/A	0.0577
C11			-0.4601	0.8629	0.8404
C12			-0.0305	-0.1151	-0.1376
C13			0.0000	0.6615	0.6378
C14			N/A	-0.1691	-0.1636
C15				N/A	-0.0225
C16				0.0226	0.0246
C17				-0.1256	-0.1256
C18				0.0352	0.0414
C19				-0.0066	-0.0066
C20				N/A	0.0104
C21					-0.0211
C22					-0.0376
C23					0.0097
C24					0.0091
C25					0.0446

Table 6.7 The coefficients (C_{mn}) of the approximate fourth mode shape derived from the measured data. C1=C_{11}, C2=C_{21}, C3=C_{31}, C4=C_{41}, C5=C_{51}, C6=C_{12}, C7=C_{22}, C8=C_{32}, C9=C_{42}, C10=C_{52}, C11=C_{13}, C12=C_{23}, C13=C_{33}, C14=C_{43}, C15=C_{53}, C16=C_{14}, C17=C_{24}, C18=C_{34}, C19=C_{44}, C20=C_{54}, C21=C_{15}, C22=C_{25}, C23=C_{35}, C24=C_{45}, and C25=C_{55} (pre-normalised).

Coefficient	1 term	4 terms	9 terms	16 terms	25 terms
C1	1.0000	0.9981	0.9874	0.9699	0.9318
C2	N/A	-0.0423	-0.0265	-0.0194	-0.0087
C3		N/A	0.1296	0.1401	0.1811
C4			N/A	0.0113	0.0131
C5				N/A	0.0681
C6		-0.0322	-0.0335	-0.0488	-0.0458
C7		-0.0297	-0.0275	-0.0428	-0.0398
C8		N/A	-0.0113	-0.0191	-0.0191
C9			N/A	-0.0029	-0.0027
C10				N/A	-0.0022
C11			0.0646	0.1652	0.2181
C12			0.0377	0.0420	0.0669
C13			0.0000	0.0520	0.1175
C14			N/A	0.0125	0.0194
C15				N/A	0.0644
C16				-0.0340	-0.0311
C17				-0.0351	-0.0326
C18				-0.0167	-0.0140
C19				-0.0087	-0.0081
C20				N/A	0.0025
C21					0.0932
C22					0.0465
C23					0.0718
C24					0.0130
C25					0.0347

Table 6.8 The normalised coefficients (C_{mn}) of the approximate fourth mode shape derived from the measured data. C1=C_{11}, C2=C_{21}, C3=C_{31}, C4=C_{41}, C5=C_{51}, C6=C_{12}, C7=C_{22}, C8=C_{32}, C9=C_{42}, C10=C_{52}, C11=C_{13}, C12=C_{23}, C13=C_{33}, C14=C_{43}, C15=C_{53}, C16=C_{14}, C17=C_{24}, C18=C_{34}, C19=C_{44}, C20=C_{54}, C21=C_{15}, C22=C_{25}, C23=C_{35}, C24=C_{45}, and C25=C_{55}.

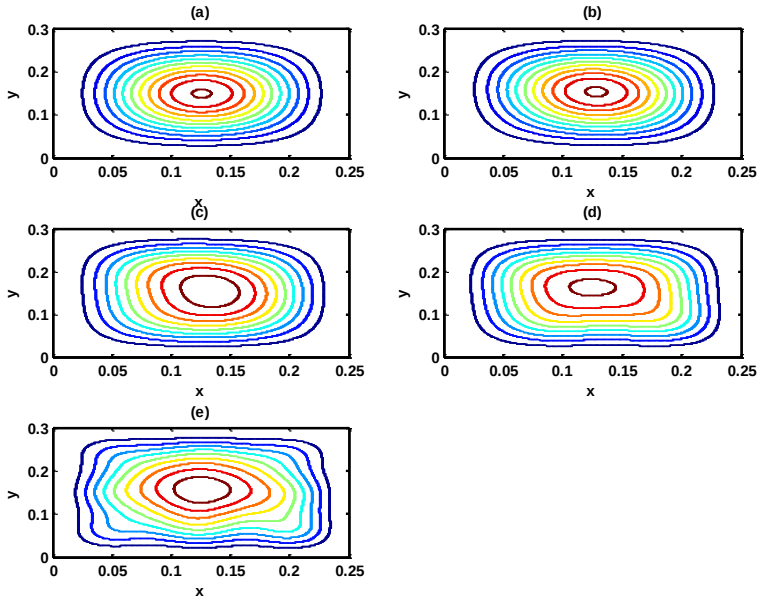

Figure 6.1 The approximate first mode shapes generated by fitting the weights into the series where the coefficient was extracted from the measured data. (a): by using 1 term (M=N=1); (b): by using 4 terms (M=N=2); (c): by using 9 terms (M=N=3); (d): by using 16 terms (M=N=4); and (e): by using 25 terms (M=N=5).

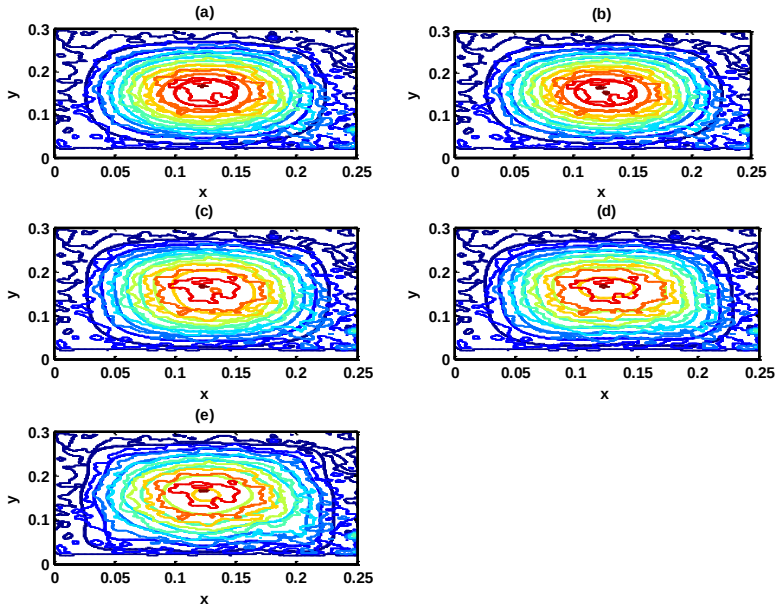

Figure 6.2 Comparison between the approximate mode shapes and the measured mode shapes for mode 1. (a) 1 term, (b) 4 terms, (c) 9 terms, (d) 16 terms, and (e) 25 terms. (-) approximate and (.) measured

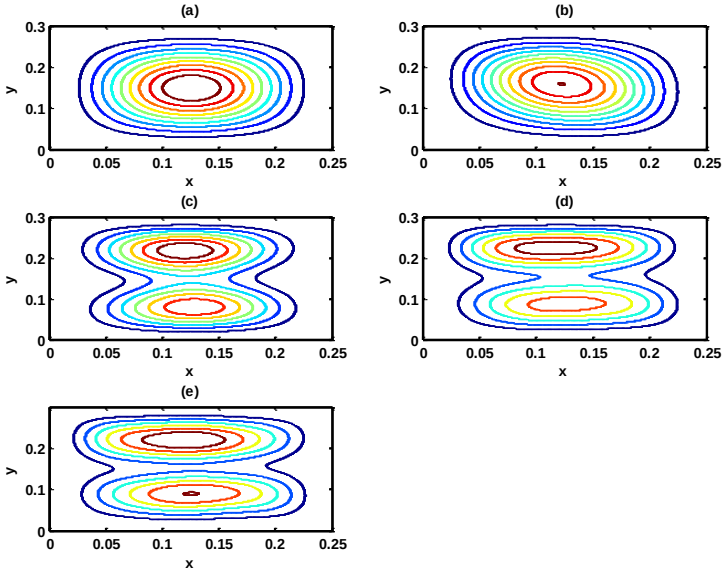

Figure 6.3 The approximate second mode shapes generated by fitting the weights into the series where the coefficient was extracted from the measured data. (a): by using 1 term (M=N=1); (b): by using 4 terms (M=N=2); (c): by using 9 terms (M=N=3); (d): by using 16 terms (M=N=4); and (e): by using 25 terms (M=N=5).

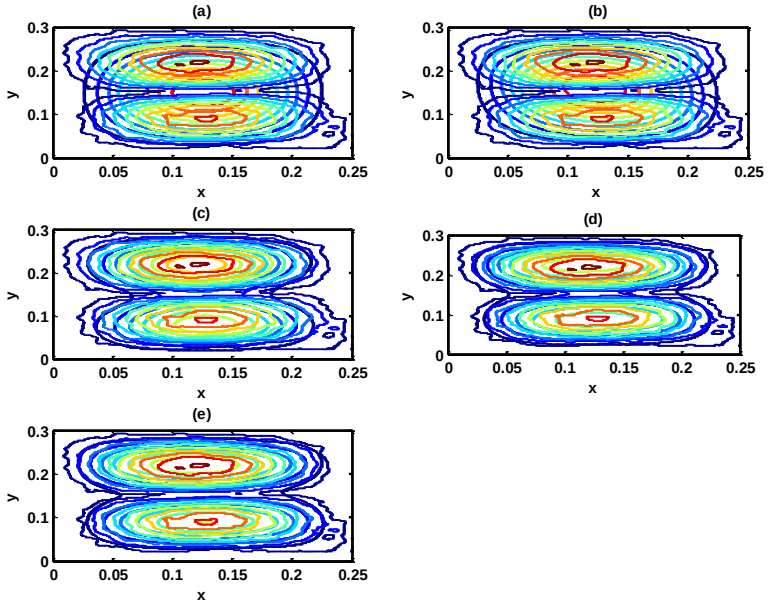

Figure 6.4 Comparison between the approximate mode shapes and the measured mode shapes for mode 2. (a) 1 term, (b) 4 terms, (c) 9 terms, (d) 16 terms, and (e) 25 terms. (-) approximate and (.) measured.

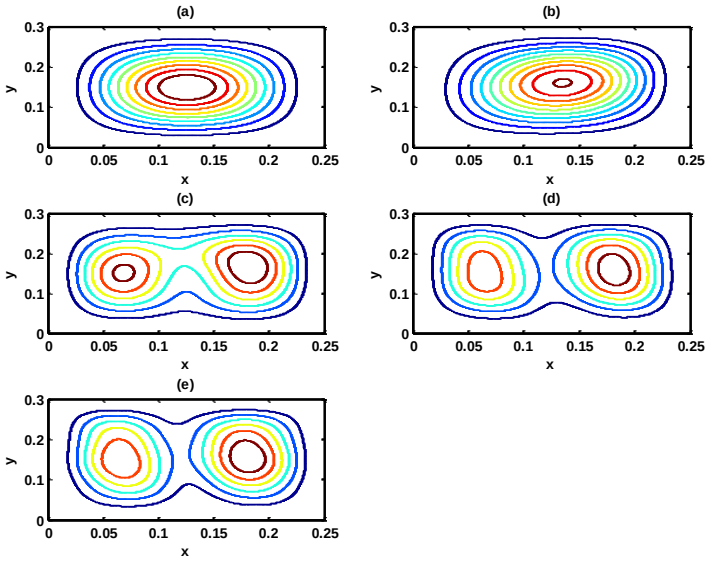

Figure 6.5 The approximate third mode shapes generated by fitting the weights into the series where the coefficient was extracted from the measured data. (a): by using 1 term (M=N=1); (b): by using 4 terms (M=N=2); (c): by using 9 terms (M=N=3); (d): by using 16 terms (M=N=4); and (e): by using 25 terms (M=N=5).

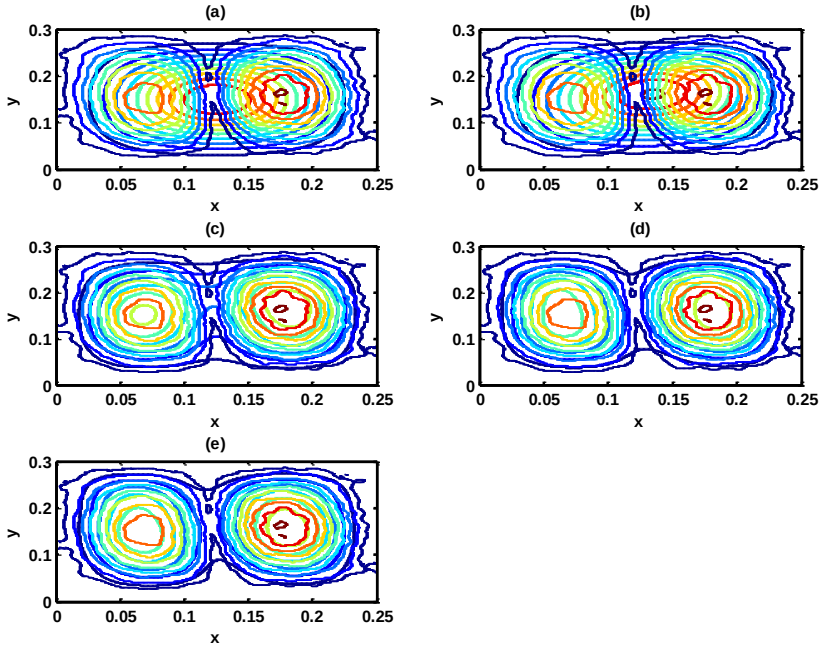

Figure 6.6 Comparison between the approximate mode shapes and the measured mode shapes for mode 3. (a) 1 term, (b) 4 terms, (c) 9 terms, (d) 16 terms, and (e) 25 terms. (-) approximate and (.) measured.

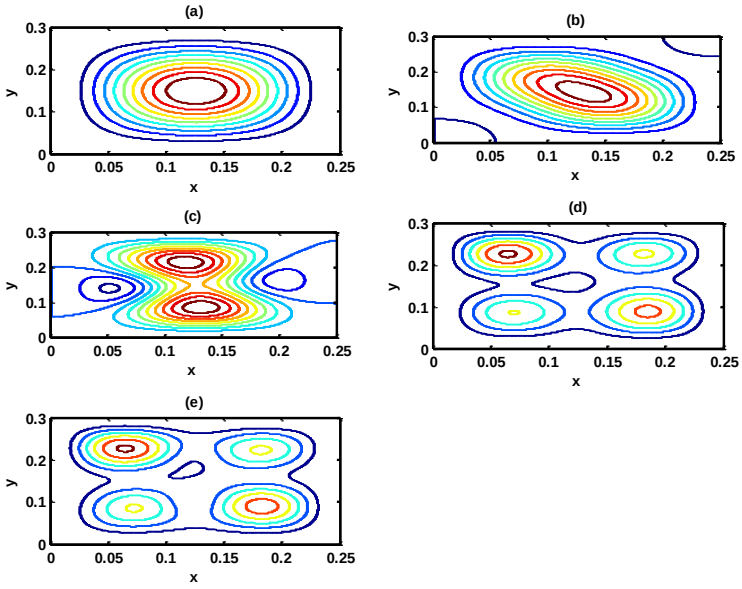

Figure 6.7 The approximate fourth mode shapes generated by fitting the weights into the series where the coefficient was extracted from the measured data. (a): by using 1 term (M=N=1); (b): by using 4 terms (M=N=2); (c): by using 9 terms (M=N=3); (d): by using 16 terms (M=N=4); and (e): by using 25 terms (M=N=5).

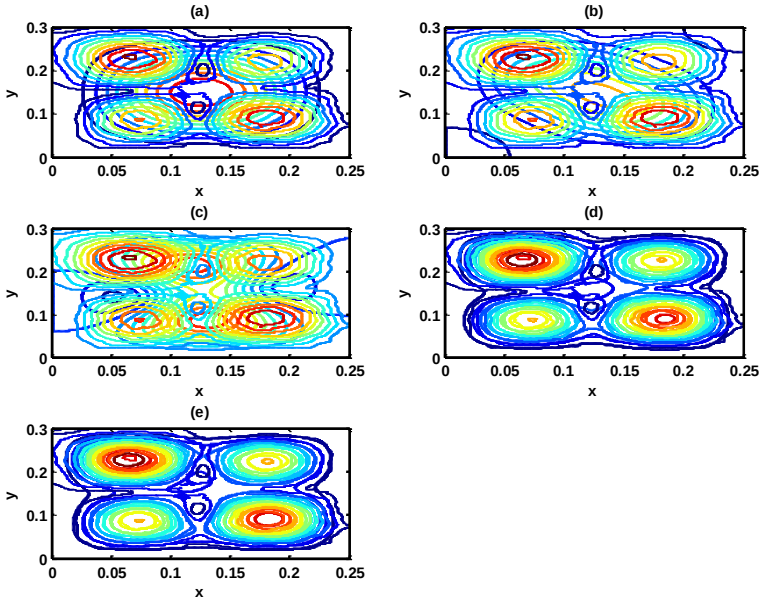

Figure 6.8 Comparison between approximate mode shapes and measured mode shapes for mode 4. (a) 1 term, (b) 4 terms, (c) 9 terms, (d) 16 terms, and (e) 25 terms. (-) approximate and (.) measured.

Figures 6.1 - 6.8 show the approximate mode shapes and a corresponding comparison for the plate without unattached mass. Table 6.9 shows the corresponding errors.

After obtaining all the coefficients and fitting them into the base function series and comparing the result with measured data it is evident that the processed mode shapes are now in a form that can be used in the plate uncertainty identification methods of Chapters 2 and 4. However, first similar results for the mode shape fitting process for the plate with an attached mass are now shown.

Number of term used to fitted the series	PE for mode 1 (%)	PE for mode 2 (%)	PE for mode 3 (%)	PE for mode 4 (%)
1 term	6.5826	24.1642	24.8095	31.8701
4 terms	6.2593	23.7814	24.2173	27.3141
9 terms	5.7746	10.3923	10.7307	29.7891
16 terms	6.1705	10.7970	10.1848	6.9137
25 terms	7.3692	10.0532	10.015	6.5380

Table 6.9 Percentage error between measured mode shapes from Vibromap and approximate fitted coefficients mode shapes

Measured data for the clamped-all-sides-rectangular-plate with an attached mass in 6 random positions.

Random positions of the point mass are generated by Monte Carlo simulation with varying mean and standard deviation values (i.e. the mean 0.1 in the x direction and 0.15 in the y direction with the standard deviation 0.05 in both x and y directions) in table 4.5 are used as a set of random positions to put a point mass on the plate structure.

For the case with unattached point mass, the pre-normalised coefficients and the coefficients normalised to magnitude 1 are respectively shown in Tables 6.10 to 6.15 for mode 1 to mode 3. The contours of the fitted mode shapes, and a comparison with the raw measured mode shape are shown respectively in Figures 6.9 to 6.14.

The measured fourth mode could not be fitted in this process possibly due to inconsistency in capturing the data. For example in one of the random mass positions, (see table 4.5) 0.146 m in the x direction, and 0.196 m in the y direction, the fourth mode could not be found.

Coefficient	1 term	4 terms	9 terms	16 terms	25 terms
C1	1.1117	1.1117	1.1897	1.2338	1.2761
C2	N/A	-0.0471	-0.0319	-0.0247	-0.0120
C3		N/A	0.1561	0.1782	0.2481
C4			N/A	0.0144	0.0180
C5				N/A	0.0932
C6		-0.0359	-0.0404	-0.0621	-0.0627
C7		-0.0331	-0.0331	-0.0545	-0.0545
C8		N/A	-0.0136	-0.0243	-0.0261
C9			N/A	-0.0036	-0.0036
C10				N/A	-0.0031
C11			0.0778	0.2101	0.2986
C12			0.0455	0.0534	0.0916
C13			0.0000	0.0662	0.1609
C14			N/A	0.0159	0.0265
C15				N/A	0.0882
C16				-0.0433	-0.0426
C17				-0.0447	-0.0447
C18				-0.0212	-0.0192
C19				-0.0110	-0.0110
C20				N/A	0.0034
C21					0.1276
C22					0.0637
C23					0.0983
C24					0.0178
C25					0.0475

Table 6.10 The coefficients (C_{mn}) of the approximate first mode shape derived from the measured data where . $C1=C_{11}$, $C2=C_{21}$, $C3=C_{31}$, $C4=C_{41}$, $C5=C_{51}$, $C6=C_{12}$, $C7=C_{22}$, $C8=C_{32}$, $C9=C_{42}$, $C10=C_{52}$, $C11=C_{13}$, $C12=C_{23}$, $C13=C_{33}$, $C14=C_{43}$, $C15=C_{53}$, $C16=C_{14}$, $C17=C_{24}$, $C18=C_{34}$, $C19=C_{44}$, $C20=C_{54}$, $C21=C_{15}$, $C22=C_{25}$, $C23=C_{35}$, $C24=C_{45}$, and $C25=C_{55}$ (pre-normalised).

Coefficient	1 term	4 terms	9 terms	16 terms	25 terms
C1	1.0000	0.9981	0.9874	-0.0488	0.9318
C2	N/A	-0.0423	-0.0265	-0.0428	-0.0087
C3		N/A	0.1296	-0.0191	0.1811
C4			N/A	-0.0029	0.0131
C5				N/A	0.0681
C6		-0.0322	-0.0335	0.1652	-0.0458
C7		-0.0297	-0.0275	0.0420	-0.0398
C8		N/A	-0.0113	0.0520	-0.0191
C9			N/A	0.0125	-0.0027
C10				N/A	-0.0022
C11			-0.0642	0.1070	0.2181
C12			-0.0365	-0.0423	0.0669
C13			0.0000	0.0829	0.1175
C14			N/A	-0.0176	0.0194
C15				N/A	0.0644
C16				0.0001	-0.0311
C17				-0.0343	-0.0326
C18				-0.0034	-0.0140
C19				-0.0141	-0.0081
C20				N/A	0.0025
C21					0.0932
C22					0.0465
C23					0.0718
C24					0.0130
C25					0.0347

Table 6.11 The normalised coefficients (C_{mn}) of approximate first mode shape derived from the measured data. C1=C_{11}, C2=C_{21}, C3=C_{31}, C4=C_{41}, C5=C_{51}, C6=C_{12}, C7=C_{22}, C8=C_{32}, C9=C_{42}, C10=C_{52}, C11=C_{13}, C12=C_{23}, C13=C_{33}, C14=C_{43}, C15=C_{53}, C16=C_{14}, C17=C_{24}, C18=C_{34}, C19=C_{44}, C20=C_{54}, C21=C_{15}, C22=C_{25}, C23=C_{35}, C24=C_{45}, and C25=C_{55}.

Coefficient	1 term	4 terms	9 terms	16 terms	25 terms
C1	0.5218	0.5218	0.6643	0.7144	0.7129
C2	N/A	-0.0880	-0.0981	-0.1499	-0.1537
C3		N/A	0.4808	0.5058	0.4850
C4			N/A	-0.1037	-0.1042
C5				N/A	-0.0440
C6		0.0137	0.0204	0.0204	0.0203
C7		-0.0522	-0.0522	-0.0673	-0.0673
C8		N/A	0.0201	0.0186	0.0183
C9			N/A	-0.0055	-0.0055
C10				N/A	-0.0004
C11			-0.0533	0.0971	0.1230
C12			-0.0303	-0.0383	-0.0495
C13			0.0000	0.0752	0.1042
C14			N/A	-0.0160	-0.0176
C15				N/A	0.0206
C16				0.0001	-0.0007
C17				-0.0311	-0.0311
C18				-0.0031	-0.0054
C19				-0.0127	-0.0127
C20				N/A	-0.0039
C21					0.0394
C22					-0.0186
C23					0.0367
C24					-0.0026
C25					0.0151

Table 6.12 The coefficients (C_{mn}) of approximate second mode shape derived from the measured data. C1=C_{11}, C2=C_{21}, C3=C_{31}, C4=C_{41}, C5=C_{51}, C6=C_{12}, C7=C_{22}, C8=C_{32}, C9=C_{42}, C10=C_{52}, C11=C_{13}, C12=C_{23}, C13=C_{33}, C14=C_{43}, C15=C_{53}, C16=C_{14}, C17=C_{24}, C18=C_{34}, C19=C_{44}, C20=C_{54}, C21=C_{15}, C22=C_{25}, C23=C_{35}, C24=C_{45}, and C25=C_{55} (pre-normalised).

Coefficient	1 term	4 terms	9 terms	16 terms	25 terms
C1	1.0000	0.9810	0.8001	0.7876	0.7878
C2	N/A	-0.1654	-0.1181	-0.1653	-0.1698
C3		N/A	0.5791	0.5577	0.5359
C4			N/A	-0.1143	-0.1152
C5				N/A	-0.0486
C6		0.0257	0.0245	0.0225	0.0224
C7		-0.0981	-0.0629	-0.0742	-0.0744
C8		N/A	0.0242	0.0205	0.0203
C9			N/A	-0.0061	-0.0061
C10				N/A	-0.0004
C11			-0.0642	0.1070	0.1359
C12			-0.0365	-0.0423	-0.0547
C13			0.0000	0.0829	0.1151
C14			N/A	-0.0176	-0.0194
C15				N/A	0.0228
C16				0.0001	-0.0008
C17				-0.0343	-0.0344
C18				-0.0034	-0.0060
C19				-0.0141	-0.0141
C20				N/A	-0.0043
C21					0.0435
C22					-0.0205
C23					0.0406
C24					-0.0029
C25					0.0167

Table 6.13 The normalised coefficients (C_{mn}) of approximate second mode shape derived from the measured data. C1=C_{11}, C2=C_{21}, C3=C_{31}, C4=C_{41}, C5=C_{51}, C6=C_{12}, C7=C_{22}, C8=C_{32}, C9=C_{42}, C10=C_{52}, C11=C_{13}, C12=C_{23}, C13=C_{33}, C14=C_{43}, C15=C_{53}, C16=C_{14}, C17=C_{24}, C18=C_{34}, C19=C_{44}, C20=C_{54}, C21=C_{15}, C22=C_{25}, C23=C_{35}, C24=C_{45}, and C25=C_{55}.

Coefficient	1 term	4 terms	9 terms	16 terms	25 terms
C1	0.9068	0.9068	1.1745	1.2421	1.2414
C2	N/A	-0.0963	-0.1199	-0.1545	-0.1583
C3		N/A	0.1046	0.1384	0.1630
C4			N/A	-0.0691	-0.0695
C5				N/A	0.0442
C6		-0.0949	-0.0870	-0.0577	-0.0565
C7		0.0746	0.0746	0.0315	0.0315
C8		N/A	0.0236	0.0260	0.0294
C9			N/A	0.0020	0.0020
C10				N/A	0.0058
C11			0.6986	0.9013	0.8817
C12			-0.0707	-0.0983	-0.1097
C13			0.0000	0.1014	0.1219
C14			N/A	-0.0552	-0.0563
C15				N/A	0.0440
C16				0.0587	0.0603
C17				-0.0996	-0.0996
C18				0.0047	0.0093
C19				-0.0227	-0.0227
C20				N/A	0.0078
C21					-0.0443
C22					-0.0190
C23					-0.0003
C24					-0.0018
C25					0.0157

Table 6.14 The coefficients (C_{mn}) of the approximate third mode shape derived from the measured data. C1=C_{11}, C2=C_{21}, C3=C_{31}, C4=C_{41}, C5=C_{51}, C6=C_{12}, C7=C_{22}, C8=C_{32}, C9=C_{42}, C10=C_{52}, C11=C_{13}, C12=C_{23}, C13=C_{33}, C14=C_{43}, C15=C_{53}, C16=C_{14}, C17=C_{24}, C18=C_{34}, C19=C_{44}, C20=C_{54}, C21=C_{15}, C22=C_{25}, C23=C_{35}, C24=C_{45}, and C25=C_{55} (pre-normalised).

Coefficient	1 term	4 terms	9 terms	16 terms	25 terms
C1	1.0000	0.9858	0.8495	0.7944	0.7962
C2	N/A	-0.1047	-0.0867	-0.0988	-0.1015
C3		N/A	0.0757	0.0885	0.1045
C4			N/A	-0.0442	-0.0446
C5				N/A	0.0284
C6		-0.1032	-0.0629	-0.0369	-0.0362
C7		0.0811	0.0540	0.0201	0.0202
C8		N/A	0.0171	0.0166	0.0189
C9			N/A	0.0013	0.0013
C10				N/A	0.0037
C11			0.5053	0.5765	0.5655
C12			-0.0511	-0.0629	-0.0703
C13			0.0000	0.0648	0.0782
C14			N/A	-0.0353	-0.0361
C15				N/A	0.0282
C16				0.0376	0.0387
C17				-0.0637	-0.0639
C18				0.0030	0.0060
C19				-0.0145	-0.0146
C20				N/A	0.0050
C21					-0.0284
C22					-0.0122
C23					-0.0002
C24					-0.0012
C25					0.0101

Table 6.15 The normalised coefficients (C_{mn}) of approximate third mode shape derived from the measured data. C1=C_{11}, C2=C_{21}, C3=C_{31}, C4=C_{41}, C5=C_{51}, C6=C_{12}, C7=C_{22}, C8=C_{32}, C9=C_{42}, C10=C_{52}, C11=C_{13}, C12=C_{23}, C13=C_{33}, C14=C_{43}, C15=C_{53}, C16=C_{14}, C17=C_{24}, C18=C_{34}, C19=C_{44}, C20=C_{54}, C21=C_{15}, C22=C_{25}, C23=C_{35}, C24=C_{45}, and C25=C_{55}.

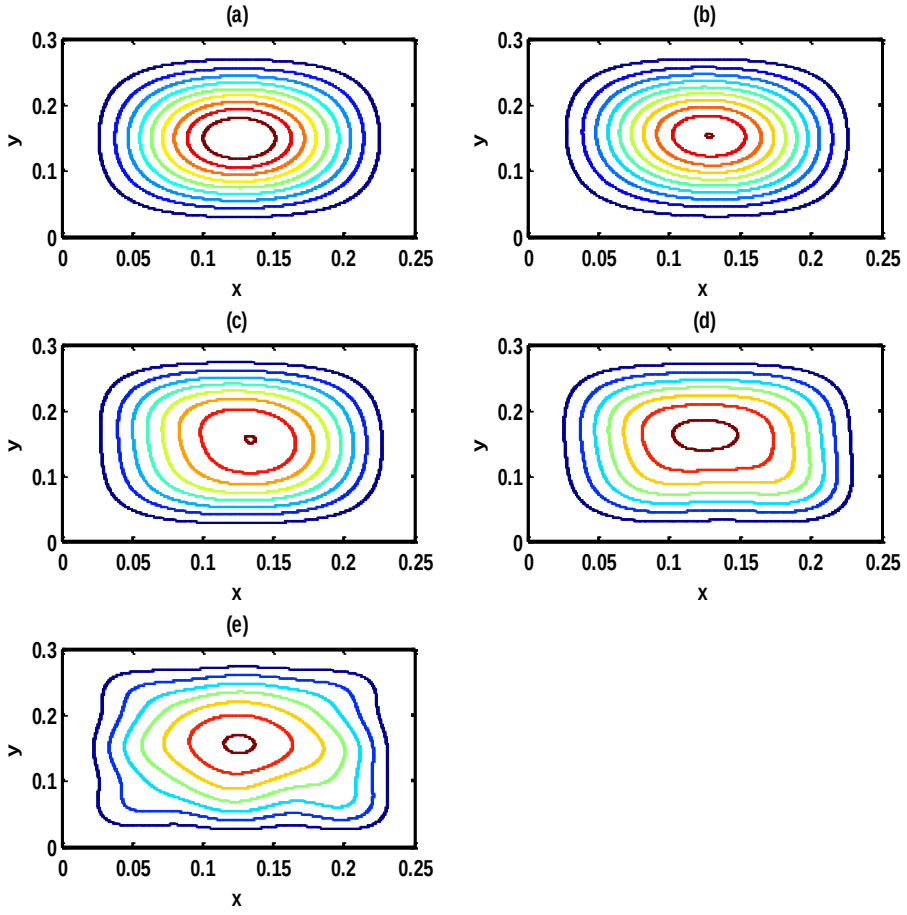

Figure 6.9 The approximate first mode shape of an all-sides-clamped rectangular plate with a point mass at 0.045 m (x direction) and 0.042 m (y direction) generated by fitting the weights into the series where the coefficient was extracted from the measured data. (a): by using 1 term (M=N=1); (b): by using 4 terms (M=N=2); (c): by using 9 terms (M=N=3); (d): by using 16 terms (M=N=4); and (e): by using 25 terms (M=N=5).

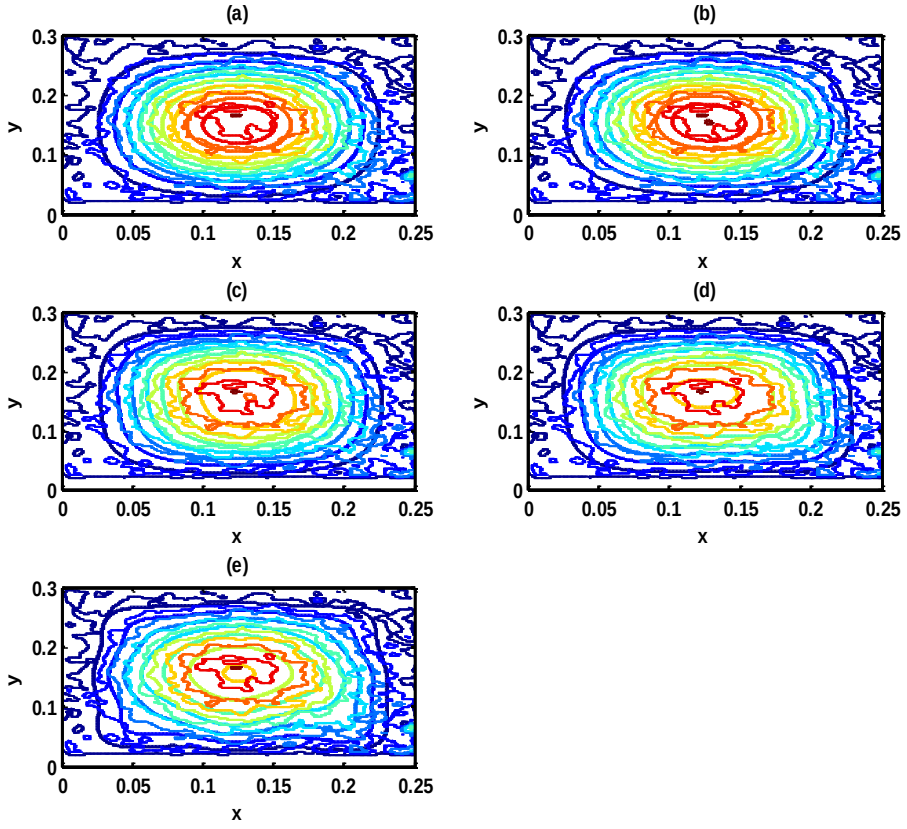

Figure 6.10 Comparison between the approximate mode shape and the measured mode shape for mode 1 of all-sides-clamped rectangular plate with a point mass at 0.045 m (x direction) and 0.042 m (y direction). (a) 1 term, (b) 4 terms, (c) 9 terms, (d) 16 terms, and (e) 25 terms. (-) approximate and (.) measured

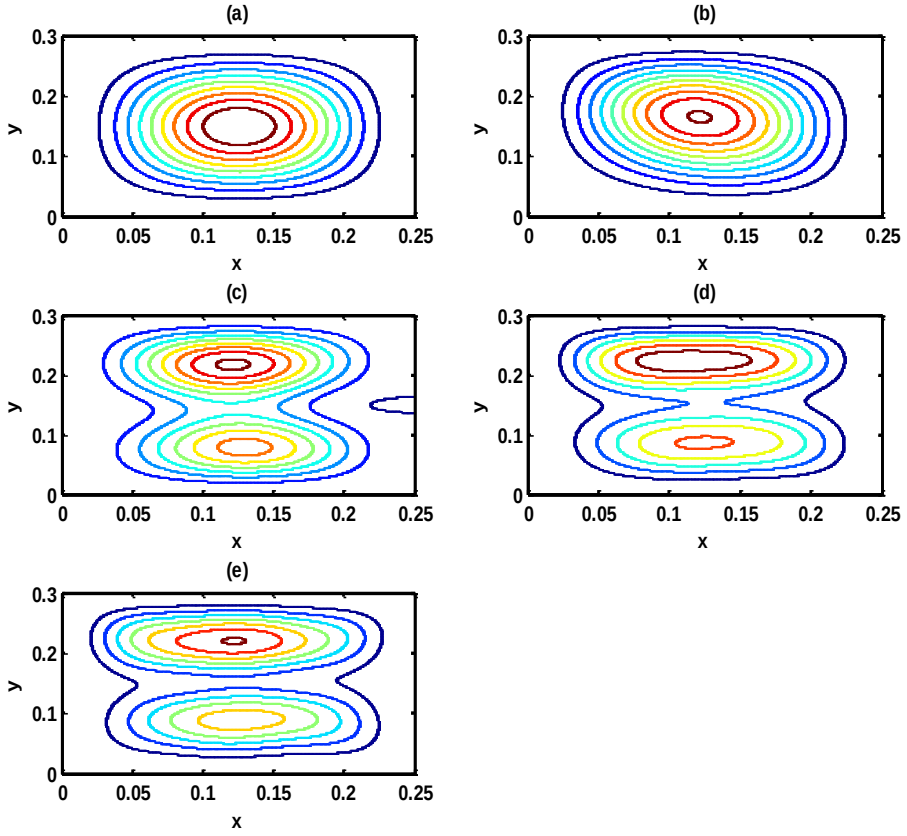

Figure 6.11 The approximate second mode shape of all-sides-clamped rectangular plate with a point mass at 0.045 m (x direction) and 0.042 m (y direction) generated by fitting the weights into the series where the coefficient was extracted from the measured data. (a): by using 1 term (M=N=1); (b): by using 4 terms (M=N=2); (c): by using 9 terms (M=N=3); (d): by using 16 terms (M=N=4); and (e): by using 25 terms (M=N=5).

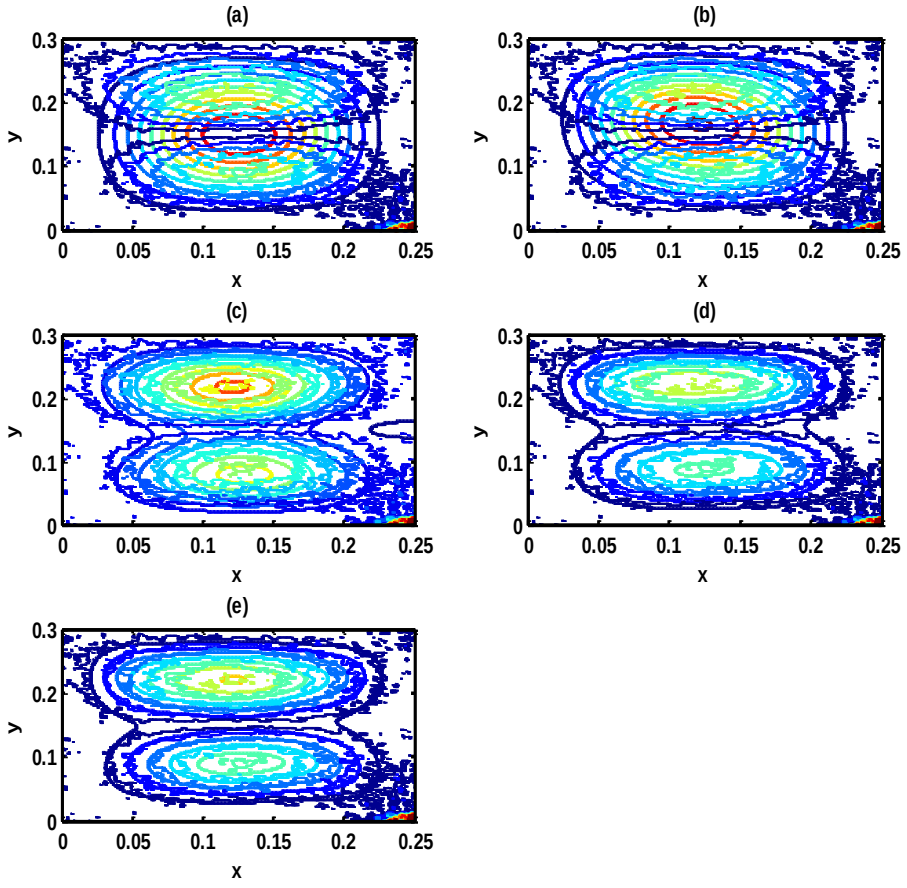

Figure 6.12 Comparison between the approximate mode shape and the measured mode shapes for mode 2 of all-sides-clamped rectangular plate with a point mass at 0.045 m (x direction) and 0.042 m (y direction). (a) 1 term, (b) 4 terms, (c) 9 terms, (d) 16 terms, and (e) 25 terms. (-) approximate and (.) measured

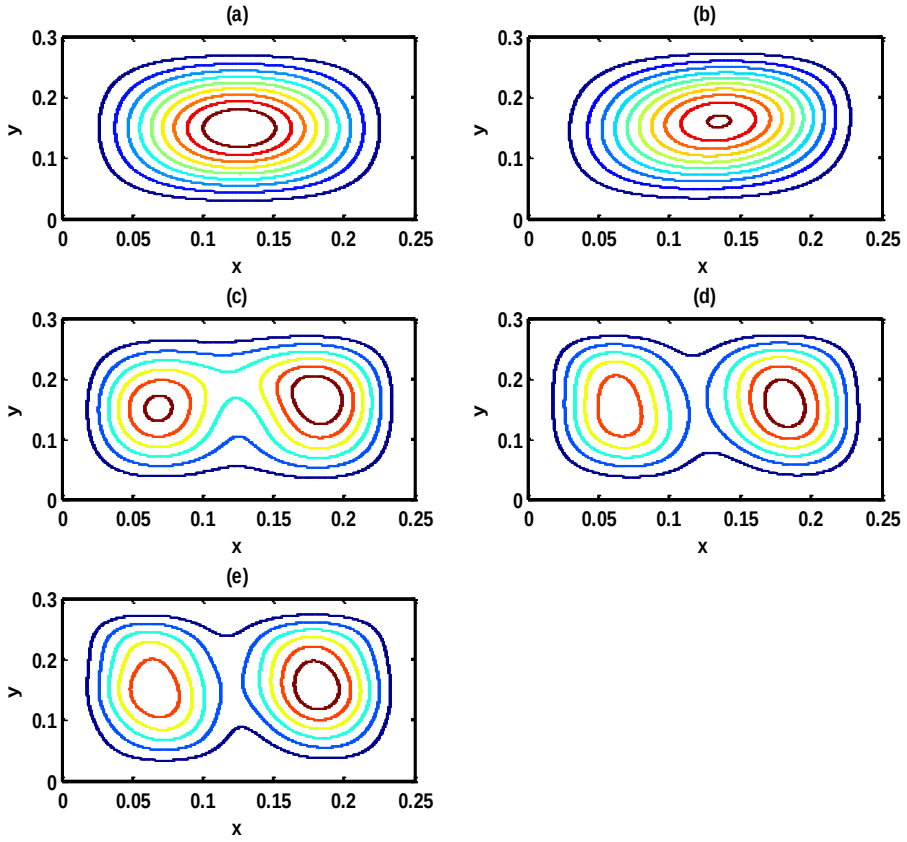

Figure 6.13 The approximate third mode shape of all-sides-clamped rectangular plate with a point mass at 0.045 m (x direction) and 0.042 m (y direction) generated by fitting the weights into the series where the coefficient was extracted from the measured data. (a): by using 1 term (M=N=1); (b): by using 4 terms (M=N=2); (c): by using 9 terms (M=N=3); (d): by using 16 terms (M=N=4); and (e): by using 25 terms (M=N=5).

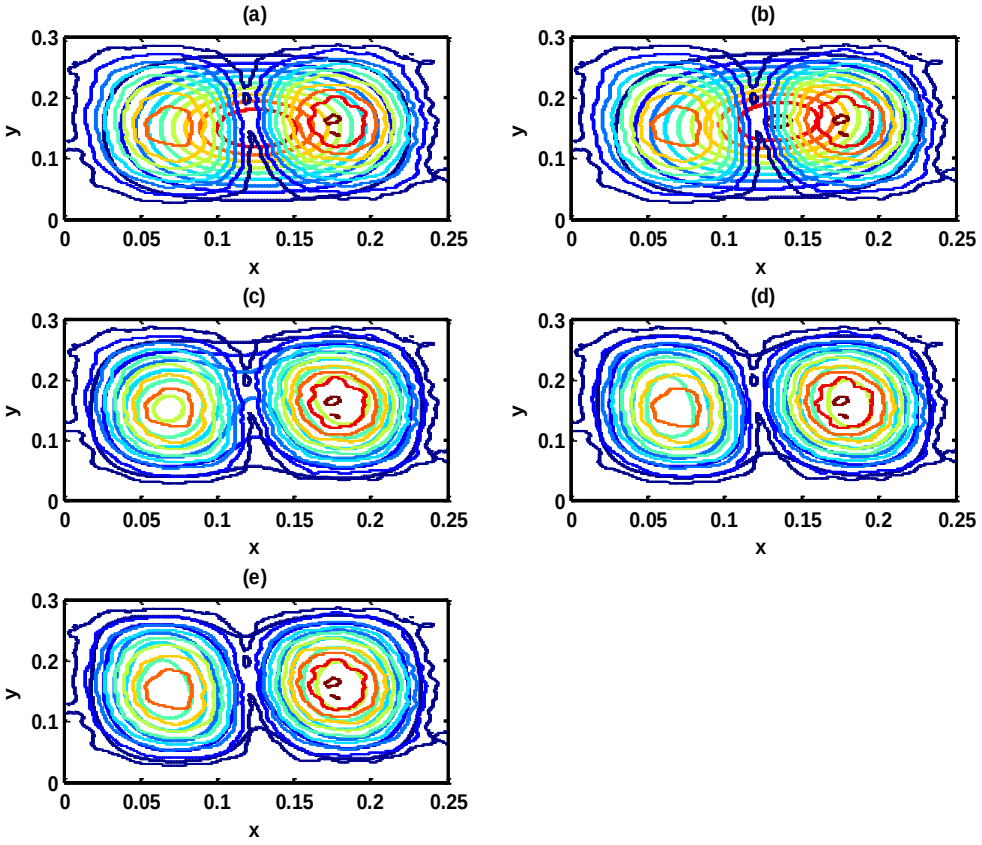

Figure 6.14 Comparison between the approximate mode shape and the measured mode shape for mode 3 of all-sides-clamped rectangular plate with a point mass at 0.045 m (x direction) and 0.042 m (y direction). (a) 1 term, (b) 4 terms, (c) 9 terms, (d) 16 terms, and (e) 25 terms. (-) approximate and (.) measured

Number of terms used to fit the series	PE for mode 1 (%)	PE for mode 2 (%)	PE for mode 3 (%)
1 term	6.5826	22.8725	24.8095
4 terms	6.2593	22.3896	24.2173
9 terms	5.7746	9.0042	10.7307
16 terms	6.1704	6.1535	10.1848
25 terms	7.3692	5.9582	10.0150

Table 6.16 Percentage errors between measured mode shapes from VibroMap and the corresponding fitted mode shapes.

6.2 Uncertainty Identification using Experimental Data

The purpose of the uncertainty identification method discussed in Chapter 2 is to estimate the statistical properties of a particular source of uncertainty using measured mode shapes. In Chapter 4, two examples were considered of a clamped-plate with attached mass in random locations. The Rayleigh-Ritz based predictions in these two cases showed that the uncertainty identification method worked well when the uncertainty was relatively low, but the method was unsuccessful when the level of uncertainty was high. Here, these two cases are repeated using the real clamped-plate structure when the mode shape information used is measured, rather than Rayleigh-Ritz predicted as in Chapter 4.

First for the high uncertainty case considered, measured mode shapes have been obtained using Vibromap1000. The generalised displacement model (similar to that used in the Rayleigh Ritz method) discussed earlier in the section, has been fitted to the measured data, with the vector of coefficients obtained, appropriately normalised to magnitude = 1. The processed results are shown in Table 6.17. The second case considered is lower-uncertainty example of Chapter 4. Again measured mode shapes have been processed and normalised again in terms Rayleigh Ritz coefficients, with results shown in Table 6.18.

Set of coefficients	Mode 1	Mode 2	Mode 3
C1&C2	0.1000	excluded	0.1000
C3&C4	0.1000	excluded	0.0590
C5&C6	excluded	0.1000	excluded
C7&C8	0.1000	excluded	0.0630
C9&C10	0.1000	excluded	0.1000
C11&C12	0.1000	excluded	0.1000
C13&C14	0.1000	excluded	0.1000
C15&C16	excluded	0.1000	excluded
C17&C18	0.1000	excluded	0.1000
C19&C20	0.1000	excluded	0.1000
C21&C22	0.1000	excluded	0.1000
C23&C24	0.1000	excluded	0.1000
Average	0.1000	0.1000	0.0922

Table 6.17 Standard deviation estimates for the uncertain position of a point mass in the x direction on an all-sides-clamped rectangular plate (using coefficients from the first three approximate fitted mode shape) obtained by using MLE and the perturbation approach using the set point mass positions given in table 4.5 (random sample each set = 6, μ_x = 0.1 m, μ_y = 0.15 m, σ_y = 0.05 m, and target σ_x = 0.05 m).

Set of coefficients	Mode 1	Mode 2	Mode 3
C1&C2	0.1000	excluded	0.1000
C3&C4	0.1000	excluded	0.1000
C5&C6	excluded	0.1000	excluded
C7&C8	0.1000	excluded	0.1000
C9&C10	0.1000	excluded	0.1000
C11&C12	0.1000	excluded	0.1000
C13&C14	0.1000	excluded	0.1000
C15&C16	excluded	0.1000	excluded
C17&C18	0.1000	excluded	0.1000
C19&C20	0.1000	excluded	0.1000
C21&C22	0.1000	excluded	0.1000
C23&C24	0.1000	excluded	0.1000
Average	0.1000	0.1000	0.1000

Table 6.18 Standard deviation estimates for the uncertain position of a point mass in the x direction on an all-sides-clamped rectangular plate (using coefficients from the first three approximate fitted mode shape) obtained by using MLE and the perturbation approach using one of the set point mass positions (random sample each set = 6, μ_x = 0.1 m, μ_y = 0.15 m, σ_y = 0.03 m, and target σ_x = 0.03 m).

Discussion of the results

Table 6.17 confirms that for high levels of uncertainty (in the random mass position) the free-vibration structural uncertainty method of Chapter 2 does not work on a mass-loaded clamped-plate structure undergoing forced vibration. But it is also evident in this case that predictions for a similar case in Chapter 4, the method also did not work. The most likely numerical cause for this problem is the linearization error in the perturbation method caused by numerical problems, particularly of singular Jacobian values.

But when the level of variability was reduced, the same method was shown in Chapter 4 to work well. Whereas here, for the lower-uncertainty forced-damped case as shown by table 6.18, the method is not working. There could be several reasons for this failure. One possible cause is that
the forced-vibration mode shape variation behaviour (as indicated by the Jacobian) is different from free-vibration behaviour. This could be a reason since the same free-vibration Jacobian values have been used. Developing a calculation method for the forced-vibration case is substantially more complicated and has not yet been attempted.

Another possible cause is that the measured mode shape is not accurate enough via Vibromap1000 in quantitative mode. Use of an alternative mode shape measurement technique would resolve this question.

Yet another possible cause is that the mode shape fitting process is not accurate enough and is not capable of adequately identifying the change in the mass position. To answer this question the fitted Rayleigh Ritz coefficients (using 25 terms) obtained from the VibroMap measurement are compared with directly obtained Rayleigh-Ritz coefficients using the method in Chapter 4. Here the mass positions in the Chapter 4 prediction have been identically chosen as those used in the experimental measurements. The comparison is shown in table 6.19. It is evident from this comparison (as indicated by the parameter ratio, which ideally should be equal to 1, that the first coefficient C1 is being

very well fitted but all the other coefficients are not similar. The reason for this difference is not yet known.

coefficients	position 1			position 2			position 3			position 4			position 5			position 6		
	RR	measured	ratio	RR	measured	ratio	RR	measured	ratio	RR	measured	ratio	RR	measured	ratio	RR	measured	ratio
C1	0.9961	0.9509	1.0475	0.9943	0.9514	1.0451	0.9946	0.9726	1.0227	0.9962	0.9243	1.0778	0.9962	0.9717	1.0252	0.9949	0.8752	1.1368
C2	-0.0213	0.0090	-2.3604	0.0185	-0.0655	-0.2822	-0.0103	-0.1039	0.0991	0.0116	-0.1484	-0.0782	-0.0190	-0.0620	0.3064	-0.0107	-0.0810	0.1321
C3	0.0627	0.1617	0.3879	0.0718	0.1811	0.3965	0.0633	0.0916	0.6907	0.0615	0.1971	0.3120	0.0623	0.1317	0.4731	0.0625	0.3020	0.2069
C4	0.0026	0.0219	0.1186	-0.0020	-0.0302	0.0663	0.0022	-0.0415	-0.0530	-0.0016	-0.0697	0.0230	0.0024	-0.0442	-0.0543	0.0020	-0.0671	-0.0298
C5	0.0128	0.0303	0.4226	0.0110	0.0076	1.4383	0.0138	-0.0051	-2.7191	0.0136	0.0458	0.2972	0.0131	0.0139	0.9397	0.0138	0.0367	0.3765
C6	0.0055	-0.0764	-0.0720	0.0215	-0.0451	-0.4767	0.0355	-0.0525	-0.6758	-0.0149	0.0294	-0.5067	0.0008	-0.0014	-0.5525	0.0355	-0.0037	-9.6094
C7	-0.0012	0.0247	-0.0486	0.0118	-0.0224	-0.5271	-0.0052	-0.0259	0.2006	-0.0018	-0.0147	0.1226	-0.0002	-0.0167	0.0120	-0.0047	-0.0100	0.4711
C8	-0.0005	-0.0237	0.0211	0.0001	-0.0029	-0.0345	-0.0057	0.0000	1892.1464	0.0017	-0.0169	-0.1005	-0.0001	0.0176	-0.0057	-0.0053	0.0061	-0.8683
C9	0.0004	0.0125	0.0320	-0.0032	-0.0056	0.5696	0.0031	-0.0105	-0.2951	0.0007	-0.0231	-0.0303	0.0000	0.0003	0.0000	0.0026	-0.0004	-6.9566
C10	0.0002	-0.0183	-0.0109	-0.0017	0.0079	-0.2145	0.0026	0.0036	0.7152	-0.0007	-0.0158	0.0444	0.0000	0.0102	0.0000	0.0025	0.0029	0.8605
C11	0.0546	0.2120	0.2575	0.0698	0.2189	0.3189	0.0706	0.1611	0.4382	0.0560	0.2334	0.2400	0.0544	0.1671	0.3256	0.0676	0.3429	0.1971
C12	-0.0002	0.0409	-0.0049	0.0078	-0.0326	-0.2393	-0.0026	-0.0366	0.0711	0.0003	-0.0456	-0.0066	-0.0001	-0.0348	0.0029	-0.0020	-0.0628	0.0319
C13	-0.0014	0.0396	-0.0353	-0.0031	-0.0449	0.0691	-0.0065	-0.0288	0.2257	-0.0017	0.0538	-0.0316	-0.0013	-0.0222	0.0585	-0.0054	-0.0460	0.1174
C14	-0.0011	0.0407	-0.0270	-0.0036	0.0044	-0.8164	0.0023	-0.0066	-0.3499	0.0005	0.0147	0.0340	-0.0010	-0.0140	0.0717	0.0014	-0.0235	-0.0595
C15	-0.0021	0.0251	-0.0837	-0.0037	0.0002	-15.4523	0.0002	0.0045	0.0443	-0.0023	0.0682	-0.0337	-0.0022	0.0075	-0.2944	-0.0004	-0.0047	0.0844
C16	-0.0007	-0.0450	0.0155	0.0047	-0.0221	-0.2125	0.0049	-0.0101	-0.4855	0.0014	0.0194	0.0722	-0.0001	0.0042	-0.0240	0.0031	0.0024	1.3035
C17	0.0002	0.0086	0.0233	0.0033	-0.0173	-0.1904	-0.0008	-0.0177	0.0453	0.0002	-0.0255	-0.0079	0.0000	-0.0215	0.0000	-0.0005	-0.0165	0.0303
C18	0.0004	-0.0158	-0.0252	-0.0007	0.0013	-0.5268	-0.0019	0.0088	-0.2156	-0.0009	-0.0135	0.0667	0.0001	0.0104	0.0096	-0.0010	0.0052	-0.1915
C19	-0.0004	-0.0025	0.1608	-0.0021	-0.0094	0.2240	0.0011	-0.0060	-0.1832	-0.0006	-0.0232	0.0259	-0.0001	-0.0066	0.0151	0.0005	-0.0045	-0.1104
C20	-0.0002	-0.0069	0.0290	-0.0013	0.0020	-0.6455	0.0009	0.0055	0.1633	0.0007	-0.0023	-0.3034	0.0000	0.0063	0.0000	0.0004	0.0045	0.0896
C21	0.0106	0.0688	0.1542	0.0124	0.0428	0.2899	0.0111	0.0241	0.4607	0.0099	0.0609	0.1626	0.0108	0.0318	0.3394	0.0098	0.0703	0.1394
C22	-0.0004	0.0382	-0.0105	0.0020	0.0065	0.3083	-0.0003	-0.0084	0.0356	0.0002	0.0161	0.0124	-0.0004	-0.0105	0.0382	-0.0002	-0.0222	0.0090
C23	-0.0017	0.0281	-0.0605	-0.0018	-0.0067	0.2668	-0.0018	-0.0115	0.1563	-0.0013	0.0627	-0.0207	-0.0018	-0.0005	3.8172	-0.0011	-0.0108	0.1017
C24	0.0006	0.0237	0.0253	-0.0016	0.0180	-0.0890	0.0004	-0.0084	-0.0478	-0.0001	0.0237	-0.0042	0.0006	-0.0022	-0.2692	-0.0001	-0.0081	0.0123
C25	-0.0004	0.0161	-0.0249	-0.0017	0.0060	-0.2820	-0.0004	0.0027	-0.1489	-0.0006	0.0352	-0.0170	-0.0003	0.0051	-0.0587	-0.0009	0.0062	-0.1450

Table 6.19 The coefficients obtained by using the Rayleigh-Ritz method using 25 terms and by using the VibroMap measurement

Conclusions of Chapter 6

This chapter has shown that real measurements of a mass-loaded plate can be processed in the same as the Rayleigh-Ritz based mode shapes in order to identify the required statistical properties of a mass-loaded plate structure. But the use of forced-damped measured data instead of the free vibration data via the Rayleigh-Ritz method, does not produce acceptable results, as they are not consistent with the successful results obtained for the low uncertainty case obtained in Chapter 4. Several possible causes for this inconsistency have been identified.

CHAPTER 7

CONCLUSIONS

This thesis has attempted to adapt an existing uncertainty identification method by making use of measure mode shapes information. The method has been developed by focusing on the identification of key statistical information associated with the location properties of a point mass on a clamped-plate. In drawing conclusions of the thesis, the objectives from Chapter 1 are recalled. These are:

i) To develop an uncertainty identification method which makes use of free-vibration dynamic response information in particular, a method that makes use of both natural frequency and free-vibration mode shape information suitable for lightly-damped structures with random uncertainty.

ii) To test the developed method on simulated free-vibration data corresponding to a representative structure.

iii) To test the method experimentally on a real, lightly-damped structure (under forced-vibration conditions) to confirm that the use of a free-vibration-based method.

With respect to objective i), an efficient method has been developed using measured frequency and free-vibration mode shapes for identifying uncertainty on simple beam and plate structures with an attached mass with uncertain positions. This is an extended form of MLE estimation based on the method of Fonseca [2005] et al. This uses frequency values in the same way as Fonseca [2005] but additionally mode shape information has been used (in summarised form) via the Rayleigh-Ritz method. The method in principle allows multiple estimates to be obtained from several different nominally independent sources including the use of different modes and different Rayleigh-Ritz coefficient groups. Averaging these multiple estimates allows for scatter reduction using small sample sizes, which is a requirement of practical value.

Turning to the second objective, the free vibration method developed in Chapter 2 has been tested on number representative cases and is shown to work well when the level of structural uncertainty is low. But it is also shown that this method does not work when the level of uncertainty is high. The cause of this failure is believed to be because in high levels of uncertainty the linearization error in the perturbation method is high.

Finally with regard to the third objective, involving testing of the free-vibration uncertainty identification method using forced-vibration mode shapes, the conclusions are difficult to interpret and inconsistent. This is because with both low and high levels of uncertainty the method developed in Chapter 2 and tested in Chapter 4 on plate structures, does not appear to work. The evidence seems to suggest that the Rayleigh-Ritz coefficients in the forced vibration of a real plate structure are different from the Rayleigh-Ritz coefficients obtained for free vibration case. There are however many other possible causes for failure of the method to work. But the main conclusion is that until this inconsistency is resolved the method is not suitable for use on more complicated structures of practical value.

Recommended Future Work

Future work needs to identify the cause of the inconsistency identified in meeting objective iii). In particular, the testing process should be simplified to precisely locate the source of the problem. The following points will hopefully answer the remaining questions:

- Test the method using simulated large-sample forced-vibration resonant frequencies rather than mode shapes.

- If the method proves successful using simulated frequency data, then it should be tested using measured forced-vibration resonant frequencies rather than mode shapes.

- Mode shapes should be measured using an alternative mode shape measurement technique in addition to use of Vibromap1000 in quantitative mode.

- A forced-vibration Jacobian calculation method should be developed for use in the uncertainty identification method rather than using the same free-vibration Jacobian as adopted in this thesis.

References

Adhiakri, S., Langley, R, 2003, *Distribution of Eigenvalues of linear stochastic systems*, Millpress.

Adhiakri, S., Friswell, M.I, 2004, *Random eigenvalue problems in structural dynamics*, AIAA/ASME/ASCE/AHS/ASC Structures, Structural Dynamics and Materials conference.

Anderson, Mark., 28th June 2001, *A definition of simulation uncertainty & a view of total uncertainty*, Uncertainty quantification working group: 4 - 5.

Arenas, Jorge. P., 2003, *On the vibration analysis of rectangular clamped plate using the virtual work principle*, Journal of Sound and Vibration, volume 266: 912-918.

Basil, Martin., Papadopoulos, Christos., Sutherland, Donald., Yeung, Hoi., 2001, *Application of probabilistic uncertainty methods (Monte Carlo Simulation) in flow measurement uncertainty estimation*, Flow measurement international conference.

Bies, David A., Hansen, Colin H., 2009, *Engineering noise control: Theory and Practice, Fourth edition, Spon Press.*

Bishop, R.E.D, Johnson, D.C, 1960, *The Mechanics of vibration*, Cambridge university press.

Chai, G.-B., 1995, *Frequency Analysis of an S-C-S-C plate carrying a concentrated mass*, Journal of Sound and Vibration, volume 179, issue 1: 170.

Chen, Su Huan., Wu, Jie., 2004, *Interval Optimization of Dynamic Response for Uncertain Structures with Natural Frequency Constraints*, Journal of Sound and Vibration, volume 26, issue 2: 221-232.

Chen, Su Huan., Wu, Jie., Chen, Yu Dong., 2004, *Interval Optimization for Uncertain Structures, Journal of Sound and Vibration*, volume 40, issue 11: 1379 -1398.

Dunne, J.F, Riefelyna, S, 2009, *Structural uncertainty identification using vibration mode shape information*, The Vibration Analysis of Structures with Uncertainties, IUTAM symposium. St Petersburg, Russia.

Ewins, D. J., 1984, *Modal Analysis: Testing and Practice*, Research studies press.

Ewins, D. J., 2001, *Mode of Vibration*, Encyclopedia of Vibration, Academic press.

Fonseca, Jose., Mares, Cris., Friswell, Mike., Mottershead, John, 2003, *The propagation of parameter uncertainty through structural dynamics models*, Proceeding of the IMAC-XXI.
Fonseca, Jose., Friswell, Mike., Mottershead, John., Lees, Arthur W., 2005a, *Uncertainty Quantification using Maximum Likelihood: Experimental Validation*, AIAA/ASME/ASCE/AHS/ASC Structures, Structural Dynamics & Materials Conference.

Fonseca, Jose, Friswell, Mike, Mottershead, John., Lees, Arthur, 2005b, *Uncertainty identification by the maximum likelihood method*, Journal of Sound and Vibration, 288: 587-599.

Fonseca, Jose, 2005c, *Uncertainty in structural dynamic models*, PhD thesis, University of Wales Swansea.

Fraccone, G. C., Ruzzene, M ., Volovoi, V., et al, 2008, *Assessment of uncertainty in response estimation for turbine engine bladed disks,* Journal of Sound and Vibration, volume 317 : 625 – 645.

Gersem, Hilde. De., Moens, David., Desmet, Wim., Vandepitte, Dirk., 6th December 2005, *A fuzzy finite element procedure for the calculation of uncertain frequency response functions of damped structures: Part 2-Numerical case studies*, Journal of Sound and Vibration, volume 288, issue 3: 463 – 486.

Gladwell, G. M. L., Bishop, R. E. D., 1960, *Interior receptances of beams*, Journal Mechanical Engineering Science.

Gorman, D. J., Sharma, R. K., 1976, *A comprehensive approach to the free vibration analysis of rectangular plates by use of the method of superposition*, Journal of Sound and Vibration, volume 47: 126-128.

Gorman, D. J., 1976, *A comprehensive approach to the free vibration analysis of rectangular plates by use of the method of superposition*, Journal of Sound and Vibration, Volume 49: 453-467.

Haldar, A., Mahadevan, S., 2000, *Probability, reliability and statistical methods in engineering design*, Acta Mechanica Sinica, John Wiley & Sons, Inc.

Haselman, Timothy., October 2001, *Quantification of Uncertainty in Structural Dynamic Models*, Journal of Aerospace Engineering, volume 14, Issue 4: 158-165.

Hazell, C.R., Mitchell, A.K., 1986, *Experimental eigenvalues and mode shapes for flat clamped plates,* Experimental mechanics 26: 337-344.

Inman, Daniel, J., 2008, *Engineering vibration*, Third edition, Pearson Prentice Hall.

Langley, R. S., July 2000, *The dynamic analysis on uncertain structures*, Proceedings of the Seventh International Conference on Recent Advances in Structural Dynamics, Southampton, 1 - 20.

Leissa, A.W., 1969, *Vibration of plates,* NASA SP-160.

Leissa, A.W., 1973, *The free vibration of rectangular plate,* Journal of Sound and Vibration, volume 31(3): 257 – 293.

Leissa, A.W., 2005, *The historical bases of the Rayleigh and Ritz methods*, Journal of Sound and Vibration, volume 287: 961-978.

Lin, Y K., 1967, *Probabilistic Theory of Structural Dynamics*, McGraw Hill.
Low, K.H., Chai, G.B., Tan, G.S., 1997, *A comparative study of vibrating loaded plates between the Rayleigh-Ritz and experimental methods*, Journal of Sound and Vibration, volume 199(2): 285-297.

Liu, B., Xing, Y., 2011, *Exact solutions for free in-plane vibrations for rectangular plates* , Acta Mechanica Solida Sinica, volume 24 Issue 6: 556 - 567.

Mace, Brian. R., Worden, Keith., Manson, Graeme., 2005, *Preface – Uncertainty in Dynamics*, Journal of Sound and Vibration volume 288: 423-429.

McGill, W. L., Ayyub, B. M., 2008, *Estimating parameter distribution in structural reliability assessment using transferable belief model,* Computers and structures, volume 86: 1052 – 1060.

Melchers, Robert E., 1999, *Structural reliability analysis and prediction*, John Wiley & Sons Ltd.

Mendenhall, W., Sincich, T., 2007, *Statistics for engineering and the sciences*, Fifth edition, Pearson Prentice Hall, Inc.

Myung, J., 2003, *Tutorial on maximum likelihood estimation*, Journal of Mathematical Psychology, volume 47: 90 - 100.

Nieves, F.J., Gascon, F., Bayon, A., 6th December 2004, *Natural Frequencies and Mode Shapes of Flexural Vibration of Plates: Laser-Interferometry Detection and Solutions by Ritz's Method*, Journal of Sound and Vibration, volume 278, issue 3: 637 – 655.

Onatski, Alexei., Williams, Noah., 10th August 2011, *Modelling model uncertainty*, http://www.princeton.edu/»noahw

Papadimitriou, P., 22nd December 2004, *Optimal Sensor Placement Methodology for Parametric Identification of Structural Systems*, Journal of Sound and Vibration, volume 278, issue 4-5: 923 - 947.

Plunt, Juha., 2003, *Predictability of Mid-and High Frequency Dynamic Properties of Industrial Products Using Simplified Modeling and NVH Design Strategy*, Keynote Presentation at VIII Int. Conf. Recent Advanced in Structural Dynamics ISVR, Southampton, United Kingdom.

Rabbiolo, G., Bernnard, R. J., Milner, F. A., 5th November 2004, *Definition of A High-Frequency Treshold for Plates and Acoustical Spaces*, Journal of Sound and Vibration, volume 277, issue 4 – 5: 647 – 667.

Ritz, W., 1908, *Ueber eine neue methode zur loesung gewisser variationsprobleme der mathematischenphysik*, J.f.Reine u. Angew. Math., volume 135: 1-61.

Shiryayev, O. V., Page, S. M, Pettit, C. L., et al., 2007, *Parameter estimation and investigation of a bolted joint model,* Journal of Sound and Vibration, volume 307, issue 3 – 5: 680 - 697.

Sung, C.-C., Jan, J. T., 1997, *The response of and sound power radiated by a clamped rectangular plate*, Journal of Sound and Vibration, volume 207: 301-317.

Szilard, Rudolph., 1974, *Theory and Analysis of Plates Classical and Numerical Methods*, Civil Engineering and Engineering Mechanics Series, Prentice-Hall, Inc.

Vickhagen, Eiof., 2005, *Vibromap 1000 Short Course Handbook*, Optonor, Norway.

Vijayakumar, K., Ramaiah, G.K., 1978, *Analysis of vibration of clamped square plates by the Rayleigh-Ritz method with asymptotic solutions from a modified Bolotin method*, Journal of sound and vibration, volume 56 Issue 1: 127-135.

Wu, Jiu Hui., Liu, A.Q., Chen, H.L., November 2007, *Exact solutions for free-vibration analysis of rectangular plates using Bessel functions*, Journal of Applied Mechanics, ASME, volume 74: 1247- 1251.

Xing, Y., Liu, B., 2009, *New exact solution for free vibrations of rectangular plates by symplectic dual method*, Acta Mechanica Sinica, volume 25 Issue 2: 265 - 270.

Xing, Y., Liu, B., 2009, *Characteristic equations and closed-form solutions for free vibrations of rectangular mindlin plates*, Acta Mechanica Solida Sinica, volume 22 Issue 2: 125 - 136.

Xing, Y., Liu, B., 2009, *New exact solutions for free vibrations of thin orthotropic rectangular plates*, Composite structures, volume 89: 567 - 574.

Young, Dana., 4th December 1950, *Vibration of rectangular plates by the Ritz method*, Journal of Applied Mechanic, ASME Trans, volume 17 (4): 448 - 453.